Damage Localization for Structural Health Monitoring

An Exploration of Three New Vibration-based Schemes

Ulriksen, Martin Dalgaard

DOI (link to publication from Publisher):
10.5278/vbn.phd.eng.00036

Publication date:
2018

Document Version
Publisher's PDF, also known as Version of record

DAMAGE LOCALIZATION FOR STRUCTURAL HEALTH MONITORING

AN EXPLORATION OF THREE NEW VIBRATION-BASED SCHEMES

BY
MARTIN D. ULRIKSEN

DISSERTATION SUBMITTED 2018

AALBORG UNIVERSITY
DENMARK

Damage Localization for Structural Health Monitoring

An Exploration of Three New Vibration-based Schemes

Martin D. Ulriksen
Department of Civil Engineering
Aalborg University

A thesis submitted for the degree of
Doctor of Philosophy

January 1, 2018

Dissertation submitted:	January 1, 2018
PhD supervisors:	Prof. Lars Damkilde (main supervisor) Aalborg University
	Dr. Dmitri Tcherniak (co-supervisor) Brüel & Kjær Sound & Vibration Measurement A/S
PhD committee:	Associate Professor Mohsen Soltani (chairman) Aalborg University
	Professor, dr.ir. Christof Devrient The Offshore Wind Infrastruture Lab
	Senior Researcher Laurent Medel INRIA Centre de Recherche ennes Bretagne Atlantique
PhD Series:	Faculty of Engineering and Science, Aalborg University
Department:	Department of Civil Engineering

ISSN (online): 2446-1636
ISBN (online): 978-87-7210-122-4

Published by:
Aalborg University Press
Langagervej 2
DK – 9220 Aalborg Ø
Phone: +45 99407140
aauf@forlag.aau.dk
forlag.aau.dk

Printed in Denmark by Rosendahls, 2018

Thesis details

Thesis title:
Damage Localization for Structural Health Monitoring: An Exploration of Three New Vibration-based Schemes

Ph.D. student:
Martin D. Ulriksen

Ph.D. supervisors:
Prof. Lars Damkilde & Dr. Dmitri Tcherniak

The main body of the present thesis is composed of the following six papers, which are enclosed in Appendix A to F:

A **Ulriksen, M. D.** and Damkilde, L. (2016). "Structural damage localization by outlier analysis of signal-processed mode shapes – Analytical and experimental validation." *Mechanical Systems and Signal Processing*, 68–69:1–14.

B **Ulriksen, M. D.**, Tcherniak, D., Kirkegaard, P. H., and Damkilde, L. (2016). "Operational modal analysis and wavelet transformation for damage identification in wind turbine blades." *Structural Health Monitoring*, 15(4):381–388.

C Bernal, D. and **Ulriksen, M. D.** (2017). "Subspace exclusion zones for damage localization." *Mechanical Systems and Signal Processing*, Under review.

D **Ulriksen, M. D.**, Tcherniak, D., Hansen, L. M., Johansen, R. J., Frøyd, L., and Damkilde, L. (2017). "In-situ damage localization for a wind turbine blade through outlier analysis of SDDLV-induced stress resultants." *Structural Health Monitoring*, 16(6):745–761.

E **Ulriksen, M. D.**, Bernal, D., and Damkilde, L. (2017). "Input shaping for steady-state damage localization." *Mechanical Systems and Signal Processing*, Under review.

F **Ulriksen, M. D.**, Bernal, D., Nielsen, M. E., and Damkilde, L. (2017). "Damage localization in offshore structures using shaped inputs." *Procedia Engineering*, 199:2282–2287.

In addition to the main papers, the following relevant publications have been made during the Ph.D. study:

- **Ulriksen, M. D.** and Bernal, D. (2017). "Sensor distributions for structural monitoring: a correlation study." *Proceedings of the International Conference on Structural Engineering Dynamics ICEDyn 2017*, Ericeira, Portugal.

- Markvart, M. K., Bull, T., Sekjær, C., Johansen, R. J., **Ulriksen, M. D.**, Tcherniak, D., and Damkilde, L. (2017). "Steady state shift damage localization in a residential-sized wind turbine blade." *Proceedings of the International Conference on Structural Engineering Dynamics ICEDyn 2017*, Ericeira, Portugal.

- Bull, T., Sekjær, C., Markvart, M. K., **Ulriksen, M. D.**, Johansen, R. J., Tcherniak, D., and Damkilde, L. (2017). "Statistical discrimination of steady state shift damage localization metrics." *Proceedings of the International Conference on Structural Engineering Dynamics ICEDyn 2017*, Ericeira, Portugal.

- Sekjær, C., Markvart, M. K., Bull, T., Johansen, R. J., **Ulriksen, M. D.**, Tcherniak, D., and Damkilde, L. (2017). "Steady state shift damage localization - a super-element approach." *Proceedings of the International Conference on Structural Engineering Dynamics ICEDyn 2017*, Ericeira, Portugal.

- Nielsen, M. E., **Ulriksen, M. D.**, and Damkilde, L. (2017). "SOFIA - A simulation tool for bottom founded and floating offshore structures." *Procedia Engineering*, 199:1308–1313.

- Gres, S., **Ulriksen, M. D.**, Döhler, M., Johansen, R. J., Andersen, P., Damkilde, L., and Nielsen, S. A. (2017). "Statistical methods for damage detection applied to civil structures." *Procedia Engineering*, 199:1919–1924.

- Gres, S., Andersen, P., Johansen, R. J., **Ulriksen, M. D.**, and Damkilde, L. (2017). "A comparison of damage detection methods applied to civil engineering structures." *Proceedings of the 7th International Conference on Experimental Vibration Analysis for Civil Engineering Structures*, San Diego, USA.

- **Ulriksen, M. D.** and Damkilde, L. (2016). "Vibration-based localization of structural deterioration in frame-like civil engineering structures." *Proceedings of INTER-NOISE 2016: 45th International Congress and Exposition on Noise Control Engineering*, Hamburg, Germany, 6574–6582.

- **Ulriksen, M. D.**, Bernal, D., and Damkilde, L. (2016). "Sensor placement for modal parameter subset estimation: A frequency response-based approach." *Proceedings of the 8th European Workshop On Structural Health Monitoring (EWSHM 2016)*, Bilbao, Spain.

- Johansen, R. J., **Ulriksen, M. D.**, and Damkilde, L. (2016). "DELORES - a system for detection and localization of structural damages." *Proceedings of the 8th European Workshop On Structural Health Monitoring (EWSHM 2016)*, Bilbao, Spain.

- **Ulriksen, M. D.** and Damkilde, L. (2015). "Damage localization by statistical evaluation of signal-processed mode shapes." *Journal of Physics: Conference Series*, 628:012121.

- Johansen, R. J., Hansen, L. M., **Ulriksen, M. D.**, Tcherniak, D., and Damkilde, L. (2015). "Damage localization in a residential-sized wind turbine blade by use of the SDDLV method." *Journal of Physics: Conference Series*, 628:012069.

- Hansen, L. M., Johansen, R. J., **Ulriksen, M. D.**, Tcherniak, D., and Damkilde, L. (2015). "Statistical evaluation of characteristic SDDLV-induced stress resultants to discriminate between undamaged and damaged elements." *Journal of Physics: Conference Series*, 628:012003.

- **Ulriksen, M. D.**, Tcherniak, D., and Damkilde, L. (2015). "Damage detection in an operating Vestas V27 wind turbine blade by use of outlier analysis." *Proceedings of the 2015 IEEE Workshop on Environmental, Energy and Structural Monitoring Systems (EESMS)*, Trento, Italy, 50–55.

Finally, the following relevant publications have been made prior to the Ph.D. study:

- **Ulriksen, M. D.**, Skov, J. F., Kirkegaard, P. H., and Damkilde, L. (2014). "Wavelet transformation for damage identification in wind turbine blades." *Structural Health Monitoring, Volume 5: Proceedings of the 32nd IMAC, A Conference and Exposition on Structural Dynamics, 2014*, 5:187–193.

- **Ulriksen, M. D.**, Skov, J. F., Dickow, K. A., Kirkegaard, P. H., and Damkilde, L. (2013). "Modal analysis for crack detection in small wind turbine blades." *Damage Assessment of Structures X, Vol. 569 of Key Engineering Materials*, Trans Tech Publications, 603-610.

- Skov, J. F., **Ulriksen, M. D.**, Dickow, K. A., Kirkegaard, P. H., and Damkilde, L. (2013). "On structural health monitoring of wind turbine blades." *Damage Assessment of Structures X, Vol. 569 of Key Engineering Materials*, Trans Tech Publications, 628–635.

The present thesis has been submitted for assessment in partial fulfillment of the Ph.D. degree. The thesis is based on the previously listed six submitted or published main scientific papers. Parts of the papers are used directly or indirectly in the extended summary of the thesis. As part of the assessment, co-author statements have been made available to the assessment committee and are also available at the Faculty. The thesis is not in its present form acceptable for open publication but only in limited and closed circulation as copyright may not be ensured.

Preface

The present Ph.D. thesis, "Damage Localization for Structural Health Monitoring: An Exploration of Three New Vibration-based Schemes", has been completed during my Ph.D. study from October 2014 to December 2017 at the Department of Civil Engineering, Aalborg University, Denmark. The thesis is presented as a collection of papers that have been written therewhile.

Acknowledgments

First and foremost, I would like to thank my main Ph.D. supervisor, Prof. Lars Damkilde, whose inventive mindset and good spirits made my Ph.D. study a rewarding experience. It was Prof. Damkilde who encouraged me to embark on not only this Ph.D. study but also, before that, an M.Sc. thesis on structural health monitoring. Needless to say, Prof. Damkilde has played a crucial role in my, so far short, academic career, and I am grateful to have had him as my main supervisor.

The gratitude is extended to my external supervisor, Dr. Dmitri Tcherniak from Brüel & Kjær Sound & Vibration Measurement A/S, with whom I have collaborated extensively and, in this context, enjoyed several technical discussions concerning structural health monitoring. Additionally, Dr. Tcherniak has introduced me to other researchers within the field and in this way helped me widen my research activities.

Special gratitude is directed to Prof. Dionisio Bernal for hosting me as a visiting scholar at the Structural Dynamics and System Identification Laboratory, Department of Civil and Environmental Engineering, Northeastern University, Boston, USA. The stay in Boston undoubtedly composes a pivotal part of my Ph.D. study, and it has been an honor to work for/with Prof. Bernal.

During the last part of my Ph.D. study, my supervisors and I have organized a structural health monitoring research group, which includes industrial partners, researchers from other universities, and other Ph.D. and M.Sc. students from Aalborg University. I would like to thank all past and present members of this group for fruitful collaboration.

Throughout the course of the Ph.D. study, I have been involved in four external projects; (1) "Torsional Stiffening of Wind Turbine Blades: Mitigating Leading Edge Damages" (EUDP Project 64013-0115), (2) "Weptos WEC Hanstholm" (ForskEL Project 2013-1-12039), (3) "Self-deployable Deorbiting Space Structure for Active Debris Removal" (Innovation Fund Denmark Project 100-2012-1), and (4) "Urban Tranquility" (under the Interreg V programme). Although the projects have not revolved around the topic of structural health

monitoring, they have played an important role in the Ph.D. study by enhancing my general knowledge within structural mechanics and dynamics. Furthermore, all the projects have provided financial support, which is gratefully acknowledged.

Finally, I want to thank my nearest and dearest for their perpetual moral support and helpfulness during the course of my Ph.D. study. I cannot even begin to quantify the importance and my appreciation of this.

Martin D. Ulriksen
Esbjerg, December 2017

Abstract

The tendency within engineering is to build increasingly large structures while minimizing material use. Needless to say, this leads to less conservative designs and, as such, an increased demand on regular inspection of the structures to ensure that they maintain adequate reliability through their life cycle. The inspections are conventionally conducted by sending out trained personnel to visually assess the integrity of the structures. This procedure can, however, be associated with high costs due to operational downtime and, for structures located in terrain not easily accessible, transportation.

A general consensus is that vibration-based structural health monitoring (SHM), which involves implementing a damage identification strategy to monitor structural integrity using vibration measurements, can play a role in reducing the inspection costs. Numerous SHM techniques have been suggested, and while the task of detecting whether damage is present or not has been resolved with reasonable success, a reliable solution has not yet been presented for the next logical step; namely, to locate the detected damage. There are many reasons as to why vibration-based damage localization has not yet found the level of industrial applicability that one would anticipate after decades of research. One of these reasons is undoubtedly that the vibration features used in the process, such as modal parameters, lack sensitivity to damage compared to the sensitivity to noise and other variabilities.

In the present thesis, three new vibration-based damage localization schemes are proposed that, in one way or another, address the noted sensitivity issue. The first exploration is the CWT-GDTKEO scheme, whose methodological premise is to seek for damage-induced changes in signal-processed mode shapes of the structure in question. More specifically, the scheme incorporates continuous wavelet transformation (CWT) and a generalized discrete Teager-Kaiser energy operator (GDTKEO) to capture these changes, and the damage location is attained using a simple metric comparing processed signals from the states prior and posterior to damage. In this way, the scheme relies on sufficiently accurate estimation of the required mode shapes, which, in many application scenarios, can be difficult to achieve due to noise and/or poor excitation.

The obvious drawbacks of the CWT-GDTKEO scheme have led to exploration of what are considered the two main contributions of this thesis. The first one is the Subspace Exclusion Zone (SEZ) scheme, which, under certain input conditions, circumvents system identification. The scheme locates damage by reconstructing shifts in measured field quantities using subspaces indexed by postulated boundaries, the so-called exclusion zones (EZs). The methodological concept rests on the fact that shifts in any field quantity outside the

boundary of an EZ encompassing the damage can be generated from stress fields acting on the aforementioned boundary. The EZs, which are formed in a theoretical model of the structure prior to damage, are of user-defined size, thus information on size and type of damage is precluded to provide a net robustness gain. Application examples are presented that clearly demonstrate the robustness of the SEZ scheme in instances allowing for a system identification-free configuration.

The second main contribution of the thesis is the Shaped Damage Locating Input Distribution (SDLID) scheme, which operates unconditionally free of system identification. The methodological premise is to deploy controllable inputs that are tailored to actively interrogate one structural subdomain at a time. When the subdomain containing damage is rendered dormant, the effect of damage and, as such, its induced shift in steady-state vibrations are canceled. In this way, the SDLID scheme facilitates damage localization using only few output sensors; in fact, one well-placed may suffice. This low demand on output sensors is an attractive feature, which is conventionally only achieved when employing an approach based on guided waves. However, unlike this approach with high-frequency waves, which is merely suitable for local integrity inspection because of small wavelengths and high damping, the SDLID scheme can operate in a broad band of frequencies.

Resumé

Tendensen inden for ingeniørvidenskab er at konstruere strukturer af tiltagende størrelse med minimalt materialeforbrug. Dette fører naturligvis til mindre konservative konstruktionsudformninger og, som konsekvens heraf, et forøget behov for regelmæssige inspektioner af strukturerne for at sikre, at de bibeholder den fornødne pålidelighed gennem deres livscyklus. Inspektionerne udføres konventionelt ved at sende uddannet personel ud for visuelt at vurdere integriteten af strukturerne. Denne procedure kan dog være forbundet med høje omkostninger grundet driftsstop og, såfremt strukturerne er placeret i svært tilgængeligt terræn, transport.

Der er generel enighed om, at vibrationsbaseret strukturovervågning (SHM), der involverer implementering af en skadesidentifikationsstrategi for at overvåge den strukturelle integritet ud fra vibrationsmålinger, kan spille en rolle i reducering af inspektionsomkostningerne. Adskillige SHM-teknikker er blevet foreslået, og mens opgaven med at opdage, om der er en skade eller ej, er blevet løst med rimelig succes, mangles der stadig en pålidelig løsning til det næste naturlige skridt; nemlig at lokalisere den opdagede skade. Der er adskillige grunde til, at vibrationsbaseret skadeslokalisering endnu ikke har opnået det industrielle applikationsniveau, som ville være ventet efter årtiers forskning. En af disse grunde er uomtvisteligt, at de vibrationskarakteristika, der anvendes i processen, såsom modale parametre, udviser manglende sensitivitet mod skade i forhold til sensitivitet mod støj og andre variationer.

I indeværende afhandling foreslås tre nye vibrationsbaserede skadeslokaliseringsmetoder, der på forskellig vis adresserer det anførte sensitivitetsproblem. Den første udforskning er CWT-GDTKEO-metoden, hvis præmis er at søge efter skadesfremkaldte ændringer i signalbehandlede egensvingningsformer for den pågældende struktur. Mere specifikt inkorporerer metoden kontinuerlig wavelettransformation (CWT) og en generaliseret diskret Teager-Kaiser energioperator (GDTKEO) for at opfange disse ændringer, og skadens placering opnås ved sammenligning af processerede signaler fra stadierne før og efter, skaden er opstået. På denne måde afhænger metoden af en tilstrækkeligt nøjagtig estimering af de krævede egensvingningsformer, hvilket i mange applikationsscenarier kan være svært at opnå grundet støj og/eller svag stimulering.

De åbenlyse ulemper ved CWT-GDTKEO-metoden har foranlediget udforskningen af, hvad der betragtes som denne afhandlings to hovedbidrag. Det første bidrag er Underrumseksklusionszone-metoden (SEZ), der undgår systemidentifikation under visse belastningsforhold. I metoden lokaliseres en skade gennem rekonstruktion af ændringer i målte feltstørrelser ved brug af underrum, der er inddelt af postulerede grænser, de såkaldte eksklusionszoner

(EZer). Det metodiske koncept hviler på det faktum, at ændringer i en hvilken som helst feltstørrelse uden for randen af en EZ, der omkredser skaden, kan genereres ud fra spændingsfelter, som virker på den førnævnte rand. Disse EZer, som etableres i en teoretisk model af strukturen i sin ubeskadiget tilstand, er af bruger-defineret størrelse, hvormed information omkring skadesstørrelse og –type undlades for at skabe en robusthedsforøgelse. Præsenterede applikationseksempler demonstrerer robustheden af SEZ-metoden i tilfælde, hvor systemidentifikation kan undgås.

Det andet hovedbidrag i afhandlingen er den Formede Skadeslokaliserende Belastningsfordelings-metode (SDLID), der opererer ubetinget uafhængigt af systemidentifikation. Den metodiske præmis er at implementere kontrollerbare belastninger, der formes til aktivt at undersøge ét strukturelt underdomæne af gangen. Når det underdomæne, der indeholder skaden, er sat i hvile, annulleres effekten af skaden i de stationære vibrationer. På denne måde muliggør SDLID-metoden skadeslokalisering ved brug af få sensorer; en enkelt velplaceret kan faktisk være tilstrækkelig. Dette lave behov for sensorer er et attraktivt særpræg, der normalt kun ses ved procedurer baseret på guidede bølger. Modsat denne fremgangsmåde med højfrekvente bølger, der udelukkende er egnet til lokal integritetsinspektion grundet små bølgelængder og høj dæmpning, kan SDLID-metoden operere inden for et bredt bånd af frekvenser.

Contents

CHAPTER 1

Introduction

There is general consensus that vibration-based structural health monitoring (SHM) can play a role in minimizing the costs needed to ensure that structures maintain adequate reliability through their life cycle. This SHM approach, which uses vibration signals as the observables from where inferences are made, has not, however, found the level of industrial applicability that one would anticipate after decades of research. There are many reasons why this is the case, and while a full discussion is beyond the scope of this thesis, it is safe to say that the ratio between sensitivity to damage and sensitivity to noise and other variabilities has been part of the roadblock. In the present chapter, the basic principles of vibration-based SHM, the theme around which the thesis revolves, are presented along with current state-of-the-art approaches and the existing challenges associated with these. The chapter is completed by outlining the focus, scope, and layout of the remainder of the thesis.

1.1 Vibration-based SHM

Vibration-based techniques for structural integrity inspection have been used for several years in different industries to enable online detection of damage in machinery (Rehorn et al., 2005; Jardine et al., 2006; Farrar and Worden, 2013). However, for structures and structural systems, such as bridges and wind turbines, the use of vibrations for remote integrity monitoring is still primarily a topic of academic research, albeit industrial platforms and companies focusing on SHM are starting to emerge. This highlights the difference between two closely related branches of vibration-based integrity inspection, namely, *condition monitoring* (CM) and *structural health monitoring* (SHM), between which the sole difference is the application area. An automated integrity inspection is referred to as CM if the application is within rotating machinery and SHM if structures and structural systems are treated (Balageas et al., 2006).

With the clear discrimination between CM and SHM, it is realized that vibration-based CM is a mature field, in the sense that is has made the transition from being a pure research topic to being applied extensively in the engineering industry with specific certification requirements (DNV GL, 2016). Contrary, vibration-based SHM is still primarily thought of as a research topic that is under the transition to become applicable in the industry as a robust and reliable alternative to regular visual inspection, which constitutes the most com-

monly adopted approach for structural integrity assessment in practice (Farrar and Worden, 2013; Burgos et al., 2015).

1.1.1 Motivation for implementing SHM systems

Nowadays, the general tendency within engineering is to build increasingly large structures while minimizing material use. Obviously, this tendency leads to less conservative designs with reduced safety margins and, accordingly, an increased demand on regular inspections to identify any critical damage. Here, damage is—as it will be throughout the entire thesis—used as a term that covers any changes to the structural properties, hence including cracks, delamination, added mass, and changes in kinematic boundary conditions.

With the increased demand on inspection due to less conservative structures, there are some obvious human, economic, and technical benefits of implementing an SHM system to replace (some of) the manual, visual inspections. One can, for instance, think in terms of safety, where it is noted that the process of inspecting especially large structures is associated with some portion of risk. This can easily be appreciated from Fig. 1.1, which depicts inspection crews in the process of looking for damage in, respectively, a wind turbine blade (Fig. 1.1a) and an offshore platform (Fig. 1.1b). Besides the safety issue, the visual inspections can also be associated with great costs due to operational downtime and, in case of structures located in terrain not easily accessible (such as offshore), transportation. Again, wind turbines and offshore platforms serve as good examples, since an inspection crew must be transported to the site and the structure to be inspected must be shut down. When the inspection crew is searching for damage, a technical issue arises, as some damages are hidden from view. In the context of the wind turbine example, some of the areas most likely to experience structural deterioration are located within the blade surfaces, hence making them difficult, and sometimes even impossible, to

(a) (b)

Fig. 1.1: Manual, visual inspection of (a) a wind turbine blade by rope access (Schroeder, 2013) and (b) an offshore platform by rope access (by courtesy of MEnD Consulting).

reach for human inspection (Ciang et al., 2008).

1.1.2 Damage identification

As defined in Subsection 1.1.1, damage is taken as changes to the physical properties of a structure, so the basic principle of vibration-based SHM is to capture these changes from dynamic response signals measured using installed sensors. Although a vast amount of different definitions of the term *structural health monitoring* are available in the literature, there seems to be the consensus that SHM, at the very minimum, involves the process of implementing a damage identification strategy to monitor structural integrity (Farrar et al., 2001; Balageas et al., 2006; Kopsaftopoulos and Fassois, 2010). In this context, *damage identification* refers to the following accumulative classification provided by Rytter (1993):

1. Detection: *is damage present?*
2. Localization: *where is the damage located?*
3. Assessment: *how big is the damage?*
4. Consequence: *what is the safety of the damaged structure?*

Damage prognosis and its application readiness

Evaluation of damage consequence, which is also referred to as *damage prognosis*, is related to the engineering fields of fracture mechanics and fatigue-life analysis and is, as such, typically treated separately from the first three steps in the identification tetrad. As can be seen in the review by Si et al. (2011), numerous studies have addressed prognostic remaining useful life (RUL) estimation for structural systems. Conventional approaches include the use of Bayesian networks (Straub, 2009) and Markov models (Banjevic and Jardine, 2006), and, at present, direct schemes with the aid of virtual sensing (as adopted from modern control theory) are also gaining attention and showing promising potential. Especially the results presented by Maes et al. (2016) and Iliopoulos et al. (2017) suggest that damage prognosis has reached a methodological maturity level that, given damage can be detected, located, and quantified, allows for application in practice.

Damage characterization and its application readiness

The triad composed of damage detection, localization, and assessment is denoted as *damage characterization* or *damage diagnosis* in the literature (Bernal, 2002; Kopsaftopoulos and Fassois, 2010). The situation one typically considers in damage characterization is that of assuming linearity in both the (typically healthy) reference state and the damaged one. Following this path, the task

of damage characterization can be viewed as a linear model updating problem (Friswell and Mottershead, 1995). However, an intrinsic deficiency in the model updating approach is that the inverse problem to be solved is often ill-conditioned, because the parameter space of the model tends to be much larger than the number of parameters identified from measurements (Udwadia, 1994; Friswell, 2007). As a consequence, a well-established strategy that has emerged in order to address these conditioning difficulties is to treat the components of the characterization triad in a cascade fashion.

Global detection of whether or not damage is present in a structure conventionally boils down to comparing some vibration features, such as vibration patterns or modal parameters, from the reference state and the current, potentially damaged state. At present, this is typically solved by use of unsupervised learning algorithms adapted from the fields of pattern classification and machine learning (Duda et al., 2001; Bishof, 2006). As such, the basic principle is to train a statistical baseline model based on the features extracted from the reference state and then compare the features from the current state to this model, hence exploiting that a structural damage will prompt changes in the stiffness, mass, and/or damping of the system. Of all unsupervised learning approaches, the by far most employed one for damage detection is classic outlier analysis, where the discordance between the current features and the baseline model is quantified via some metric (Worden et al., 2000); with a popular choice being the Mahalanobis distance (Mahalanobis, 1936). Another popular technique is the subspace-based scheme proposed by Basseville et al. (2000) and further developed by Döhler et al. (2014). Here, an identified model from the reference state is compared to vibration data from the possibly damaged state using a subspace-based residual function and hypothesis testing. The potential of these mentioned techniques has been demonstrated in the context of damage detection by Mevel et al. (1999) for different industrial structures, by Ulriksen et al. (2015) and Tcherniak and Mølgaard (2017) for an operating wind turbine blade, by Gres et al. (2017) for a decommissioned bridge, and so forth. It is thus contended that the detection component, although still a topic of active research, has reached a technical maturity level that enables implementation in industrial applications.

Damage localization has, just like the detection component, gained extensive research attention during the last decades (Salawu, 1997; Fan and Qiao, 2011). Localization is typically resolved in a setup where differences in features, such as transfer functions or modal parameters, from the reference and damaged states are mapped to the structural domain; either directly, referred to as *data-driven*, or by use of a theoretical model of the structure in question, referred to as *model-based*. Here, the theoretical model can be established analytically (when the structure is sufficiently "simple") or, more generally, based on a finite element (FE) formulation. While numerous studies, such as those more recent by Cao et al. (2014), Marin et al. (2015), and Markvart et al. (2017), document successful localization of different damages under laboratory conditions, there has, to the author's knowledge, not yet been presented a ro-

bust, scalable solution reliable for in-service applications. Obviously, this lack of success is most likely due to a combination of several aspects, but one general issue is the robustness to noise when, as done in many investigated schemes, compressing the vibration signals into a modal model through system identification (that is, inferring a mathematical model of the system/structure from measured data).

Once damage has been located, its quantification is known to be amenable to a solution in a model updating framework (Hà and Golinval, 2010; Bernal, 2014; Simoen et al., 2015). In this context, the general procedure is to parametrize the damage in a physically meaningful fashion (Friswell and Penny, 2002), formulate a cost function that measures the discordance between the model and the measurements, and then, finally, select the values of the parameters that minimize the cost function. Only few examples of in-situ studies on damage quantification, as that by Teughels and De Roeck (2004), have been presented, but it is the author's conviction that this is due to the lack of robust solutions to the localization component. Consequently, the focus of the present thesis will be dedicated to this central piece of the damage characterization triad.

1.2 Approaches to damage localization

A common approach in the early vibration-based damage localization schemes is to map direct changes in the modal parameters, namely, eigenfrequencies, damping ratios, and mode shapes, to the structural domain. However, since noise and varying environmental and operational conditions can account for at least 5 % shifts in modal parameters (Creed, 1987; Farrar et al., 1997; Devriendt et al., 2014), this general approach has limited robustness in practice. In fact, it can be shown theoretically that damage-induced shifts of more than 5 % in the lower modes typically excited by ambient sources will, for most structures and structural systems, require a deterioration extent above what can be accepted in practice. This argumentation is supported by numerous experimental findings; such as that by Larsen et al. (2014), who find the changes in the first seven eigenfrequencies of a 34 m long wind turbine blade introduced to a 1.2 m long edge debonding to be statistically insignificant.

Different measures have been taken to cope with the lack of sensitivity to damage of the modal parameters of the lower modes. Before going into details with these, it appears convenient to separate the localization approaches based on the prevailing operating condition as;

- output-only cases, where only spatial and statistical characteristics of the load are known, or can be reasonably assumed, and
- input-output cases, where one has control over the loading or, at least, can measure it.

Needless to say, it requires more from a practical point of view to implement input-output schemes, as some measurable and, potentially, controllable input

must be available. The gain is, on the other hand, that more information is available, which, when exploited properly, can increase the localization robustness. Additionally, some input sources can be tailored to excite a high frequency range where the modes, as a rule of thumb, are more sensitive to damage. In Subsections 1.2.1 and 1.2.2, we will discuss the two classes separately, and despite what one may find logical, we start by discussing the output-only techniques. This is chosen for three reasons; namely, because output-only techniques can also operate in input-output scenarios, because most methods can actually operate under output-only conditions, and because there are application scenarios in which implementation of external input sources is infeasible.

Another classification that is often employed, at least when referring to machine learning terminology (Bishof, 2006), is the distinction between supervised and unsupervised learning approaches. Supervised learning approaches have been employed successfully for damage localization in the context of numerical analyses and laboratory experiments by, for example, Kopsaftopoulos and Fassois (2010) and Sakaris et al. (2016). However, from a general application point of view, the requirement of having access to data from different damaged states prior to the actual damage identification seems troublesome, and therefore only unsupervised techniques will be treated further in this thesis.

1.2.1 Output-only techniques

The format of the output-only approach is attractive from an industrial application point of view, since many engineering structures are excited strictly by ambient and operational sources. The output-only techniques are conventionally implemented with the assumption that the (ambient) excitation is distributed randomly both temporally and spatially (Heylen et al., 1998). In this way, operational modal analysis (OMA) can be applied to infer a modal model from the measurements.

As documented in the reviews by Salawu (1997) and Fan and Qiao (2011), many of the early methods dealing with damage localization are model-based schemes in which shifts in eigenfrequencies are mapped to the structural domain using an analytical model (Adams et al., 1978; Cawley and Adams, 1979; Ju and Mimovich, 1988). Most of these methods, however, include damage severity in the formulation, as they require some estimate of the damage-induced reduction in local stiffness. Later on, model-based methods have been proposed that focus strictly on localization; with an example being the Best Achievable Eigenvector technique (Lim and Kashangaki, 1994), which interrogates one element at a time in the model and announces damage when the span of a subspace that depends on the element being considered contains the identified eigenvectors. A shortcoming of this method, and many other of the early model-based localization schemes, is that the experimental feature needs to be available at all the coordinates of the theoretical model. In practice, this requirement will never be satisfied, thus the missing experimental entries must be estimated through coordinate expansion (Heylen et al., 1998), which will often degrade

the localization results considerably.

A series of output-only model-based damage localization methods not requiring a coordinate match is the Stochastic Damage Locating Vector (SDLV) family, which is proposed by Bernal (2006, 2010) as an extension to the deterministic DLV schemes (Bernal, 2002, 2007). In the SDLV schemes, damage is localized from stress fields computed in a model subjected to load vectors extracted from the null space of changes in identified surrogates of the flexibility or transfer matrix. An extension of the SDLV methods has been proposed by Marin et al. (2015), who take into account the statistical uncertainties associated with the embedded output-only realizations and propagate these to the stress estimates. Subsequently, these stress estimates are aggregated to a single damage indicator for each element in the model, which is then analyzed in a hypothesis test for final, element-wise discrimination. Based on a laboratory experiment with a cantilevered beam, Marin et al. (2015) demonstrate the robustness enhancement obtained by adding the statistical evaluation to reduce the effects of noise. Another model-based method that rests on statistical evaluation has been proposed by Basseville et al. (2004) as an extension of the subspace-based detection technique by Basseville et al. (2000). This method seeks to locate damage using sensitivities of a residual that is computed from changes in the observability block with respect to the parameters of a model; the residual being the one used for detection. A drawback of this method is that it depends on clustering to reduce the number of unknowns (Balmès et al., 2008), and the applicability of the method has, to this author's knowledge, only been tested numerically.

As an alternative to model-based schemes, data-driven schemes have been employed since the early studies by Savage and Hewlett (1978), Yuen (1985), and Pandey et al. (1991). One straightforward, data-driven technique is to circumvent system identification by inspecting the feature shifts extracted during damage detection and, from these, directly announce damage near the sensor(s) registering the biggest shifts. This strategy has been adopted by, for example, García et al. (2015), who attempt to locate damage based on the shifts in principal components used for detection in the scheme by García and Trendafilova (2014). While the localization proves successful in some cases, it is clear that the technique lacks robustness.

In more recent studies adhering to the data-driven principle, a popular procedure is to seek for damage-induced changes in signal-processed mode shapes, or their spatial derivatives, by use of, for example, Laplacian operators (Ratcliffe, 1997; Cao and Qiao, 2009) or wavelet transformation (Douka et al., 2003; Loutridis et al., 2005; Rucka and Wilde, 2006). In particular, wavelet transformation has been employed extensively to filter noise and enhance damage-induced irregularities, and this approach has demonstrated potential in tests on, respectively, simple beam- and plate-like structures (Douka et al., 2003; Loutridis et al., 2005; Rucka and Wilde, 2006) and more advanced structures, such as small-scale wind turbine blades (Doliński and Krawczuk, 2009). Extensions of this wavelet transformation-based approach have been proposed by,

for example, Cao et al. (2014) for increasing noise robustness, but a general, intrinsic drawback of all data-driven methods (when recalling that we only treat unsupervised techniques) is that the spatial damage localization resolution is determined exclusively by the deployed grid of output sensors. Thus, a fine grid must be available if a high spatial localization resolution is required.

Most of the mentioned localization schemes, both model-based and data-driven, rely on a *parametric model* identified from the measurements to provide transfer matrices, modal parameters, and so forth. Since accurate system identification can be difficult to achieve from experimental data due to noise and/or poor excitation, this parametrization poses an issue in the context of localization robustness. To circumvent this, Bernal and Kunwar (2016) have proposed the Steady State Shift Damage Localization (S3DL) scheme, which, under certain input conditions, can operate in a system identification-free procedure where model-based postulated damage patterns are compared to the experimental data in a forward manner. The requirements for the input (which is not used explicitly in the scheme) are that it is spatially invariant and, as a minimum, proportional in the reference and damaged states. These two constraints make the scheme inapplicable, at least in a system identification-free reference, for structures subjected solely to ambient excitation. Another methodological issue is that a decision as to whether the damage is stiffness- or mass-related must be made, so if one wishes to interrogate a structure for both types, it has to be done separately.

1.2.2 Input-output techniques

The use of frequency response functions (FRFs) to localize damage has been explored extensively in the literature (Doebling et al., 1998; Fan and Qiao, 2011). One of the attractive features of this approach is that the FRFs can be directly computed when both the input and the output are known (the scenario prevailing in Fig. 1.2a), thus system identification is avoided. An example of a model-based FRF technique is given by the deterministic Dynamic Damage Location Vector (DDLV) scheme by Bernal (2007), which, like its stochastic counterpart discussed in Subsection 1.2.1, operates on the premise of localizing damage from fictitious stress fields, with damage revealing itself at locations of zero stress. The stress fields are computed by use of a theoretical model, which is subjected to load vectors extracted from the null space of the difference in the frequency response matrix prior and posterior to damage.

Another popular approach is to employ FRFs as parameters in a model updating context, which has been done, for example, by Wang et al. (1997) to localize damage in a laboratory frame structure. Data-driven FRF-based techniques include that by Hà and Golinval (2010), who extract sensitivities of FRF principal components and conduct sensor-level localization by announcing damage where the biggest shifts in these sensitivities occur. By doing so, Hà and Golinval (2010) succeed in locating damage in experimental campaigns with different structures, including an exploration of a decommissioned bridge.

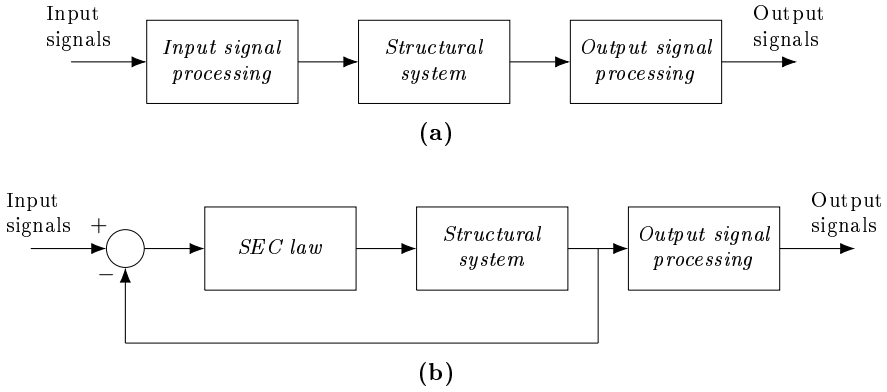

Fig. 1.2: Block diagram, as sketched by Ray and Tian (1999), of a linear dynamic system in (a) open loop and (b) closed loop with sensitivity-enhancing control (SEC).

Thus far, the discussed techniques within both input-output and output-only approaches are all based on—or, at least, applicable for—systems where the excitation signals only carry frequencies within the modal range. Another popular class of techniques is the one based on guided waves, where one or multiple input sources, such as piezoelectric or electro-mechanical transducers, are installed on the structure in question to excite high-frequency content. Damage is then located from observed changes in the reflections of the (guided) Lamb or ultrasonic waves that propagate within the structure (Hellier, 2001). The high frequency content typically ensures relatively high sensitivity to damage, and as documented in the reviews by Su et al. (2006) and Guan et al. (2017), guided waves have been employed successfully to locate rather small damages in, for instance, composite structures and steel pipelines. However, due to the high frequencies and, as such, small wavelengths and high damping, guided waves are merely suitable for local integrity inspection under controlled conditions (Raghavan and Cesnik, 2007).

It is evident that there is a trade-off between sensitivity to damage and the size of the area that can be examined. Given that the external input is not only measurable but also controllable, closed-loop system control schemes, as illustrated very simplistically in Fig. 1.2b, can be adopted to design conditions in which the modal model identified from data has increased sensitivity to damage (when compared to that of the open-loop system). The initial idea to employ such a sensitivity-enhancing control (SEC) approach dates back to Ray and Tian (1999), who, from a single-degree-of-freedom (SDOF) consideration about the sensitivity of the eigenvalue, suggested to select the controller gain to shift the poles towards lower frequencies. Later on, studies have been presented that address placement of both eigenvalues and eigenvectors for increasing the eigenfrequency sensitivity to damage (Jiang et al., 2007), and some of the few available experimental investigations, as those by Ray et al. (2000) and

Solbeck and Ray (2005), demonstrate the effectiveness of SEC-based damage localization in beam and frame structures. Obviously, the major drawback of the SEC-based approach is the amount of hardware required, which can be impossible to implement in some applications due to technical and/or economic reasons. Furthermore, one could, from a practical standpoint, argue that the use of active control poses a restriction, as many civil and mechanical engineers are still not familiarized with this topic.

1.3 Thesis focus and contributions

All vibration-based localization schemes can, independently of whether they are based on the output-only or the input-output approach, be classified according to the block diagram in Fig. 1.3, where some state-of-the-art schemes are included to exemplify the premises. One gathers that the predominant issue in the context of vibration-based damage localization, where the guided waves-based approach is excluded due to its limited use for in-service applications, is the ratio between sensitivity to damage and sensitivity to noise and other variabilities. As it has been outlined in the review in the previous section, there are two obvious paths that one can follow in the attempt to improve this ratio. The first is to reduce the impact of noise and other variabilities, which can be done by taking into account the uncertainties linked to the system identification or, if the specific situation allows for it, by reducing or even eliminating the need for extracting a modal model. The other path is, of course, to increase the sensitivity to damage by designing a closed-loop system with an, in the strict

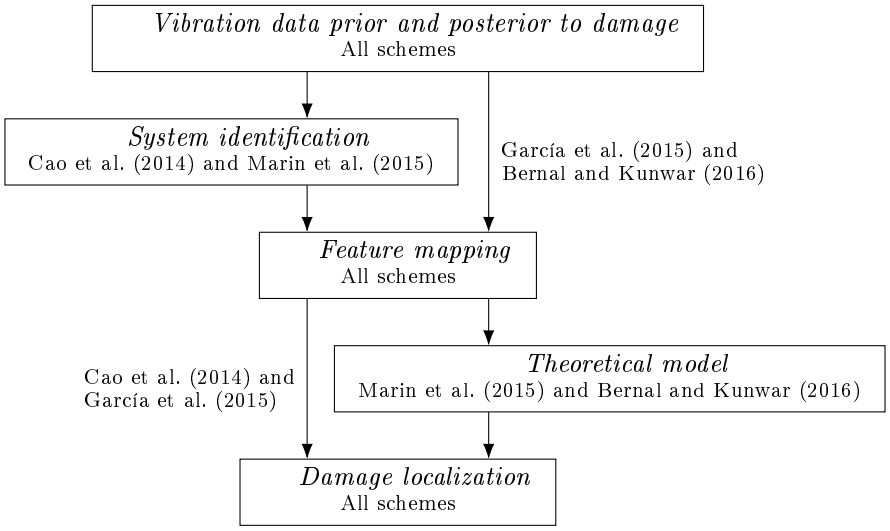

Fig. 1.3: Block diagram of (unsupervised) output-only and input-output approaches to vibration-based damage localization, with examples of schemes adhering to particular paths.

sense of damage sensitivity, optimized eigenstructure and then proceed with a modal-based localization scheme.

Another aspect that should be considered in the attempt to improve the sensitivity ratio is the deployment of output and, potentially, input transducers. Generally, one has to accept that for most applications only a limited number of transducers can be used during in-situ explorations, thus the deployment challenge boils down to distributing these in an optimal way. In this context, numerous studies have focused on distributing sensors to maximize the probability of detection (Worden and Burrows, 2001; Parker, 2011; Döhler et al., 2013), but when it comes to optimal sensor placement for locating damages, only a few investigations, such as those by Shi et al. (2000) and Ulriksen and Bernal (2017), have been conducted. Although these clearly demonstrate how the likelihood of successful localization strongly depends on the sensor distribution, it is, with the exception of a particular application example in Chapter 5, not a path pursued in the present thesis.

With focus on fundamental research concerning vibration-based damage localization, the objective of the present thesis is to develop methods that, in one way or another, confront the governing sensitivity issue. It is realized that to optimize the effectiveness of a damage localization procedure, it must be customized to the particular application in question and, accordingly, the governing operational and environmental conditions. This implies that no single localization approach is optimal in all cases, and therefore different paths in the block diagram in Fig. 1.3 are explored. To be specific, the contributions of the present thesis are the following:

1. The parametric, data-driven CWT-GDTKEO scheme, which
    - enhances damage-induced mode shape changes by continuous wavelet transformation (CWT) and application of a generalized discrete Teager-Kaiser energy operator (GDTKEO);
    - localizes damage by comparison of the signal-processed mode shape signals prior and posterior to damage;
    - operates independently of whether the damage is a stiffness or a mass perturbation;
    - can, in principle, be used in both an output-only and an input-output context.
2. The conditionally non-parametric, model-based Subspace Exclusion Zone (SEZ) scheme, which
    - localizes damage from orthogonality between model-based subspaces and an experimental feature;
    - operates in a forward procedure where system identification is circumvented if certain input conditions are met;

- allows for a user-defined spatial localization resolution with postulated model-based boundaries;
- interrogates the structural domain independently of whether the damage is a stiffness or a mass perturbation;
- can, in principle, be used in both an output-only and an input-output context.

3. The non-parametric, model-based Shaped Damage Locating Input Distribution (SDLID) scheme, which
   - localizes damage by shaping inputs to render structural subdomains dormant and, from this, isolate damage;
   - operates in a forward procedure where system identification is unconditionally circumvented;
   - allows for a user-defined spatial localization resolution with postulated damage areas;
   - facilitates, in principle, the use of a single output sensor;
   - requires controllable inputs.
4. In-situ and in-service application examples with a wind turbine introduced to damage in one of its blades.

The CWT-GDTKEO scheme can be regarded as a further development of the parametric, data-driven method proposed by Cao et al. (2014). In the new scheme, a generalization of the discrete Teager-Kaiser energy operator (DTKEO), as defined by Kaiser (1990), is formulated and applied to increase the robustness to noise and other variabilities. Additionally, a simple damage metric is proposed for final discrimination between damage-induced discontinuities and other signal irregularities in the processed mode shapes.

The SEZ scheme bares strong resemblance to the S3DL scheme by Bernal and Kunwar (2016). The major difference is that the former rests on a theoretical premise allowing for structural interrogation without prior distinction between stiffness- and mass-related damage. System identification can be circumvented if the input is spatially invariant and, as a minimum, proportional prior and posterior to damage. If these input requirements are not complied with, system identification is necessary. Yet, in this context, it is worth noting that the experimental feature is less demanding in accuracy compared to that of the conventional parametric, model-based techniques (Bernal, 2010; Marin et al., 2015), as the SEZ scheme employs the difference between two vectors and not the kernel of the difference between two matrices.

The SDLID scheme constitutes a conceptual alternative to conventional input-output-based localization approaches, as controllable inputs are shaped by use of a theoretical model to "deactivate" the damage for determining its location. The methodological premise of the SDLID scheme is, as such, to

compare the responses obtained prior and posterior to damage when applying the shaped inputs; a procedure that, in principle, allows for the use of a single output sensor. Compared to the SEC-based format, the major difference is that the SDLID scheme operates in open loop, thus active control is circumvented.

1.4 Thesis outline

The remainder of the thesis consists of five chapters, including a conclusion, and six appendices that contain the papers constituting the body of the thesis. A brief outline of the content in Chapters 2 to 6 and Appendices A to F is given below.

Chapter 2 presents the background theory on the vibration analysis, system identification, and basic principles of damage localization needed to, respectively, formulate the three schemes and apply them in relevant contexts.

Chapter 3 introduces the CWT-GDTKEO scheme as an incremental refinement of an existing damage localization method. The new scheme is examined experimentally based on laboratory tests with a full-scale wind turbine blade.

Chapter 4 presents the SEZ scheme, which operates non-parametrically under certain input conditions. The scheme is tested through simulations, in laboratory experiments, and in the context of a real-life operating wind turbine blade.

Chapter 5 explores the SDLID scheme, which rests on the requirement that controllable inputs are available to shape the vibration response for damage isolation. The scheme is tested in the context of different numerical examples.

Chapter 6 concludes the main body of the thesis with a summary and discussion of the material presented. The main results achieved in the project are outlined and suggestions for future work are provided.

Appendix A contains Paper A by Ulriksen and Damkilde (2016); that is, "Structural damage localization by outlier analysis of signal-processed mode shapes – Analytical and experimental validation."

Appendix B contains Paper B by Ulriksen et al. (2016); that is, "Operational modal analysis and wavelet transformation for damage identification in wind turbine blades."

Appendix C contains Paper C by Bernal and Ulriksen (2017); that is, "Subspace exclusion zones for damage localization."

Appendix D contains Paper D by Ulriksen et al. (2017); that is, "In-situ damage localization for a wind turbine blade through outlier analysis of SDDLV-induced stress resultants."

Appendix E contains Paper E by Ulriksen et al. (2017a); that is, "Input shaping for steady-state damage localization."

Appendix F contains Paper F by Ulriksen et al. (2017b); that is, "Damage localization in offshore structures using shaped inputs."

CHAPTER 2

Background theory

This chapter provides an overview of the fundamental theory common for the explored damage localization schemes. In Section 2.1, linear vibration analysis is addressed, and concepts such as modal parametrization and state-space modeling are introduced. Next, the concept of system identification, one of the governing challenges within vibration-based damage localization, is outlined in Section 2.2, and finally the basic principles of vibration-based damage localization are presented in Section 2.3. It is important to note that this chapter by no means attempts to provide an exhaustive explanation of the included theory, so references will appear to background material. Furthermore, details concerning each of the three localization schemes appear in the relevant chapters.

2.1 Linear vibration analysis

Consider a linear and time-invariant (LTI) structural domain, $\mathcal{A}$, that is discretized with n DOF and subjected to p independent inputs that are gathered in $u(t) \in \mathbb{R}^p$ and distributed to $\mathcal{A}$ by $B_2 \in \mathbb{R}^{n\times p}$. With $x(t)$, $\dot{x}(t)$, $\ddot{x}(t) \in \mathbb{R}^n$ being the nodal displacement, velocity, and acceleration vectors, the governing temporal equation of viscously damped motion is

$$M\ddot{x}(t) + C\dot{x}(t) + Kx(t) = B_2u(t), \qquad x(0) = x_0, \dot{x}(0) = \dot{x}_0, \tag{2.1}$$

where K, C, $M \in \mathbb{R}^{n\times n}$ are the stiffness, damping, and mass matrices for which it, in general, holds that $K \succeq 0$, $C \succeq 0$, and $M \succ 0$ (with $\succ$ denoting positive definiteness). When $\mathcal{A}$ is supported such that rigid body motion is prevented, one gets $K \succ 0$ and $C \succ 0$.

Laplace transformation of Eq. (2.1) yields

$$M\big(-\dot{x}_0 - sx_0 + s^2X(s)\big) + C\big(-x_0 + sX(s)\big) + KX(s) = B_2U(s), \tag{2.2}$$

as $X(s) = \mathcal{L}(x(t))(s)$ and $U(s) = \mathcal{L}(u(t))(s)$ are the Laplace transforms of the output and the input. In Fig. 2.1a, the coupling between the Laplace variable, s, and the eigenvalues of the system in Eq. (2.2) is illustrated. The eigenvalue of the ith mode can, from the homogeneous part of Eq. (2.1), be derived to

$$\lambda_i, \lambda_i^* = -\zeta_i\omega_i \pm \omega_i j\sqrt{1-\zeta_i^2}, \tag{2.3}$$

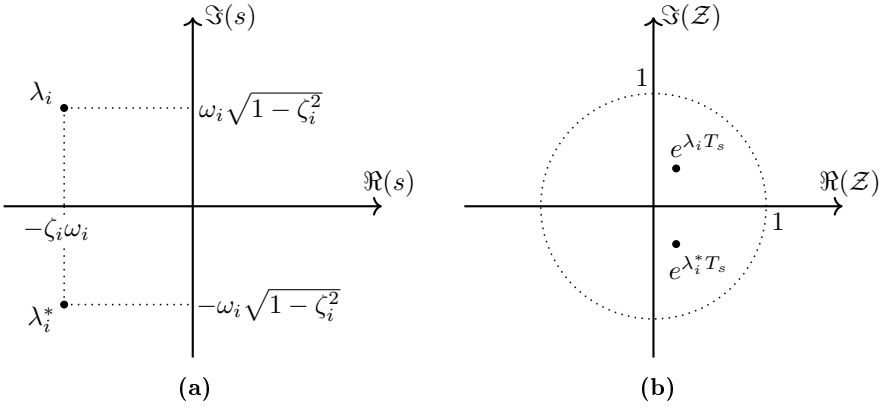

Fig. 2.1: The ith pole of $\mathcal{A}$ in (a) s-domain and (b) $\mathcal{Z}$-domain with inter-sample time T_s.

where $j = \sqrt{-1}$ is the imaginary unit while $\omega_i = |\lambda_i|$ and $\zeta_i = -\Re(\lambda_i)/|\lambda_i|$ are, respectively, the undamped eigenfrequency and the damping ratio. The latter is here restricted to satisfy $\zeta_i \in [0, 1)$, thus the damping is either omitted or assumed undercritical. The eigenvalues are gathered in the spectral matrix $\Lambda = \mathrm{diag}\,[\lambda_1, \lambda_2, \ldots, \lambda_n] \in \mathbb{C}^{n\times n}$ and inserted to form

$$\Lambda_c = \begin{bmatrix} \Lambda & 0 \\ 0 & \Lambda^* \end{bmatrix}. \tag{2.4}$$

When solving Eq. (2.2) for $X(s)$ and assuming $x_0 = \dot{x}_0 = 0$ and/or steady-state conditions, one gets

$$X(s) = \left(Ms^2 + Cs + K\right)^{-1} B_2 U(s) = G(s) B_2 U(s) \tag{2.5}$$

with $G(s) \in \mathbb{C}^{n\times n}$ being the receptance matrix coupling the force input to the displacement output. It is noticed that evaluation of $G(s)$ along the imaginary axis yields the frequency response matrix composed of the FRFs, while $G(t) = \mathcal{L}^{-1}(G(s))(t)$ is the impulse response matrix.

2.1.1 Modal parametrization

Define $\Lambda_0 = \mathrm{diag}\left[\omega_1^2, \omega_2^2, \ldots, \omega_n^2\right] \in \mathbb{R}^{n\times n}$ and $\Phi = [\phi_1\ \phi_2\ \ldots\ \phi_n] \in \mathbb{R}^{n\times n}$, where ϕ_i is the mass-normalized mode shape of the ith undamped eigenmode. Since $\mathrm{rank}\,(\Phi) = n$, it holds that $\Phi^T M \Phi = \bar{M} = I$ and $\Phi^T K \Phi = \bar{K} = \Lambda_0$. Additionally, if the damping distribution is classical, which, as proved by Caughey and O'Kelly (1965), is the case when $M^{-1}C$ and $M^{-1}K$ commute, then $\Phi^T C \Phi = \bar{C} = \mathrm{diag}\,[2\zeta_1\omega_1, 2\zeta_2\omega_2, \ldots, 2\zeta_n\omega_n]$. From this, the transfer matrix can be expressed in terms of the modal matrices as

$$
\begin{aligned}
G(s) &= \left(\left(\Phi^T\right)^{-1}\bar{M}\Phi^{-1}s^2 + \left(\Phi^T\right)^{-1}\bar{C}\Phi^{-1}s + \left(\Phi^T\right)^{-1}\bar{K}\Phi^{-1}\right)^{-1} \\
&= \left(\left(\Phi^T\right)^{-1}\left(\bar{M}s^2 + \bar{C}s + \bar{K}\right)\Phi^{-1}\right)^{-1} = \Phi\left(\bar{M}s^2 + \bar{C}s + \bar{K}\right)^{-1}\Phi^T \\
&= \sum_{i=1}^{n}\frac{\phi_i\phi_i^T}{\bar{m}_{ii}s^2 + \bar{c}_{ii}s + \bar{k}_{ii}} = \sum_{i=1}^{n}\frac{\phi_i\phi_i^T}{s^2 + 2\zeta_i\omega_i s + \omega_i^2},
\end{aligned}
\tag{2.6}
$$

and—since Laplace transformation is a linear operation such $\mathcal{L}^{-1}(g_1 + g_2) = \mathcal{L}^{-1}(g_1) + \mathcal{L}^{-1}(g_2)$—the impulse response matrix becomes

$$
G(t) = \sum_{i=1}^{n}\frac{\phi_i\phi_i^T}{\omega_i\sqrt{1-\zeta_i^2}}e^{-\zeta_i\omega_i t}\sin\left(\omega_i\sqrt{1-\zeta_i^2}t\right). \tag{2.7}
$$

As deduced from Eqs. (2.6) and (2.7), LTI conditions and a classical damping distribution imply that the vibration characteristics of the ith eigenmode are governed solely by the modal triplet $\{\omega_i, \zeta_i, \phi_i\}$. Introducing the modal transformation $f : x \mapsto \bar{x}$, where $f(x) = \Phi^{-1}x$, provides

$$
x(t) = \Phi\bar{x}(t) = \sum_{i=1}^{n}\phi_i\bar{x}_i(t), \tag{2.8}
$$

which evidences that an n-DOF LTI system with classical damping can be treated as a sum of n SDOF systems in modal coordinates, $\bar{x}_i(t)$. This superposition principle is illustrated in Fig. 2.2. For additional theory on basic modal analysis, the reader is referred to the book by Heylen et al. (1998).

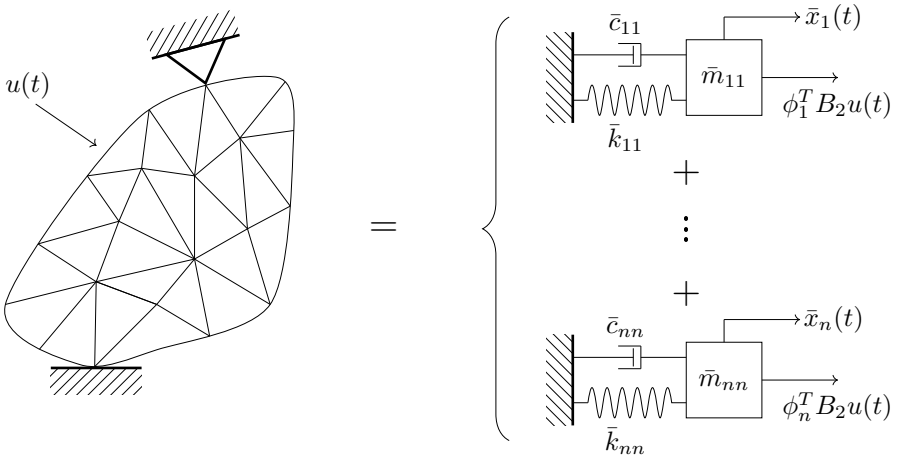

Fig. 2.2: Modal decoupling of a classically damped LTI n-DOF system with input $u(t)$.

2.1.2 State-space representation

Continuous-time

We define the state vector $z(t)^T = [x(t)^T \ \dot{x}(t)^T]$ and rewrite Eq. (2.1) into the state-space form

$$\dot{z}(t) = A_c z(t) + B_c u(t) \tag{2.9a}$$

$$y(t) = C_c z(t) + D_c u(t), \tag{2.9b}$$

where the output vector $y(t)$ is some linear combination of displacements, velocities, and/or accelerations, while $A_c \in \mathbb{R}^{2n\times 2n}$, $B_c \in \mathbb{R}^{2n\times p}$, $C_c \in \mathbb{R}^{n\times 2n}$, and $D_c \in \mathbb{R}^{n\times p}$ are the state transition, input, output, and input-output transmission matrices. The solutions to Eqs. (2.9a) and (2.9a) are

$$z(t) = e^{A_c t} z(0) + \int_0^t e^{A_c(t-\tau)} B_c u(\tau)\, d\tau \tag{2.10a}$$

$$y(t) = C_c e^{A_c t} z(0) + C_c \int_0^t e^{A_c(t-\tau)} B_c u(\tau)\, d\tau + D_c u(t), \tag{2.10b}$$

in which the first term of the right-hand-side (in both equations) is the response due to initial conditions, while the remaining are governed by the input. It follows that the impulse response matrix can be extracted as

$$\mathcal{G}(t) = C_c e^{A_c t} B_c + D_c \delta(t) \tag{2.11}$$

when $\delta(t)$ is the delta function. Obviously, $\mathcal{G}(t)$ equals $G(t)$ defined in Eq. (2.7) for displacement measurements and the first and second derivatives of $G(t)$ for, respectively, velocities and accelerations.

Laplace transformation of $\mathcal{G}(t)$ yields the transfer matrix

$$\mathcal{G}(s) = C_c \left(sI - A_c\right)^{-1} B_c + D_c, \tag{2.12}$$

which for displacement measurements coincides with the receptance matrix derived from Eq. (2.5) and restated in Eq. (2.6). Again, if velocities or accelerations are measured, $\mathcal{G}(s)$ corresponds to the mobility matrix, $sG(s)$, or the accelerance matrix, $s^2G(s)$. Now, situations may occur where, for example, accelerations are measured but the receptance matrix is required. In order to handle this, Bernal (2007) derives the general expression

$$\mathcal{G}(s) = C_c A_c^{-b} \left(sI - A_c\right)^{-1} B_c \tag{2.13}$$

for computing the receptance matrix; with $b = 0, 1, 2$, depending on whether displacements, velocities, or accelerations are measured.

The term $\left(sI - A_c\right)^{-1}$, which appears in $\mathcal{G}(s)$, can be rewritten by use of Cramer's rule, such

$$\left(sI - A_c\right)^{-1} = \frac{\operatorname{adj}\left(sI - A_c\right)}{\det\left(sI - A_c\right)} \tag{2.14}$$

with adj(∘) and det(∘) denoting matrix adjoint and determinant. The denominator in Eq. (2.14) is recognized as the characteristic polynomial of A_c, thus the poles of the state-space system, corresponding to the complex conjugated eigenvalue pairs defined for the second order system in Eq. (2.3) and gathered in Λ_c, are collected as the eigenvalues of A_c. Similarly, the eigenvectors of A_c are collected in

$$\Psi_c = \begin{bmatrix} \Psi & \Psi^* \\ \Psi\Lambda & \Psi^*\Lambda^* \end{bmatrix}, \tag{2.15}$$

where, in general, $\Psi \in \mathbb{C}^{n\times n}$ contains the eigenvectors/mode shapes of the second order system in Eq. (2.1). However, if classical damping is assumed, which will be the case throughout this thesis, $\Psi = \Phi \in \mathbb{R}^{n\times n}$.

Discrete-time

In real applications, vibration responses from a structure are captured with some sampling frequency, hence yielding discrete signals. If the dynamic system in question is sampled with an inter-sample time of T_s, the solution to Eq. (2.9a) at time instant $t = (k+1)T_s$, where $k \in \mathbb{N}_0 = \mathbb{N} \cup \{0\}$, is

$$z_{k+1} = e^{A_c T_s} z_k + \int_{kT_s}^{(k+1)T_s} e^{A_c\left((k+1)T_s - \tau\right)} B_c u(\tau)\, d\tau. \tag{2.16}$$

Thus, if the zero-order-hold (ZOH) rule is employed, such $\forall t \in [kT_s, (k+1)T_s) : u(t) = u_k$, one gets the discrete state-space representation

$$z_{k+1} = A_d z_k + B_d u_k \tag{2.17a}$$

$$y_k = C_d z_k + D_d u_k \tag{2.17b}$$

with $A_d = e^{A_c T_s}$, $B_d = \int_{kT_s}^{(k+1)T_s} e^{A_c\left((k+1)T_s - \tau\right)}\, d\tau B_c = A_c^{-1}\left(A_d - I\right) B_c$, $C_d = C_c$, and $D_d = D_c$.

The poles of the discrete-time system are placed in the $\mathcal{Z}$-domain (with $\mathcal{Z} = e^{sT_s}$) and found as the eigenvalues of A_d. If the ZOH rule is applied, one obtains the discrete-time eigencharacteristics

$$\Lambda_d = e^{\Lambda_c T_s} \tag{2.18a}$$

$$\Psi_d = \Psi_c, \quad C_d \Psi_d = \Phi \tag{2.18b}$$

for a classical damping distribution. In Fig. 2.1b, the locations in the $\mathcal{Z}$-domain of the ith pole of A_d and its complex conjugate are shown.

2.2 System identification

One could argue that since only one of the three explored damage localization schemes is unconditionally parametric, system identification falls under the category of specific details and should, as such, be described in Chapter 3.

However, as the remaining two schemes are developed, partially, to circumvent this system parametrization, it seems appropriate to introduce the topic in a general context

In Subsection 2.1.2, the forward procedure for determining the modal parameters of an LTI state-space system is outlined. In practice, one does, of course, not typically know the actual system parameters, K, M, and C, so system identification is used to infer a model and, as such, the modal parameters of the system through measured data. In the present thesis, it has been chosen to employ a subspace-based approach due to, among other reasons, its limited extent of parametrization; in principle, only the order of the system must be selected (Overschee and De Moor, 1996). For a thorough survey of subspace-based techniques, the reader is referred to the work by Overschee and De Moor (1996) and Prevosto et al. (1991), while a more general description of system identification has been provided by Ljung (1987) and, in the context of structural dynamics, by Peeters and De Roeck (2001).

2.2.1 Basic concepts of subspace identification

If one should derive the quadruplet $\{A_d, B_d, C_d, D_d\}$ in practice, the dimensions would, of course, be governed by the number of output sensors and a pre-defined parametric model order (referred to as system order) and not the number of DOF in the theoretical model. By letting n_s and $m_s < n$ denote, respectively, the selected system order and the number of output sensors/measurement DOF, such $z_k \in \mathbb{R}^{n_s}$ and $y_k \in \mathbb{R}^{m_s}$, the quadruplet follows as $A_d \in \mathbb{R}^{n_s \times n_s}$, $B_d \in \mathbb{R}^{n_s \times p}$, $C_d \in \mathbb{R}^{m_s \times n_s}$, and $D_d \in \mathbb{R}^{m_s \times p}$. Obviously, the state and output vectors along with the system quadruplet are now truncated editions of those listed in Eqs. (2.17a) and (2.17b), but they are denoted identically to ease the notation.

The state-space models established thus far are deterministic, since the input is assumed known and no measurement noise is present. In a more general context, we define the combined deterministic-stochastic model

$$z_{k+1} = A_d z_k + B_d u_k + w_k \tag{2.19a}$$

$$y_k = C_d z_k + D_d u_k + v_k \tag{2.19b}$$

by adding process noise, $w_k \in \mathbb{R}^{n_s}$, and measurement noise, $v_k \in \mathbb{R}^{m_s}$, for which it is assumed that $w_k \sim \mathcal{N}(0, \Sigma_w)$ and $v_k \sim \mathcal{N}(0, \Sigma_v)$. Fairly simplified, the concept of subspace system identification is to estimate the state using the output and the input—with the latter being either known deterministically or characterized statistically—and, from this, compute the quadruplet $\{A_d, B_d, C_d, D_d\}$ or a subset hereof (A_d and C_d).

In the review of existing vibration-based damage localization techniques, see Section 1.2, a clear distinction was made between input-output and output-only approaches. This is also the case in system identification, where *experimental modal analysis* (EMA) and *operational modal analysis* (OMA) are system

identification branches treating structural modal analysis in, respectively, a deterministic (input-output) and a stochastic (output-only) reference. It is contended that if the input is known, the best approach in terms of damage localization will be to compute a feature, for example, based on the frequency response function(s), directly from the input-output relation. Therefore, system identification will only be used in the present thesis in stochastic scenarios.

2.2.2 Covariance-driven subspace-based OMA

OMA is conducted from the outset of unmeasured input that complies with the previously noted assumptions for w_k and v_k. Thus, Eqs. (2.19a) and (2.19b) reduce to

$$z_{k+1}^{(st.)} = A_d z_k^{(st.)} + w_k \tag{2.20a}$$

$$y_k = C_d z_k^{(st.)} + v_k \tag{2.20b}$$

in which superscript $(st.)$ denotes stochastic. Let $\mathcal{P} = \mathbb{E}(z_k^{(st.)} y_k^T)$ denote the cross-correlation between the state and the output and $R_i = \mathbb{E}(y_k y_{k-i}^T) = C_d A_d^i \mathcal{P}$ the output correlations, then

$$\mathcal{H}_{q_1+1,q_2} = \begin{bmatrix} R_0 & R_1 & \dots & R_{q_2-1} \\ R_1 & R_2 & \dots & R_{q_2} \\ \vdots & \vdots & \ddots & \vdots \\ R_{q_1} & R_{q_1+1} & \dots & R_{q_1+q_2-1} \end{bmatrix} \tag{2.21}$$

is the block Hankel matrix; with q_1 and q_2 being time lags (here, $q_2 = q_1 + 1$). The block Hankel matrix possesses the factorization property

$$\mathcal{H}_{q_1+1,q_2} = \mathcal{O}_{q_1+1} \mathcal{C}_{q_2}, \tag{2.22}$$

where

$$\mathcal{O}_{q_1+1} = \begin{bmatrix} C_d \\ C_d A_d \\ \vdots \\ C_d A_d^{q_1} \end{bmatrix} \quad \text{and} \quad \mathcal{C}_{q_2} = \begin{bmatrix} \mathcal{P} & A_d \mathcal{P} & \dots & A_d^{q_2-1} \mathcal{P} \end{bmatrix} \tag{2.23}$$

are the observability and controllability matrices. Evidently, C_d can be extracted directly as the first block-row of $\mathcal{O}_{q_1+1} \in \mathbb{R}^{(q_1+1)m_s \times n_s}$, while A_d is found from the least squares solution of

$$\mathcal{O}_{q_1+1}^{\uparrow} A_d = \mathcal{O}_{q_1+1}^{\downarrow} \tag{2.24}$$

with

$$\mathcal{O}_{q_1+1}^{\uparrow} = \begin{bmatrix} C_d \\ C_d A_d \\ \vdots \\ C_d A_d^{q_1-1} \end{bmatrix} \quad \text{and} \quad \mathcal{O}_{q_1+1}^{\downarrow} = \begin{bmatrix} C_d A_d \\ C_d A_d^2 \\ \vdots \\ C_d A_d^{q_1} \end{bmatrix}. \tag{2.25}$$

When A_d and C_d have been identified, the eigencharacteristics of the discrete system, $\{\Lambda_d, \Psi_d\}$, can, as described in Subsection 2.1.2, be derived from A_d. Subsequently, the modal parameters can be collected by use of Eqs. (2.18a) and (2.18b), where it is recalled that the last condition in Eq. (2.18b) holds only for classically damped systems.

Practical implementation

In the covariance-driven subspace identification, an estimate of $\mathcal{H}_{q_1+1,q_2}$, denoted $\hat{\mathcal{H}}_{q_1+1,q_2}$, is obtained by plugging in the empirical output correlations, that is,

$$\hat{R}_i = \frac{1}{N-i} \sum_{k=i+1}^{N} y_k y_{k-i}^{(\mathrm{ref})T} \tag{2.26}$$

with y_k^{ref} denoting the $m_0 < m_s$ reference sensors/projection channels, which are typically selected to reduce the size of the matrices in the identification. Subsequently, an estimate of the observability matrix is computed as

$$\hat{\mathcal{O}}_{q_1+1} = \hat{\mathscr{U}}_1 \hat{\Delta}_1^{1/2}, \tag{2.27}$$

where $\hat{\mathscr{U}}_1$ and $\hat{\Delta}_1^{1/2}$ are the major left singular vectors and the associated singular values of $\hat{\mathcal{H}}_{q_1+1,q_2}$. Finally, $\{\hat{A}_d, \hat{C}_d\}$ and, as such, $\{\hat{\Lambda}_d, \hat{\Psi}_d\}$ can be determined using the outlined procedure.

There are numerous reasons as to why $\{\hat{A}_d, \hat{C}_d\} \neq \{A_d, C_d\}$. As listed by Reynders et al. (2008), some of these are introduction of spurious poles, improper selection of n_s, that w_k and v_k are not truly white noise sequences, and that the structure may experience substantial non-linearity and/or non-stationarity. While some of the bias errors can be removed by use of stabilization diagrams, the variance errors can, at best, be estimated but not removed. Procedures for this estimation have been proposed by Pintelon et al. (2007) and Reynders et al. (2008) and employed in the context of damage localization by, for example, Marin et al. (2015). This path is, however, not pursued in the present thesis.

2.3 Basic principles of damage localization

In the preceding sections within this chapter, we have described a structural domain, $\mathcal{A}$, in the reference state sketched, without elements for illustrative purposes, in Fig. 2.3a. Consider now the scenario depicted in Fig. 2.3b, where $\mathcal{A}$ is introduced to some local damage in $\mathcal{A}_D$ and let $\tilde{(\circ)}$ denote a quantity in this state. Then,

$$\tilde{M}\ddot{\tilde{x}}(t) + \tilde{C}\dot{\tilde{x}}(t) + \tilde{K}\tilde{x}(t) = \tilde{B}_2\tilde{u}(t), \tag{2.28}$$

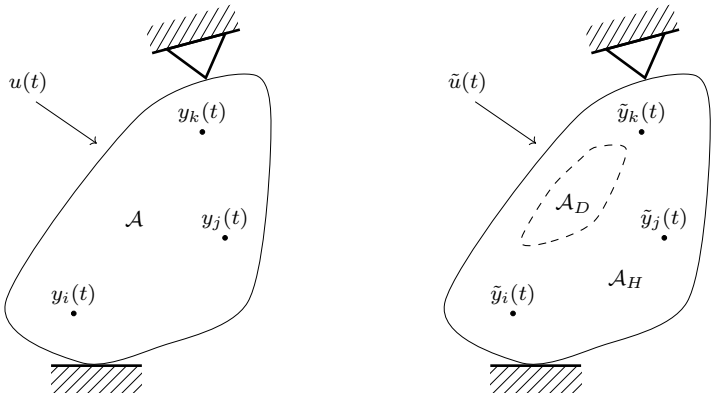

Fig. 2.3: Structural domain, $\mathcal{A}$, with output sensors ($\bullet$) measuring in (a) reference state with loading $B_2u(t)$ and (b) damaged state with perturbation in $\mathcal{A}_D$ and with loading $\tilde{B}_2\tilde{u}(t)$.

and, since damage will be emulated as either a mass or a stiffness perturbation in the numerical analyses, we also define

$$(M - \Delta M)\ddot{\tilde{x}}(t) + C\dot{\tilde{x}}(t) + K\tilde{x}(t) = \tilde{B}_2\tilde{u}(t) \tag{2.29a}$$

$$M\ddot{\tilde{x}}(t) + C\dot{\tilde{x}}(t) + (K - \Delta K)\tilde{x}(t) = \tilde{B}_2\tilde{u}(t). \tag{2.29b}$$

In Laplace domain, the generalized formulation

$$\tilde{X}(s) = \tilde{G}(s)\tilde{B}_2\tilde{U}(s) \tag{2.30}$$

is used for a damaged state with some perturbation of the system properties in the subdomain $\mathcal{A}_D$.

Now, as mentioned in Subsection 1.1.2, vibration-based damage localization is typically resolved in a setup where differences in features from the reference and damaged states are mapped—either directly or using a model—to the structural domain, $\mathcal{A}$, in order to pinpoint $\mathcal{A}_D$. The features are computed based on the output captured in m_s sensors that, according to Eq. (2.9b), is denoted $y(t)$ and contains displacements, velocities, accelerations, or some combination hereof.

2.3.1 Sensitivity to damage

To locate, or even detect, a structural damage, it obviously has to introduce a shift in (some of) the system properties. Section 2.1 outlines how an LTI system can be described fully by means of the modal parameters, and therefore it makes sense to discuss the sensitivity to damage of a structural system in the context of these parameters. As defined by, for example, Heylen et al. (1998), the sensitivities of the undamped eigenfrequencies and mass-normalized mode

shapes with respect to some parametrization of damage, $\mathscr{D}$, are given as

$$\frac{\partial \omega_i}{\partial \mathscr{D}} = \frac{1}{2}\phi_i^T \left(-\omega_i \frac{\partial M}{\partial \mathscr{D}} + \frac{1}{\omega_i}\frac{\partial K}{\partial \mathscr{D}} \right) \phi_i \tag{2.31a}$$

$$\frac{\partial \phi_i}{\partial \mathscr{D}} = -\frac{1}{2}\phi_i^T \frac{\partial M}{\partial \mathscr{D}} \phi_i \phi_i + \sum_{r \in [1,n]\setminus\{i\}} \frac{1}{\omega_i^2 - \omega_r^2} \phi_r^T \left(-\omega_i^2 \frac{\partial M}{\partial \mathscr{D}} + \frac{\partial K}{\partial \mathscr{D}} \right) \phi_i \phi_r. \tag{2.31b}$$

As noted previously, one of the roadblocks for modal parameter-based damage localization is the limited magnitudes of these sensitivities compared to the magnitudes of the sensitivities to noise and other variabilities of the modal parameter estimates. In this regard, the statement made in Section 1.3, saying that the sensor deployment is paramount in the attempt to maximize the ability to locate damage, stands obvious, as the mode shapes enter in both the sensitivity formulations in Eq. (2.31).

2.3.2 Selecting interrogation conditions

For damage localization approaches employing modal parameters, one gathers from Eq. (2.31) that the selection of eigenmodes with which the interrogation is conducted is of great importance. Furthermore, numerous model-based schemes not incorporating modal parameters operate by projection of subspaces, which are formed from realizations along $\Im(s)$. As such, the selection of frequencies at which to interrogate for the location of damage is also pivotal for these schemes.

The particular application might pose some constraints on the selection of interrogation frequencies. If, for instance, a structure is subjected to a harmonic input driving at a fixed frequency, the choice is evident. However, in cases where a band of frequencies are excited, it is advantageous to select multiple interrogation frequencies, as this will filter noise and, accordingly, increase robustness. These frequencies should, ideally, be selected such that sensitivity to any type of damage one attempts to locate is ensured.

When evaluating along $\Im(s)$, one should select locations with a certain minimum distance to the nearest pole to avoid unduly discrepancy between the actual structure and its model representation. In this context, Bernal (2010) asserts that one should generally exclude frequencies that belong to the interior of circles centered at the identified poles and having radii of $0.125\Im(\lambda_i)$, where it is recalled that λ_i is the ith pole of the reference state described by Eq. (2.1).

CHAPTER 3

Locating damage through signal-processed mode shapes

Modal parameters are utilized extensively in the context of vibration-based damage localization. Especially the mode shapes appear auspicious, as these inherently provide structural information on a local level. In this chapter, we introduce yet another mode shape-based damage localization scheme, which stands as an incremental refinement of an existing method. The new scheme, which is titled CWT-GDTKEO, uses continuous wavelet transformation (CWT) and a generalized discrete Teager-Kaiser energy operator (GDTKEO) to seek for damage-induced shifts in mode shapes. Following a dissemination in Section 3.1, the motivation for developing the CWT-GDTKEO scheme is summarized in Section 3.2. Details of CWT and the GDTKEO are outlined in Section 3.3, and subsequently, in Section 3.4, their deployment in the context of damage localization is described. A summary of the scheme is provided in Section 3.5, and in Section 3.6 an application example with a full-scale wind turbine blade is presented. Lastly, some concluding remarks are drawn in Section 3.7.

3.1 Dissemination

Parts of this chapter have been published in the following:

- Paper A by Ulriksen and Damkilde (2016).
- Paper B by Ulriksen et al. (2016).

3.2 Motivation for the CWT-GDTKEO scheme

The premise of mode shape-based damage localization is to exploit that a damage, in theory, will induce discontinuities in these signals, which, ideally, can be captured by use of some processing technique(s). Continuous wavelet transformation (CWT) has, in particular, been utilized extensively in this context, but by being based on distinguishing damage-induced discontinuities from other signal irregularities, a deficiency of this approach is the rather low robustness to measurement noise.

In order to treat the noted robustness issue, Cao et al. (2014) have proposed a scheme in which wavelet-transformed mode shapes are processed by use of the discrete Teager-Kaiser energy operator (DTKEO) to filter noise in the wavelet

transforms. Continuing along this path, the scheme introduced in this chapter, titled the CWT-GDTKEO scheme, stands as an incremental refinement of the approach by Cao et al. (2014). The refinement consists of a generalization of the DTKEO (to the GDTKEO) to further enhance robustness to noise and the implementation of a simple damage metric to ease the damage localization.

Some of the notable merits of the CWT-GDTKEO scheme are that it, in principle, can work in both deterministic (input-output) and stochastic (output-only) configurations, that it can be adopted for single- and multi-damage scenarios, and that it is data-driven and, as such, does not rely on a theoretical model of the structure in question. When it comes to shortcomings, the obvious ones include, as will be demonstrated in the application example in Section 3.6, that system identification is required (to extract the mode shapes) and that the spatial localization resolution is on sensor level. The latter implies that indications of damage are restricted to locations at which output sensors are placed.

3.3 Processing spatial mode shape signals

Let $\mathscr{Z}(\mathcal{X}) \in \mathbf{L}^2(\mathbb{R})$ be a signal-processed version of the mode shape $\phi_i \in \mathbb{R}^{m_s}$. Here, the signal processing typically consists of oversampling through cubic spline interpolation to remove discontinuities arisen due to a sparse number of measurement points, extension to remove boundary distortions, and so forth. This will be described further in the application example in Section 3.6. In Subsections 3.3.1 and 3.3.2, we outline how $\mathscr{Z}(\mathcal{X})$ is further processed by use of CWT and the GDTKEO for subsequent damage localization purposes.

3.3.1 Continuous wavelet transformation

Since the CWT-GDTKEO scheme is based on standard theory on wavelet transformation and, as such, does not contain any advancements for this, only those CWT aspects deemed most relevant for the particular purpose are presented here. For a thorough introduction to CWT, the reader is referred to any textbook on the topic; of which those by Antoine et al. (2004) and Mallat (2009) are good examples.

In analogy to the well-known Fourier transformation, the one-dimensional CWT uses inner products to measure the similarity between a spatial or temporal signal and an analyzing function. In Fourier transformation, the analyzing function is a complex exponential, whereas CWT employs a so-called wavelet function, $\gamma(\mathcal{X}) \in \mathbf{L}^2(\mathbb{R})$. A wavelet has zero mean, that is,

$$\int_{-\infty}^{\infty} \gamma(\mathcal{X})\, d\mathcal{X} = 0, \tag{3.1}$$

and is a wave-like oscillation over some interval of space (or time). In Fig. 3.1a, a particular wavelet function, namely, the fourth-order Gaussian, is depicted

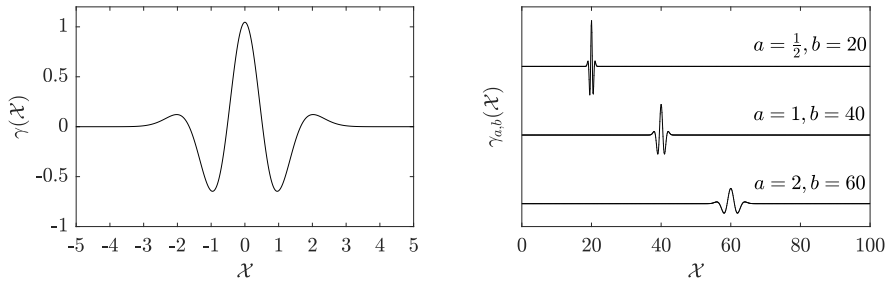

Fig. 3.1: Illustration of (a) fourth-order Gaussian wavelet and (b) some dilations and translations of it.

according to its definition as the fourth derivative of the Gaussian function (Antoine et al., 2004).

Generally, the CWT provides a transform that localizes a function in space (or time) and scaling. Let $\gamma_{a,b}(\mathcal{X}) \in \mathbf{L}^2(\mathbb{R})$ be a family of wavelets,

$$\gamma_{a,b}(\mathcal{X}) = |a|^{-\frac{1}{2}} \gamma \left(\frac{\mathcal{X} - b}{a} \right), \tag{3.2}$$

with scales $a \neq 0$ and positions $b \in \mathbb{R}$ dilating and translating the wavelet as illustrated in Fig. 3.1b. Then, the CWT of the processed mode shape signal, $\mathscr{Z}(\mathcal{X})$, is given by

$$\mathscr{T}(a, b) = \int_{-\infty}^{\infty} \mathscr{Z}(\mathcal{X}) \gamma_{a,b}^*(\mathcal{X}) \, d\mathcal{X}, \tag{3.3}$$

thus $\mathscr{T}(a, b)$ is the inner product of $\mathscr{Z}$ and $\gamma_{a,b}$, which implies that $\mathscr{T}(a, b)$ is non-negligible only if $\gamma_{a,b}$ matches $\mathscr{Z}(\mathcal{X})$.

An important property of wavelets is their number of vanishing moments, denoted m_v. Assume $r \in \mathbb{N}$, then

$$\forall r < m_v : \int_{-\infty}^{\infty} \gamma(\mathcal{X}) \mathcal{X}^r \, d\mathcal{X} = 0, \tag{3.4}$$

which states that a wavelet with m_v vanishing moments is orthogonal (or, more loosely, blind) to polynomials up to degree $m_v - 1$.

Example 3.1. To further clarify the principle and implications of vanishing moments, the piecewise function, $f(\mathcal{X})$, illustrated in Fig. 3.2a is analyzed with the Gaussian wavelet of different orders. f is zero for $\mathcal{X} \in [0, 0.25)$ and $\mathcal{X} \in (0.75, 1]$, linear for $\mathcal{X} \in [0.25, 0.5)$, and quadratic for $\mathcal{X} \in [0.5, 0.75]$. Figs. 3.2b to 3.2d show the results obtained by analyzing f with, respectively, a first-, a second-, and a third-order Gaussian wavelet.

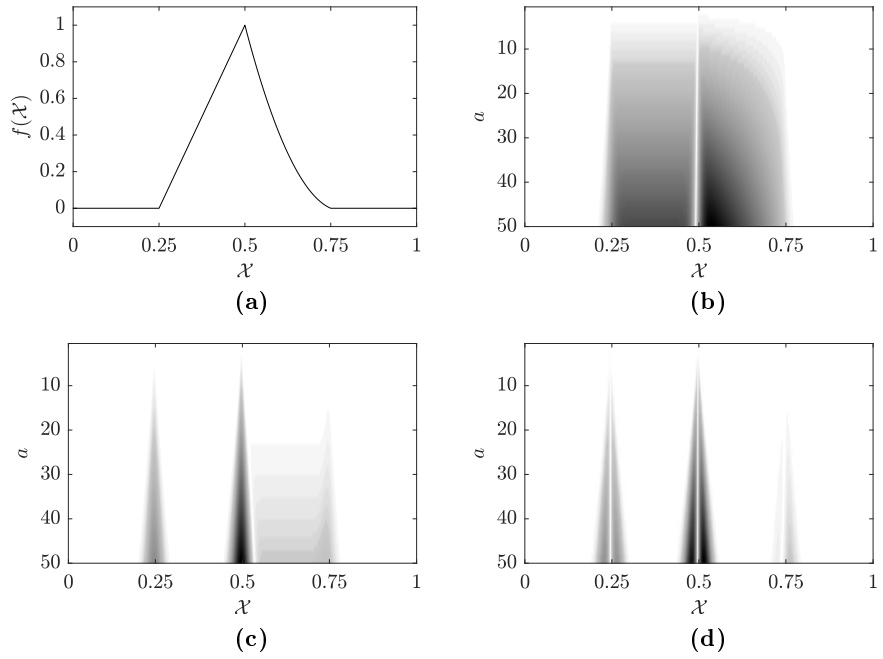

Fig. 3.2: Illustration of the concept of vanishing moments. (a) A function f. CWT of f with Gaussian wavelet of order (b) 1, (c) 2, and (d) 3.

As seen in Fig. 3.2, the first-order Gaussian wavelet, which has a single vanishing moment, is blind to the constant part of f, whereas the second-order wavelet is orthogonal to the constant and linear parts. Finally, due to its three vanishing moments, the third-order wavelet only sees the three singularities at $\mathcal{X} \in \{0.25, 0.5, 0.75\}$. □

Example 3.1, and, more particularly, Fig. 3.2d, illustrates how the CWT can be used as a signal discontinuity scanner. This has been exploited, successfully, in the context of damage localization by, for example, Douka et al. (2003), Rucka and Wilde (2006), Ulriksen et al. (2014), and Janeliukstis et al. (2017). However, as noise is added to the signal, the performance is severely reduced since the discrimination between noise and damage becomes troublesome; especially at the lower wavelet scales. For the higher scales, at which noise is better filtered, the low spatial frequency reduces the potential for capturing damage-induced signal discontinuities.

3.3.2 Teager-Kaiser operator

Since the DTKEO was proposed, originally as a discrete signal energy estimator by Kaiser (1990), it has been utilized extensively in speech processing

(Maragos et al., 1991), image processing (Maragos and Bovik, 1995), and pattern recognition (Cexus and Boudraa, 2007). In recent years, the DTKEO has been adopted to the field of damage localization by, among others, Cao et al. (2014) and Xu et al. (2015), who have applied the operator to post-damage wavelet-transformed mode shapes for damage localization in beam and plate structures.

Replacing $\mathscr{X}$ by the sequence $\{\mathcal{X}_j\}_{j=1}^{N_s}$, where N_s is the number of sample points taken in $\mathscr{X}$, the DTKEO of $\mathscr{T}$ at scale a can be found as

$$\mathscr{E}_{a,j} = \mathscr{T}_{a,j}^2 - \mathscr{T}_{a,j-1}\mathscr{T}_{a,j+1} \tag{3.5}$$

for $j \in (1, N_s)$. To appreciate the physical concept of this energy operator, we present Example 3.2 in which we, for the sake of simplicity, move from processing wavelet transforms to processing a free-vibration response of a mechanical SDOF system.

Example 3.2. This example, more or less, summarizes the operations made by Kaiser (1990) to derive the concept of Eq. (3.5). Consider the undamped eigenresponse of an SDOF system (depicted in Fig. 3.3) with eigenfrequency ω and subjected to some non-zero initial conditions. It can easily be shown that the response becomes

$$x(t) = \mathscr{A}\cos(\omega t - \mathscr{B}), \tag{3.6}$$

where $\mathscr{A}$ and $\mathscr{B}$ are the displacement amplitude and phase angle, respectively.

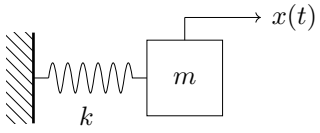

Fig. 3.3: SDOF system subjected to non-zero initial conditions.

Now, if samples $x_j = \mathscr{A}\cos(\Omega j - \mathscr{B})$ are available, replacing $\mathscr{T}_{a,j}$ in Eq. (3.5) by x_j yields

$$\mathscr{E}_j = x_j^2 - x_{j-1}x_{j+1} = \mathscr{A}^2\sin^2(\Omega), \tag{3.7}$$

and, if one assumes Ω is small, $\mathscr{E}_j \approx \mathscr{A}^2\Omega^2$. Recalling that the mechanical energy in the SDOF system in Fig. 3.3 is given by

$$E_{\text{mek}} = \frac{1}{2}m\mathscr{A}^2\omega^2 \propto \mathscr{A}^2\omega^2, \tag{3.8}$$

the justification of the energy operator term in DTKEO is clear. □

As previously noted, the DTKEO has been applied to wavelet-transformed mode shapes for damage localization purposes by Cao et al. (2014) and Xu et al. (2015); with the aim of magnifying the damage-induced singularities. In

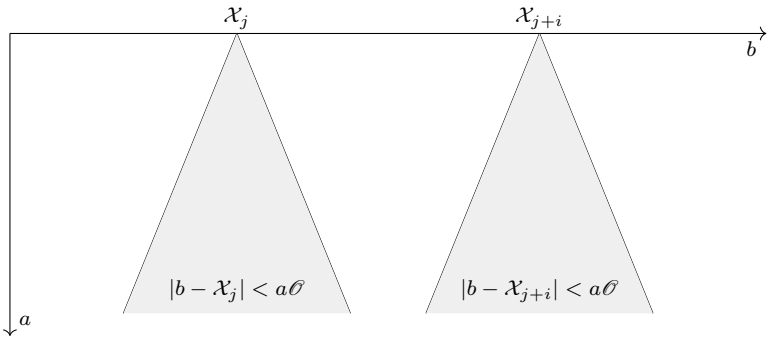

Fig. 3.4: Cone of influences for CWTs evaluated at $\mathcal{X}_j$ and $\mathcal{X}_{j+i}$.

the CWT-GDTKEO scheme, we generalize Eq. (3.5) to the GDTKEO

$$\mathcal{E}_{a,j,\varrho} = \mathscr{T}_{a,j}^2 - \mathscr{T}_{a,j-\varrho}\mathscr{T}_{a,j+\varrho}, \quad j \in (\varrho, N_s - \varrho], \tag{3.9}$$

by introduction of the lag parameter $\varrho \in \mathbb{N}$. This parameter serves to further alleviate the adverse noise effects and should, in general, be chosen on the basis of signal characteristics such as number of sample points and noise conditions. A simple approach for selecting ϱ is to use the well-known modal assurance criterion (MAC) proposed by Allemang and Brown (1982). More specifically, $\mathcal{E}_{a,\varrho}$ is calculated for $a = \max(a)$ and different ϱ-values. Then, the MAC-value between the signals with ϱ and $\varrho + 1$ is calculated in accordance with

$$\mathrm{MAC}_\varrho = \frac{\left(\mathcal{E}^T_{\max(a),\varrho}\mathcal{E}_{\max(a),\varrho+1}\right)^2}{\mathcal{E}^T_{\max(a),\varrho}\mathcal{E}_{\max(a),\varrho}\mathcal{E}^T_{\max(a),\varrho+1}\mathcal{E}_{\max(a),\varrho+1}} \in [0,1], \tag{3.10}$$

and ϱ is chosen as the value at which MAC_ϱ exceeds some threshold, Θ, that has been defined a priori. An upper bound for ϱ is given from the cone of influence, which, as illustrated in Fig. 3.4, is the set of all $\mathcal{X}$ included in the effective support[1], $[b - a\mathscr{O}, b + a\mathscr{O}]$, of the wavelet at particular values of a and b. In other words, for a given b, the cone of influence encompasses the CWT coefficients affected by the signal value at that point. Thus, if one applies the GDTKEO with the aim of gaining insight into the transform at $\mathcal{X}_j$ and $\mathcal{X}_{j+i}$, ϱ is bounded above to prevent disturbances between the cone of influences.

3.4 Locating damage in processed mode shapes

For the purpose of damage localization, CWT is applied to scan the spatial mode shape signal(s) for discontinuities, and, subsequently, the GDTKEO serves to facilitate clear distinction between damage- and noise-induced dis-

[1] The support of γ is the set of points in $\mathcal{X}$ for which $\gamma(\mathcal{X}) \neq 0$

continuities. When choosing what wavelet to use, the concept of vanishing moments comes into play, as the ability to capture any abrupt shift in the signal depends on the regularity of the analyzing wavelet. Here, regularity is related to the number of continuous derivatives a function has and, accordingly, the number of vanishing moments. As the number of vanishing moments increases, so does the ability to capture discontinuities; including those *not* associated with damage (such as noise and/or border distortions). Thus, there is a certain maximum for the operable amount of vanishing moments, which can be determined based on the signal-processed mode shapes in the reference state. A thorough discussion on the topic of selecting wavelets for damage localization has been provided by Rucka (2011).

When the mode shape signals have been processed using CWT and the GDTKEO, a decision must be made as to the damage location. If multiple measurements are conducted in the reference state, or if the uncertainties associated with estimating the mode shapes are stored, the localization should, as demonstrated in Paper A by Ulriksen and Damkilde (2016), be done in a statistical framework. If only one realization of modal parameters is available for each structural state (reference and damaged), we simply compute the discordance between transformed pre- and post-damage mode shapes through the ℓ_2-norm of the residuals,

$$\mathcal{J}_l = \sqrt{\sum_{i=1}^{N} \left(\tilde{\mathcal{E}}_{l,\varrho}(\omega_i) - \mathcal{E}_{l,\varrho}(\omega_i) \right)^2}, \tag{3.11}$$

where N modes (each associated with an eigenfrequency, ω_i) are evaluated in m_s sensor DOF. Damage is, as such, attained at/near sensor DOF k if $\forall l \neq k : \mathcal{J}_k > \mathcal{J}_l$. Additionally, it is worth noting that other sensor DOF locations at which $\mathcal{J}_l$ is high (relative to the general tendency) can be regarded as damaged. However, for a robust and explicit selection of damaged areas in such scenarios, a statistical approach should be implemented.

3.5 Summary of the CWT-GDTKEO scheme

1. Extract the spatial mode shape signal, ϕ_i.
2. Smooth ϕ_i to avoid/reduce sampling-related singularities. The smoothing can be done using cubic splines.
3. Extend the smoothed mode shape signal to avoid/reduce border distortions by use of, for example, the isomorphism approach (Messina, 2008).
4. Select a wavelet function (following the discussion in Section 3.4) and calculate the wavelet transform from Eq. (3.3).
5. Apply the GDTKEO in accordance to Eq. (3.9), with a lag parameter, ϱ, chosen as described in Subsection 3.3.2.

6. If possible, repeat steps 1 to 5 for other modes to increase the robustness.
7. Compute $\mathcal{J} = [\mathcal{J}_1 \ \mathcal{J}_2 \ \ldots \ \mathcal{J}_{m_s}]$ using Eq. (3.11) with the results for $N \geq 1$ mode(s).
8. Declare damage at/near sensor DOF k if $\forall l \neq k : \mathcal{J}_k > \mathcal{J}_l$. If multiple damages are sought for, a statistical procedure is required.

3.6 Application example

In Paper A by Ulriksen and Damkilde (2016), the applicability of the CWT-GDTKEO scheme has been tested, successfully, in the context of a numerical study of a beam and experiments with a residential-sized wind turbine blade. These examples demonstrate the basic principles of the scheme, including the robustness gained by using the GDTKEO instead of the DTKEO, so in the present section, we will address a more advanced example; namely, the SSP 34-m wind turbine blade seen mounted on an indoor test rig in Fig. 3.5.

(a)

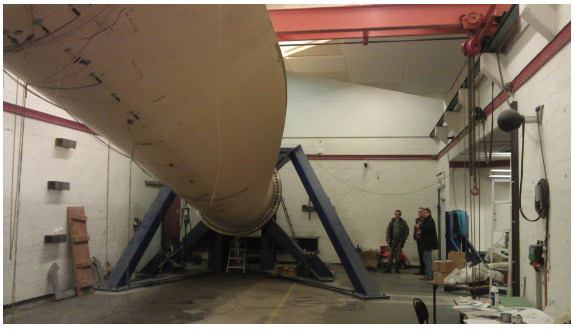

(b)

Fig. 3.5: SSP 34-m blade on test rig in (a) root-to-tip view and (b) tip-to-root view.

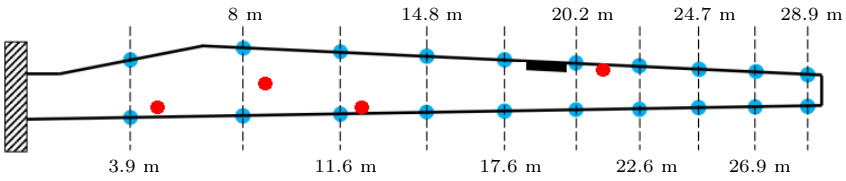

Fig. 3.6: Inputs sources (●), output sensors (●), and damage (■) along the SSP 34-m blade.

The SSP 34-m blade, which is made from epoxy fiberglass and has a length and mass of, respectively, 34 m and 4,600 kg, is analyzed in the reference state and a damaged one with a 1.2 m trailing edge debonding, whose location is illustrated in Fig. 3.6. In both states, the blade is excited by several people hitting it, around the positions highlighted in Fig. 3.6, with heavy wooden sticks wrapped in foam. This excitation type is chosen in order to resemble the conditions required when conducting OMA, namely, as stated in Subsection 1.2.1, that the input is distributed randomly both temporally and spatially.

The measurement system consists of 20 triaxial accelerometers (B&K type 4524-B) mounted on the leading and the trailing edge at ten stations along the blade, see Fig. 3.6. Data from the accelerometers are recorded during approximately seven minutes (corresponding to at least 500 oscillations at the lowest frequency of interest) through five 12-channel B&K LAN-XI data acquisition modules of type 3053-B-120. In each of the two structural states, four measurement sequences are conducted.

3.6.1 System identification

The modal parameters of the blade in both structural states are estimated using the stochastic subspace identification algorithm described in Section 2.2.

Table 3.1: 95 % confidence intervals for estimated eigenfrequencies, ω_i, and damping ratios, ζ_i, of the SSP 34-m blade. Here, FW=flapwise, EW=edgewise, and TO=torsion.

	Reference state		Damaged state	
Mode	$\frac{\omega_i}{2\pi}$ (Hz)	ζ_i (%)	$\frac{\tilde{\omega}_i}{2\pi}$ (Hz)	$\tilde{\zeta}_i$ (%)
1st FW	1.36 ± 0.01	0.99 ± 0.42	1.35 ± 0.01	0.64 ± 0.69
1st EW	1.86 ± 0.01	0.76 ± 0.14	1.86 ± 0.01	0.62 ± 0.27
2nd FW	4.21 ± 0.00	0.19 ± 0.08	4.21 ± 0.01	0.26 ± 0.10
2nd EW	7.12 ± 0.00	0.30 ± 0.08	7.12 ± 0.01	0.32 ± 0.06
3rd FW	9.19 ± 0.06	1.32 ± 0.21	9.17 ± 0.01	1.07 ± 0.20
1st TO	12.40 ± 0.02	0.53 ± 0.06	12.37 ± 0.01	0.55 ± 0.14
3rd EW/4th FW	14.16 ± 0.10	1.18 ± 0.50	14.19 ± 0.06	1.11 ± 0.06
4th FW/3rd EW	14.99 ± 0.01	0.55 ± 0.07	14.98 ± 0.01	0.61 ± 0.06

In all the eight measurement sequences (four per structural state), the eight lowest eigenmodes have been identified, and in Tb. 3.1 the eigenfrequencies and damping ratios are listed with their 95 % confidence intervals. Here, it is noted that, with reference to Fig. 3.6, edgewise is in-plane and flapwise is out-of-plane, and the seventh and eighth modes are, as such, combinations of edge- and flapwise bending modes. As can be deduced from Tb. 3.1, the introduction of the 1.2 m long trailing edge debonding does not cause a consistent, significant shift in any of the identified eigenfrequencies or damping ratios.

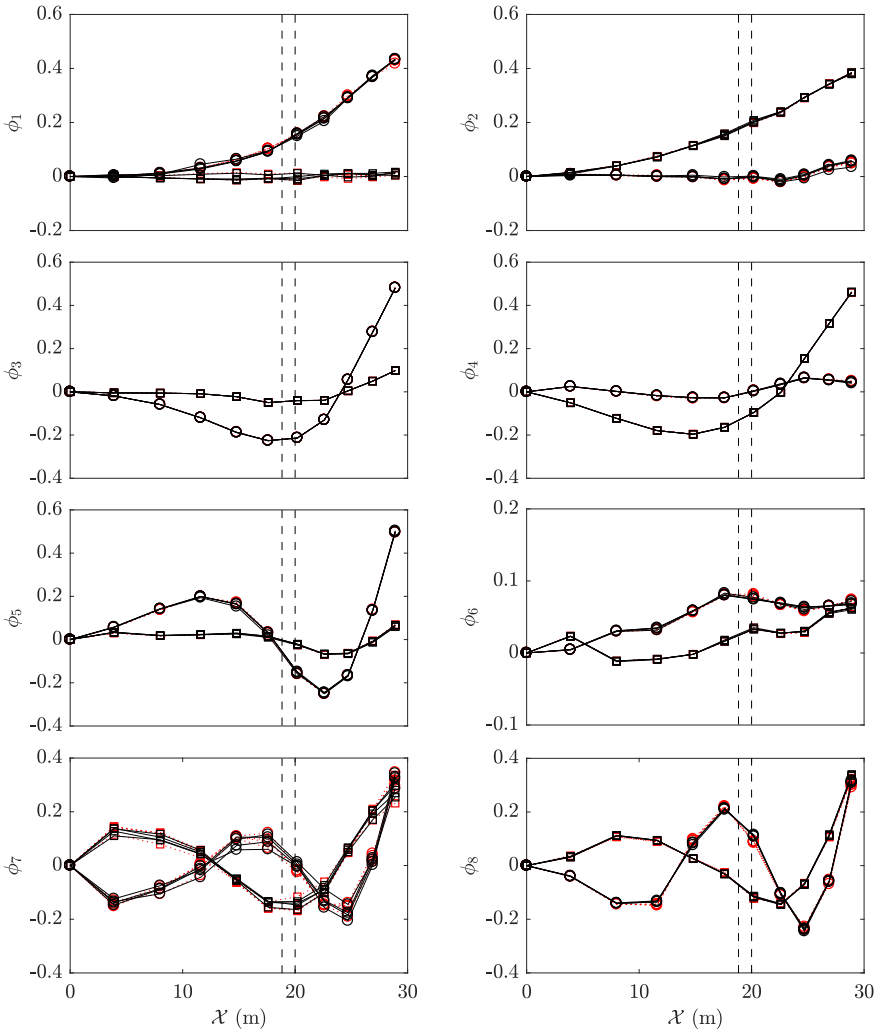

Fig. 3.7: Flapwise (○) and edgewise (□) components of the first eight mode shapes of the SSP 34-m blade in reference (—) and damaged (···) state. Damage is located at $\mathcal{X} \in [18.8, 20]$.

The identified mode shapes are sketched in Fig. 3.7, with each modal displacement value taken as a combination of the extracted values at the same radial coordinate of the blade, see Fig. 3.6. In this way, the sketched bending modes represent the mean of these pairs, while the torsion mode, as described further by Larsen et al. (2014), is found solely from the flapwise components. By close inspection, it becomes clear that direct comparisons of the mode shapes—for example, through the coordinate modal assurance criterion (COMAC) proposed by Lieven and Ewins (1988)—do not provide consistent information on the actual location of the damage.

3.6.2 Localization results

The CWT-GDTKEO scheme is applied to the flapwise components[2] of the mode shapes presented in Fig. 3.7 in the attempt to locate the trailing edge debonding at $\mathcal{X} \in [18.8, 20]$. Each mode shape is smoothed using cubic spline interpolation with a spatial sample increment of 0.1 m, and, subsequently, the isomorphism approach by Messina (2008) is implemented to extend the mode shape signals to shift the boundary distortions outside the physical domain, $\mathcal{X}$.

Based on the processed mode shapes signals in the reference state, it has been chosen to conduct the CWT using the Gaussian fourth-order wavelet depicted in Fig. 3.1, as it is the highest order of wavelet functions not yielding severe boundary distortion within $\mathcal{X}$. Subsequently, the procedure outlined in Subsection 3.3.2 is employed to select the lag parameter, ϱ, in the GDTKEO. Here, the threshold is set, rather heuristically, to $\Theta = 0.99$, which yields $\varrho = 3$.

With the selected settings, and if all $N = 8$ modes are used in Eq. (3.11), the CWT-GDTKEO scheme provides the results shown in Fig. 3.8a. The results are for one measurement sequence from the reference state and one from the damaged, and we see that the damage is correctly localized. In this context,

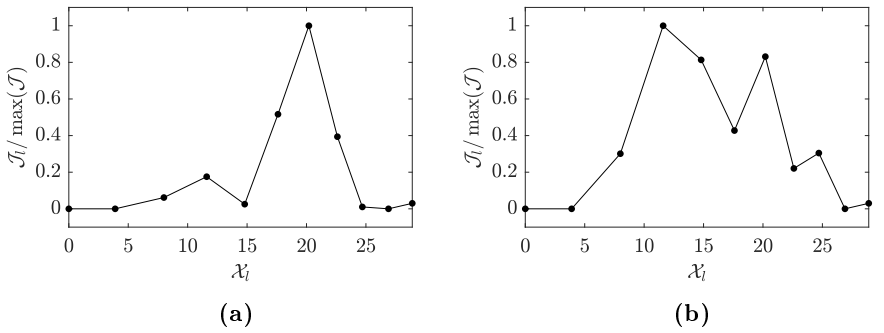

Fig. 3.8: Localization of damage at $\mathcal{X} \in [18.8, 20]$ in SSP-34m blade using the CWT-GDTKEO scheme with $\varrho = 3$ and (a) $N = 8$ and (b) $N = 6$ (first six modes).

[2] Preliminary studies have shown that the damage cannot be localized using the edgewise mode shape components.

it is worth stating that similar results are obtained for all combinations of reference- and damaged-state sequences. If we, instead of using all eight modes, only process the first $N = 6$, the results depicted in Fig. 3.8b are obtained. Under these conditions, the CWT-GDTKEO scheme evidently fails to locate the damage, which is a direct consequence of the insufficient information on the damage contained in the mode shape estimates for the first six modes.

3.7 Concluding remarks

This chapter has been dedicated to the parametric CWT-GDTKEO scheme, whose methodological premise is to seek for damage-induced changes in signal-processed mode shapes of the structure in question. More particularly, the scheme incorporates CWT and a GDTKEO to capture these changes, and the discrimination between undamaged and damaged locations is obtained using a simple metric comparing signals from the states prior and posterior to damage. As such, the CWT-GDTKEO scheme is an incremental refinement—cast to increase robustness to noise—of an existing method.

The applicability of the proposed scheme has been examined in the context of experimental work with a 34 m long wind turbine blade introduced to a 1.2 m trailing edge debonding. It is found that the damage can be located using the CWT-GDTKEO scheme if all the identified blade modes is treated, which clearly points out the issue related to using system identification in the context of damage localization. Namely, even in the controlled laboratory conditions explored in the example, the damage-induced shifts in the modal parameters of the lower modes are generally camouflaged by the uncertainties associated with the parameter estimation. Only by inspecting higher modes, in this setting the seventh and eighth, we are able to capture the damage-induced shift in the mode shapes. Since excitation of such high modes typically requires an external input source, the previous claim of the scheme being generally operable in output-only scenarios is questionable. It seems reasonable to conclude that the CWT-GDTKEO scheme, in general practice, merely applies to deterministic scenarios, in which the input can be tailored to excite higher modes. As such, the argument made in Subsection 2.2.1 is recalled; namely, that if the input is known, the best approach in terms of damage localization will be to circumvent system identification.

CHAPTER 4

Model-based subspace projections for damage localization

The observations made in the previous chapter call for exploration of non-parametric approaches for damage localization. This chapter presents the model-based Subspace Exclusion Zone (SEZ) damage localization scheme, which operates in a forward and, under certain input conditions, non-parametric procedure. The methodological premise is to form subspaces indexed by model-based postulated boundaries, so-called exclusion zones (EZs), and then declare damage within the particular EZ with which a reconstruction of the damage-induced response shifts is possible. After a dissemination in Section 4.1, the chapter proceeds by providing the reasoning behind introducing the SEZ scheme. This is done in Section 4.2, and then the physical principle of EZs is described in Section 4.3. Subsequently, the implementation of EZs for damage localization is outlined in Section 4.4, followed by a brief summary of the scheme in Section 4.5. The chapter ends with numerical and experimental application examples in Section 4.6 and conclusions in Section 4.7.

4.1 Dissemination

Parts of this chapter have been published in the following:

- Paper C by Bernal and Ulriksen (2017).
- Paper D by Ulriksen et al. (2017).

4.2 Motivation for the SEZ scheme

The application example in Section 3.6 emphasizes the issue of compressing vibration data into a modal model while preserving sufficient information on the damage. Motivated by this, Bernal and Kunwar (2016) have developed the S3DL scheme, which operates in a non-parametric configuration if certain input conditions are complied with. With reference to Eqs. (2.29a) and (2.29b), these conditions are $\tilde{B}_2 = B_2$ and $\tilde{u} \propto u$; with the latter being guaranteed in Laplace domain for single-source excitation.

As described in Subsection 1.2.1, the premise of the S3DL scheme is to compare an experimental feature to model-based analytical subspaces and declare damage based on orthogonality (or parallelism) between the subspaces and the

feature. Since each analytical subspace is derived by postulating a specific damage pattern in a model of the reference structure, the structural interrogation rests on an assumption of the nature of the damage. More specifically, a decision has to be made a priori as to whether a stiffness- or mass-related damage is to be located. This is exemplified in Example 4.1.

Example 4.1. Fig. 4.1a depicts a cantilever beam, which has a length of L and is assigned a material model corresponding to typical structural steel. A damaged state is formed by smearing extra mass across the fourth element in the FE model, and in both structural states the single-source excitation, $F(s)$, acts. Since the example is treated analytically, the further nature of the input is without relevance.

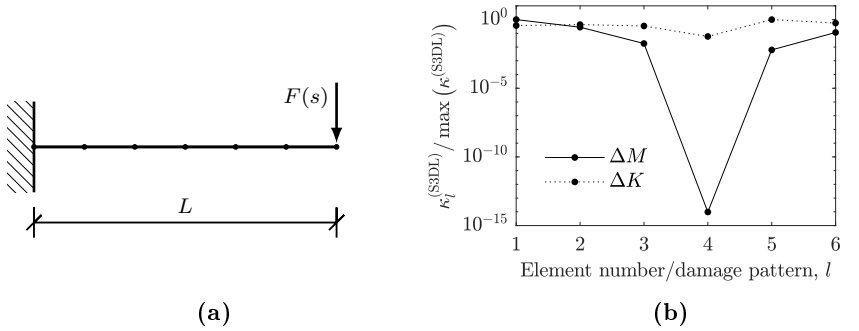

Fig. 4.1: Locating mass added to element 4 of a cantilever beam model. (a) Beam model with boundary conditions. (b) Localization results obtained by postulating element-wise mass (ΔM) and stiffness (ΔK) damages in the S3DL scheme.

Now, if the S3DL scheme is implemented with damage patterns corresponding to mass perturbations across entire elements, it is seen in Fig. 4.1b how the scheme works as intended, as $\kappa_l^{\mathrm{S3DL}} = 0$ indicates damage. However, if damage is postulated as being stiffness-related, the scheme evidently fails to provide localization. □

In practice, one can obviously choose to carry out interrogations separately for the two damage types using the S3DL scheme, but since it operates in a forward procedure, this can quickly become too time-consuming for large structures and structural systems. We therefore introduce the SEZ scheme as an alternative that, compared to the S3DL scheme, distinguishes itself by operating without the requirement of explicit discrimination between stiffness- and mass-related damages. Besides this clear distinction, the two schemes are almost identical in the way they operate. In the SEZ platform, so-called exclusion zones (EZs) of user-defined sizes are used as "damage patterns" to interrogate for damage. In this way, information on size and type of the damage is precluded, hereby providing a net robustness gain. Also worth noting are the facts that no inverse problem is solved (hence ensuring scalability) and that arbitrary non-linear behavior in the damaged region fits within the theory.

4.3 Exclusion zones

Generally, an EZ is any closed region (not necessarily simply connected) within a domain. As such, an arbitrary field quantity outside the boundary of an EZ can be reconstructed by removing the interior of the EZ and adding stress fields on the noted boundary. The principle is demonstrated in Example 4.2.

Example 4.2. To appreciate the principle of EZs and, more particularly, the reconstruction of a field quantity outside an EZ, consider the fixed-fixed linear Euler-Bernoulli beam system illustrated in Fig. 4.2a. The beam is partitioned into three subdomains, namely, $\mathcal{A}_1$, $\mathcal{A}_2$, and $\mathcal{A}_3$, of which the second is now taken as an EZ. This yields the configurations sketched in Fig. 4.2b, where the resulting forces and moments have been applied to ensure static equilibrium.

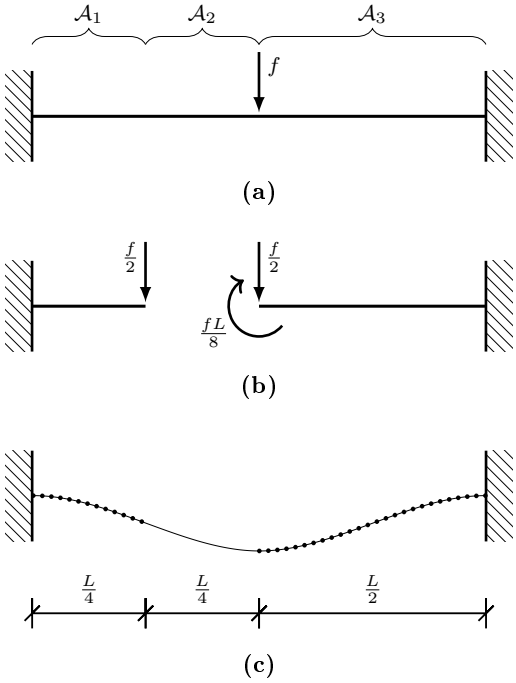

Fig. 4.2: Static beam system. (a) Full system with three subdomains, $\mathcal{A}_i$. (b) $\mathcal{A}_2$ taken as an EZ (with the bending moment being zero at the free end of $\mathcal{A}_1$ according to the full system). (c) Displacement fields for the full (—) and reconstructed (•) systems.

Using a standard way of determining the displacement fields for the systems in Figs. 4.2a and 4.2b, the results in Fig. 4.2c are obtained. Clearly, the displacement field outside the EZ has been reconstructed by removing the EZ interior and adding "stresses" to the boundary. For more information on how to compute displacement fields, the reader is referred to any textbook on beam mechanics; of which that by Krenk and Høgsberg (2013) is an example. □

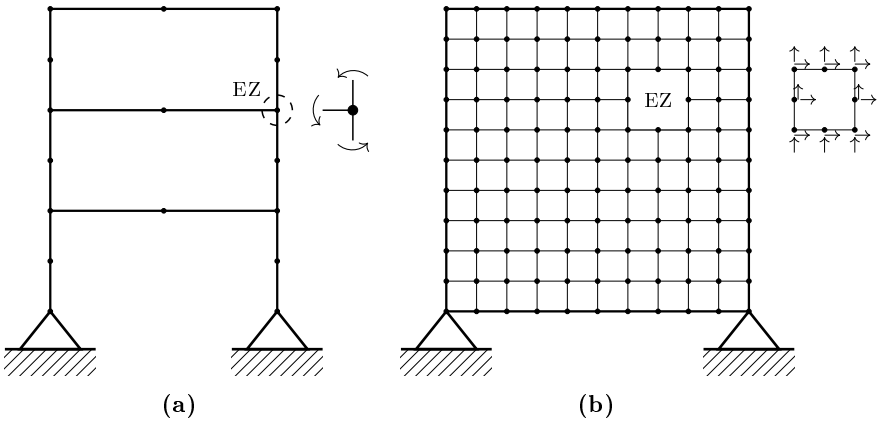

Fig. 4.3: EZ composed of (a) decoupling rotational DOF in adjacent beam elements and (b) void with translational DOF on its boundary.

While the system treated in Example 4.2 is extremely simple, it is obvious that the EZ principle is general for linear (and, in a dynamic context, time-invariant) systems. Other examples can be seen in Fig. 4.3, where an EZ is taken as, respectively, the decoupling of rotational DOF in an FE frame model (Fig. 4.3a) and a void within a two-dimensional FE model formulated using first-order quadrilateral elements (Fig. 4.3b).

4.4 Locating damage using exclusion zones

Thus far, the EZ discussion has been focusing on reconstructing an absolute field quantity. In the present section, we show how this principle adapts to reconstructing *shifts* in field quantities using the SEZ damage localization scheme.

Now, if the structural domain $\mathcal{A}$ is introduced to a damage that yields some system perturbation, it follows directly from Eq. (2.30) that

$$\tilde{X}(s) = \tilde{G}(s)B_2U(s), \tag{4.1}$$

as it, temporarily, is assumed that the loading is the same in the damaged state and the reference one. This perturbed configuration is depicted in Fig. 4.4a, where the domain is partitioned such $\mathcal{A} = \mathcal{A}_H \cup \mathcal{A}_D$. $\mathcal{A}_H$ and $\mathcal{A}_D$ are, respectively, the healthy subdomain and the subdomain containing the damage, hence implying that $\mathcal{A}_D$ is unperturbed in the reference state seen in Fig. 4.4b.

Theorem 4.1. *Let the domain $\mathcal{A} = \mathcal{A}_H \cup \mathcal{A}_D$ be excited by $B_2U(s)$ in both the reference state and a damaged one with some change in $\mathcal{A}_D$. Let the boundary between $\mathcal{A}_H$ and $\mathcal{A}_D$ be denoted by Γ, which is discretized to n_Γ DOF. Then, a change in any field quantity observed at m_s locations in $\mathcal{A}_H$ can be generated from n_Γ linearly independent stress fields acting on Γ if $m_s > n_\Gamma$.*

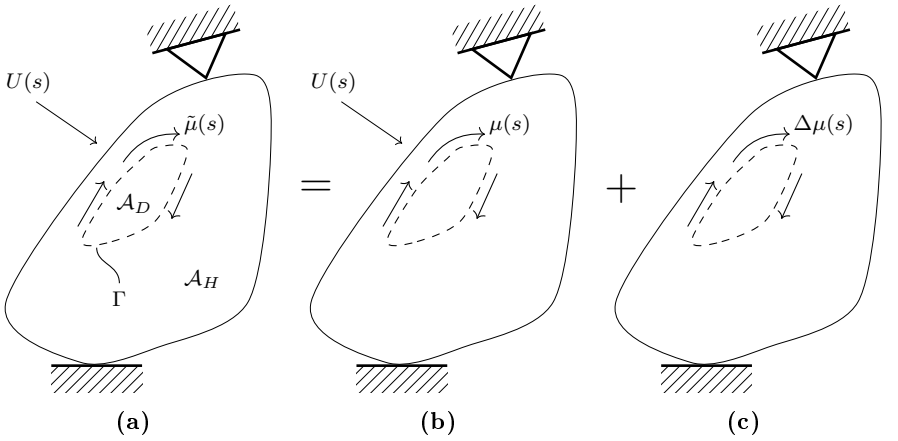

Fig. 4.4: Domain $\mathcal{A}$ subjected to loading $B_2U(s)$, with (a) showing the perturbed state, (b) the reference state, and (c) the difference between the two states.

Proof. With $\mu(s)$ and $\tilde{\mu}(s)$ denoting the linearly independent stress fields acting on Γ in, respectively, the reference state and the damaged one, then $\tilde{\mu}(s) = \mu(s) + (\tilde{\mu}(s) - \mu(s)) = \mu(s) + \Delta\mu(s)$. Define $\Delta Y(s) = \tilde{Y}(s) - Y(s)$, where $Y(s)$ is the Laplace transform of the temporal output as defined in Eq. (2.10b), and assume linearity in $\mathcal{A}_H$ from which m_s realizations of $\Delta Y(s) = \tilde{Y}(s) - Y(s)$ are captured for $\tilde{B}_2\tilde{U}(s) = B_2U(s)$. Given $m_s > n_\Gamma$, it follows directly from Fig. 4.4 that $\exists f : \Delta\mu(s) \mapsto \Delta Y(s)$. □

Remark 4.1. *A condition for Theorem 4.1 to hold is that $\mathcal{A}_H$ is linear in both states. $\mathcal{A}_D$ can, however, contain any non-linearity in the damaged state.*

Remark 4.2. *Note that Γ does not need to be the boundary of $\mathcal{A}_D$. As long as Γ encompasses a region in which $\mathcal{A}_D$ is fully contained, Theorem 4.1 holds. For the sake of simplicity, the acting stress field is still denoted $\Delta\mu(s)$.*

Remark 4.2 points to a central feature of the SEZ scheme, namely, that it operates with user-defined EZs in the interrogation. The premise is to locate damage by reconstructing the observed field quantity shifts using a model of the structure, in which the EZs are cast one at a time. The approach, therefore, does not point directly to the location of damage, but rather allows one to test whether it is in the interior of any cast EZ. From Fig. 4.4, it is evident that the reconstruction is possible when the implemented EZ encompasses the damage.

4.4.1 Reconstructing field quantity shifts

The actual stress field acting on Γ is generally unknown and will therefore not be used explicitly for reconstruction purposes. Instead, we define

$$\mathcal{W}(s)\Delta\mu(s) = \Delta Y(s), \tag{4.2}$$

where $\mathcal{W}(s) \in \mathbb{C}^{m_s \times n_\Gamma}$, with $m_s > n_\Gamma$, is a basis for all the possible differences in the observed field derived from n_Γ linearly independent stress fields on Γ.

The premise of the SEZ scheme is to compute the matrix $\mathcal{W}(s)$ for one EZ at a time in an analytical model of the structure in its reference state and then compare this to the observed shifts, $\Delta Y(s)$. Assume that the lth EZ is implemented and let $\beta_l(s)$ denote the stress pattern on the boundary of this EZ. Since $\operatorname{rank}\big(\mathcal{W}_l(s)\big) = n_{\Gamma_l}$, there exists a pseudo-inverse

$$\mathcal{W}_l^\dagger(s) = \big(\mathcal{W}_l^T(s)\mathcal{W}_l(s)\big)^{-1}\mathcal{W}_l^T(s) \tag{4.3}$$

such that the least squares solution to Eq. (4.2) for EZ l is

$$\hat{\beta}_l(s) = \underset{\beta_l(s)}{\operatorname{argmin}} \left\|\mathcal{W}_l(s)\beta_l(s) - \Delta Y(s)\right\|^2 = \mathcal{W}_l^\dagger(s)\Delta Y(s), \tag{4.4}$$

which will yield a residual

$$\epsilon_l(s) = \Big(I - \mathcal{W}_l(s)\mathcal{W}_l^\dagger(s)\Big)\,\Delta Y(s) \tag{4.5}$$

that, for $\Delta Y(s) \neq 0$ and under ideal conditions, will be a zero vector if and only if the correct EZ is postulated. Here, *correct* adheres to Remark 4.2 and implies that the interior of the specific EZ contains the structural damage. So, if k is assumed to be the correct one, we get

$$\Delta Y(s) \in \mathcal{R}\big(\mathcal{W}_k(s)\big), \tag{4.6}$$

where $\mathcal{R}$ denotes range, which, accordingly, implies rank deficiency of the matrix $\big[\mathcal{W}_k(s) \;\; \Delta Y(s)\big]$.

4.4.2 The analytical subspace

With reference to Eqs. (4.4) and (4.5), the experimental feature is, of course, fixed throughout the structural interrogation, so the operation with this is merely restricted to estimating it and subsequently treating it as a constant. The analytical subspace for each implemented EZ must be populated by theoretical quantities computed using a linear (and, in a dynamic context, time-invariant) model of the structure in its reference state. Since the content of the analytical subspace depends on whether the context is static or dynamic, we treat these scenarios separately in the following. For notational convenience, we skip the explicit reference to the lth EZ.

Static context

If the interrogation is conducted in a static context, that is, $s = 0$, and there are no probing loads in the interior of $\mathcal{A}_D$, the constraint of $m_s > n_\Gamma$ can be relaxed to $m_s + m_c > n_\Gamma$, where m_c is the number of static equilibrium conditions. Define $\mathscr{W}^T = \big[\mathcal{W}^T \;\; \Xi^T\big] \in \mathbb{R}^{n_\Gamma \times (m_s + m_c)}$ and $\theta^T = \big[\Delta Y^T \;\; 0\big] \in \mathbb{R}^{1 \times (m_s + m_c)}$,

where $\Xi \in \mathbb{R}^{m_c \times n_\Gamma}$ and $0 \in \mathbb{R}^{1 \times m_c}$ express the static constraints for the EZ. Then, the residual in Eq. (4.5) is expanded to

$$\epsilon = \left(I - \mathscr{W}\mathscr{W}^\dagger\right)\theta, \tag{4.7}$$

where $\mathcal{W}$ is determined from static analyses with n_Γ linearly independent stress fields acting on the boundary of the EZ in an n_0-DOF model with a stiffness matrix, $\mathscr{K} \in \mathbb{R}^{n_0 \times n_0}$, incorporating the EZ.

Dynamic context

The dynamic extension of the static context follows by operating at $s \neq 0$ and, of course, without static constraints, thus $m_s > n_\Gamma$ must be imposed. If the damping is assumed classically distributed, which is not required but allows for efficiency in the approach, the receptance matrix for the model implementing a particular EZ can be expressed as

$$\mathscr{G}(s) = \left(\mathscr{M}s^2 + \mathscr{C}s + \mathscr{K}\right)^{-1} = \sum_{i=1}^{n_0} \frac{\bar{\phi}_i \bar{\phi}_i^T}{s^2 + 2\bar{\zeta}_i\bar{\omega}_i s + \bar{\omega}_i^2}, \tag{4.8}$$

where $\bar{\omega}_i$, $\bar{\zeta}_i$, and $\bar{\phi}_i$ are the eigenfrequency, damping ratio, and mass-normalized eigenvector of the ith mode in the n_0-DOF system with mass, damping, and stiffness matrices, $\mathscr{M}$, $\mathscr{C}$, $\mathscr{K} \in \mathbb{R}^{n_0 \times n_0}$, that all incorporate the EZ.

Define, for all $h \in [1, n_\Gamma]$, a load vector, $\mathscr{F}^{(h)}(s) \in \mathbb{C}^{n_0}$, that holds only one non-zero entry, located at DOF $\mathcal{T}_h$, and define the resulting steady-state displacement response as $\mathscr{X}^{(h)}(s) \in \mathbb{C}^{m_s}$. If $\mathcal{Y}$ contains the indexes of the m_s measurement DOF, one finds

$$\mathscr{X}^{(h)}(s) = \mathscr{G}_{\mathcal{Y}\bullet}(s)\mathscr{F}^{(h)}(s) = \sum_{i=1}^{n_0} \frac{\bar{\phi}_{\mathcal{Y}i}\bar{\phi}_{\mathcal{T}_h i}}{s^2 + 2\bar{\zeta}_i\bar{\omega}_i s + \bar{\omega}_i^2} \mathscr{F}^{(h)}_{\mathcal{T}_h}(s) \tag{4.9}$$

from which steady-state velocities, accelerations, and strains can, if required, be computed; with the last one as a linear map of the displacements. In this way, the hth column in the interrogation matrix, $\mathcal{W}(s)$, is composed of $\mathscr{X}^{(h)}(s)$ or some spatial or temporal derivative hereof.

4.4.3 Structural interrogation

Assume that the system change is due to structural damage and let, as previously, the kth EZ be the correct one; in the sense that it fully contains the damage. Hereby, we find, under ideal conditions and with reference to Eq. (4.5), that $\epsilon_k \equiv 0$, which implies that the singular value

$$\sigma_k = \sqrt{\epsilon_k^T(s)\epsilon_k(s)} \tag{4.10}$$

will be zero. Obviously, this will not be the case in real applications where different discrepancies will arise. The effects of these in the context of operating

with the SEZ scheme will be treated in the following.

Handling load discrepancy between the experimental states

In real applications, there may be a pronounced discrepancy between the inputs during the experimental campaign in the different structural states, hence precluding the use of $\Delta Y(s)$ in a non-parametric context. In those cases where there is proportionality between the loading in the different states, which, for instance, is always the case in the Laplace domain when the excitation is a single source kept spatially fixed, the SEZ scheme can still operate non-parametrically if the experimental feature is taken as $\left[\tilde{Y}(s)\ Y(s)\right]$.

Proposition 4.1. *Let $B_2 \in \mathbb{R}^{n\times p}$ be the input distribution matrix for $U(s)$, $\tilde{U}(s) \in \mathbb{C}^p$, which are the Laplace domain input histories in, respectively, the reference state and the damaged one. If $p = 1$ and $\tilde{U}(s) \neq U(s)$, replacing $\Delta Y(s)$ by $\left[\tilde{Y}(s)\ \ Y(s)\right]$ will, with reference to Eq. (4.5), yield a residual $\epsilon_k(s) \in \mathbb{C}^{m_s\times 2}$, whose smallest singular value is zero if EZ k encompasses the damage.*

Proof. The proof follows, in full analogy to the approach adopted by Bernal and Kunwar (2016), by letting $Y(s)$ and $\tilde{Y}(s)$ be the displacements in the two structural states obtained by applying, respectively, $U(s)$ and $\tilde{U}(s)$ with B_2. Then, it can be shown that

$$Y(s) = G(s)B_2U(s) \tag{4.11a}$$

$$\tilde{Y}(s) = G(s)B_2\tilde{U}(s) + \mathcal{W}_k(s)\beta_k(s), \tag{4.11b}$$

where Eq. (4.11a) follows directly while Eq. (4.11b) is derived through simple manipulation of previous equations. Subtracting Eq. (4.11a) from Eq. (4.11b) and defining $\Delta U(s) = \tilde{U}(s) - U(s)$ yield

$$-\tilde{Y}(s) + Y(s) + G(s)B_2\Delta U(s) + \mathcal{W}_k(s)\beta_k(s) = 0, \tag{4.12}$$

which, when letting

$$G(s)B_2\Delta U(s) = Y(s)\frac{\Delta U(s)}{U(s)} = Y(s)\eta(s), \tag{4.13}$$

can be written as

$$\begin{bmatrix}\tilde{Y}(s) & Y(s) & \mathcal{W}_k(s)\end{bmatrix}\begin{bmatrix}-1\\ 1+\eta(s)\\ \beta_k(s)\end{bmatrix} = 0. \tag{4.14}$$

This leads to the assertion since $[\tilde{Y}(s)\ Y(s)\ \mathcal{W}_k(s)]$ will be rank deficient when EZ k fully contains the damage; independently of what experimental feature is employed. □

When operating with $\left[\tilde{Y}(s)\ \ Y(s)\right]$, the smallest singular value of the residual $\epsilon_l(s) \in \mathbb{C}^{m_s\times 2}$ computed from Eq. (4.5) will, as in the case with $\epsilon_l(s) \in \mathbb{C}^{m_s}$, be denoted σ_l. As such, $\sigma_k = 0$ in cases where $\tilde{B}_2 = B_2 \in \mathbb{R}^n$ and $\tilde{U}(s) \neq U(s)$.

On discrepancies between the subspaces

In order to establish each analytical subspace, a model is used and loads are applied to the corresponding EZ boundary. Needless to say, the actual loads acting on the boundary are not known, so a discrepancy between the model formulation and the experimental conditions will generally be introduced. To parametrize this discrepancy, the scalar $\alpha \in \mathbb{R}$ is introduced such we, in the cases where $\tilde{B}_2 = B_2$ and $\tilde{U}(s) = U(s)$, can write

$$\alpha \mathcal{W}_l(s)\beta_l(s) = \Delta Y(s) \Longrightarrow \Delta Y(s) - \alpha \mathcal{W}_l(s)\frac{1}{\alpha}\mathcal{W}_l^{\dagger}(s)\Delta Y(s) = \epsilon_l(s), \quad (4.15)$$

as expected since, by definition of subspaces, $\mathcal{R}\big(\alpha \mathcal{W}_l(s)\big) = \mathcal{R}\big(\mathcal{W}_l(s)\big)$. Thus, if the loads differ by a scaling between the model formulation and the experimental interrogation, the SEZ scheme still operates as intended.

Besides discrepancies between the actual loading and the one applied to the model, factors such as measurement noise, signal truncation, environmental and operational variability, and model errors will inevitably be present. Let $\delta_Y(s)$ and $\delta_{\mathcal{W}_l}(s)$ denote such perturbations/variabilities in, respectively, the experimental feature and the model implementing EZ l, and define

$$\mathscr{H}_l(s,\alpha) = \Big[\Delta Y(s) + \delta_Y(s) \quad \alpha\Big(\mathcal{W}_l(s) + \delta_{\mathcal{W}_l}(s)\Big)\Big], \quad (4.16)$$

which, in order to be rank deficient when $l = k$ and hereby provide $\sigma_k = 0$, must comply with $\mathcal{R}\big(\Delta Y(s)+\delta_Y(s)\big) \subseteq \mathcal{R}\big(\mathcal{W}_k(s)+\delta_{\mathcal{W}_k}(s)\big)$ and, as a consequence of Eq. (4.6), $\delta_Y(s) \in \mathcal{R}\big(\delta_{\mathcal{W}_k}(s)\big)$. The latter seems as an unrealistic assumption, because $\delta_Y(s)$ stems from sources related to the measurements whereas $\delta_{\mathcal{W}_k}(s)$ is governed by modeling errors. Consequently, the SEZ scheme will operate with $\sigma_k > 0$ under realistic, experimental conditions.

Insufficient set of sensors

The constraint $m_s > n_{\Gamma_l}$ (relaxed to $m_s+m_{c_l} > n_{\Gamma_l}$ in static cases) is necessary for the SEZ scheme to work according to the theory. However, in practice, one expects the effective range of $\mathcal{W}_l$ to have a small dimension. Thus, for cases where the constraints are violated, the SEZ scheme should, theoretically, be usable (albeit with reduced performance) if a truncated basis of the model matrix, $\mathcal{W}_l$ (or $\mathscr{W}_l$ in the static case), is employed. For $\mathcal{W}_l$, this basis is here taken as

$$\acute{\mathcal{W}}_l = \mathscr{U}_{\mathcal{W}_l}\acute{\mathscr{S}}_{\mathcal{W}_l}\mathscr{V}^*_{\mathcal{W}_l} \quad (4.17)$$

where $\acute{(\cdot)}$ denotes a truncated quantity, while $\mathscr{U}_{\mathcal{W}_l}$, $\mathscr{S}_{\mathcal{W}_l}$, and $\mathscr{V}^*_{\mathcal{W}_l}$ are, respectively, the left singular vectors, the singular values, and the conjugate transpose of the right singular vectors of $\mathcal{W}_l$. Through this singular value decomposition and subsequent truncation of $\mathscr{S}_{\mathcal{W}_l}$, $\mathcal{W}_l$ can be reconstructed into a matrix, $\acute{\mathcal{W}}_l$, with a rank that obeys the existing constraint.

Damage metric

Interrogations should, when possible, be made for multiple s-values to provide an aggregation that, in general, improves robustness as stochastic errors are filtered. If, for example, N s-realizations are available, any statistical evaluation can be used to aggregate the results. Here, we choose to take the mean of σ_l,

$$\kappa_l = \frac{1}{N}\sum_{i=1}^{N}\sigma_l\left(s_i\right), \tag{4.18}$$

as the SEZ damage metric, and we close this by noting how a low value of κ_l will indicate that $l = k$ (with EZ k, of course, containing the damage).

With the preceding outline of the SEZ scheme, it is evident that if one was to apply it to the system treated in Example 4.1 with element-wise interrogation, the scheme would, qualitatively, yield the same results as those obtained using mass-related damage patterns in the S3DL approach (see Fig. 4.1b).

4.4.4 Extracting the experimental feature

Given $\tilde{B}_2 = B_2$ with $\tilde{U}(s) \propto U(s)$, the SEZ scheme operates non-parametrically. In a static context, this allows for direct extraction of the experimental feature, while, for dynamic tests, the experimental feature can be taken as the Fourier transforms of the steady-state temporal signals for some s-value(s) placed along the imaginary axis of the s-plane. For the cases where the inputs do not comply with the aforementioned constraints, the experimental feature must be derived through system identification, as outlined in Section 2.2.

4.5 Summary of the SEZ scheme

1. Select an s-value (see the notes provided in Subsection 2.3.2).
   (a) Extract a kinematic field quantity from the reference and damage states, $Y(s)$ and $\tilde{Y}(s)$.
   (b) Form the experimental feature, $\Delta Y(s)$ or $[\tilde{Y}(s) \;\; Y(s)]$ (depending on the input conditions).
   (c) Establish a model incorporating EZ l to compute the analytical subspace, $\mathcal{W}_l(s)$ or $\mathscr{W}_l(s)$.
   (d) Formulate $\epsilon_l(s)$ from Eq. (4.5) using either $\Delta Y(s)$ or $[\tilde{Y}(s) \;\; Y(s)]$.
   (e) Calculate the (lowest) singular value, σ_l, of $\epsilon_l(s)$.
2. If possible, repeat step 1 for other s-values to increase the robustness.
3. Compute κ_l using Eq. (4.18) with the results for $N \geq 1$ s-values.
4. Repeat steps 1 to 3 for each of the remaining EZs and declare damage in EZ k if $\forall l \neq k : \kappa_k < \kappa_l$.

4.6 Application examples

To examine the applicability of the SEZ scheme and exemplify some of the observations previously made, three examples are presented. In Subsection 4.6.1, a numerical study with a chain system introduced to a non-linearity is conducted, and in Subsection 4.6.2 a small-scale wind turbine blade is treated experimentally in a laboratory setup. Finally, in Subsection 4.6.3, the SEZ scheme is applied to a full-scale wind turbine blade under in-service conditions.

4.6.1 Non-linear chain system

We consider the 11-DOF chain system in Fig. 4.5, with the purpose of demonstrating that the SEZ scheme can work with non-linearities in the EZ containing the damage. In any consistent set of units, $m_i = 1$, $c_i = 20$, and (now for $i \in [1, 12]$) $k_i = 1000$, and damage is introduced by a 10 % reduction in k_5 and addition of a cubic spring, $k_{13} = 1000$, in parallel with k_5 (so $k_{13} = 0$ in the reference state). It does not make physical sense to have a damage adding stiffness, but theoretically it is without importance in this particular context.

The experimental feature is computed from temporal signals measured in DOF 3, 6, and 9 that contain forced vibrations and subsequent free decay. The forced vibrations are introduced using a harmonic excitation in DOF 3 with the driving frequency $\Omega = 1.2\omega_1$, where ω_1 is the fundamental eigenfrequency in the reference state. Since the purpose of this example is to demonstrate the

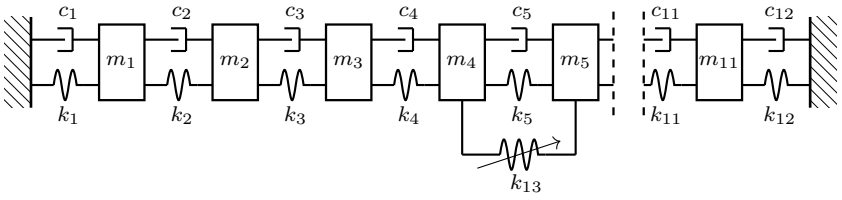

Fig. 4.5: 11-DOF chain system with damage emulated as a 10 % reduction in k_5 and addition of a cubic spring, k_{13}.

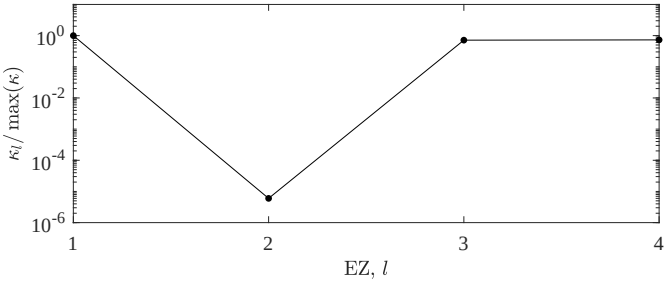

Fig. 4.6: Damage localization in 11-DOF chain system (no model errors or noise).

performance of the SEZ scheme with non-linearities in the damaged zone, no noise or model errors are included. The interrogation is conducted using EZs containing multiple springs; with the first EZ containing springs 1 to 3, the second 4 to 6 and 13, the third 7 to 9, and the fourth 10 to 12. In this way, the results shown in Fig. 4.6 are obtained. Since the second EZ contains springs 5 and 13, the damage is located unambiguously.

4.6.2 Small-scale wind turbine blade

In the present example, the applicability of the SEZ scheme is tested in the context of experiments with the small-scale wind turbine blade depicted in Fig. 4.7a. The blade, which is introduced to a mass perturbation to emulate damage, has previously been utilized to test different damage localization schemes by, among others, Johansen et al. (2015), Hansen et al. (2015), García et al. (2015), Markvart et al. (2017), Bull et al. (2017), and Sekjær et al. (2017).

The blade itself is approximately 800 mm long and weighs 720 g (including accelerometers and bolts), and it consists of two carbon fiber-reinforced polymer parts that are bolted together along the leading and trailing edges. As seen in Fig. 4.7a, the blade is fixed at the root and excited at the tip with a shaker providing a harmonic load; driving with a frequency of $\Omega = 150\pi$ rad/s. This

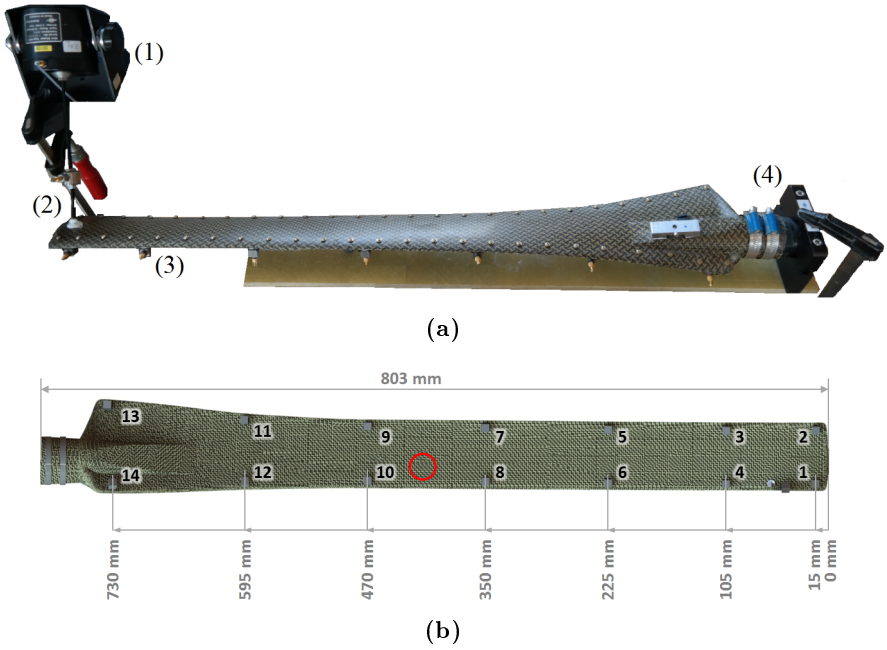

Fig. 4.7: Small-scale wind turbine blade. (a) Indication of (1) the shaker, (2) the connection between the shaker and the blade, (3) an accelerometer, and (4) the fixed support. (b) Location of the mass perturbation (on opposite surface) and the 14 accelerometers.

frequency has been chosen due to the results obtained in a preliminary damage detection study. Accelerations are captured by use of 14 uniaxial accelerometers (B&K type 4507-B-004 and B&K type 4508-B-002), which, as seen Fig. 4.7b, are mounted close to the edges underneath the blade and measure perpendicular to the surface. For data acquisition, three B&K type 3050 6-channel input systems are used. The mass perturbation is introduced by attaching a "point" mass of 30 g at the location indicated in Fig. 4.7b. Here, it should be noticed that the mass is actually placed on the opposite surface.

FE model representation

The model representation of the blade, which is fixed at the blade root to emulate the clamping mechanism, is established in the commercial software platform ANSYS® Workbench™ using a formulation with 3450 first-order shell elements. The model is assigned an orthotropic material model, whose properties are calibrated to the modal parameter estimates obtained in an OMA study by Johansen et al. (2015). In this OMA study, the first and second flapwise bending modes are found to have eigenfrequencies of, respectively, 15.9 Hz and 87.9 Hz, while the first edgewise bending mode has an eigenfrequency somewhere in between (the mode was not identified during the OMA). For more information about this and the FE modeling, the reader is referred to the studies by Johansen et al. (2015) and Markvart et al. (2017).

Damage localization results

Experiments are conducted with a fixed duration of 10 s steady-state vibration. To transform the temporal signals to frequency domain, the least-squares technique proposed by Bernal and Kunwar (2016) is employed. Subsequently, the experimental feature is formed as $[\tilde{Y}(j\Omega) \;\; Y(j\Omega)]$ (with $j = \sqrt{-1}$), which is chosen, instead of $\Delta Y(j\Omega)$, to cope with non-damage associated changes in the vibration response.

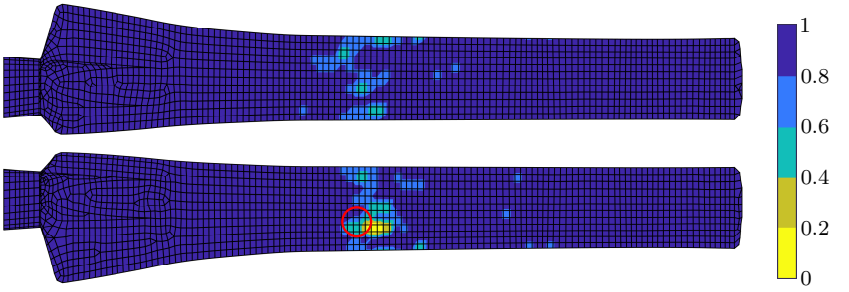

Fig. 4.8: Localization of extra mass added to small-scale blade. The colormap is according to $\kappa_l / \max(\kappa)$, and the red circle encompasses the true mass location.

The damage interrogation is conducted by taking each single element as an EZ, which yields the results depicted in Fig. 4.8. Evidently, an unambiguous localization is achieved for the mass perturbation, albeit the SEZ scheme points to damage slightly shifted from the actual location. Additionally, it is seen that the scheme provides a clear resolution in terms of undamaged and damaged elements. It is worth noting that several similar experiments have been conducted, and they all provide almost identical results.

4.6.3 Operating wind turbine

In this example, the Vestas V27 wind turbine depicted in Fig. 4.9a is analyzed. The wind turbine has a rotor diameter of 27 m, and it supports two operating regimes, namely, one at 32 rotations per minute (RPM) and one at 43 RPM. The V27 turbine has previously been examined, with success, in the context of damage detection by Ulriksen et al. (2015) and Tcherniak and Mølgaard (2017). In both of these studies, a mechanical actuator is implemented to excite a broad band of frequencies, and the damage detection schemes are implemented using vibrations governed by this input source.

Here, we seek to locate the 0.45 m trailing edge debonding seen in Fig. 4.9b, with the location pinpointed in Fig. 4.9c. This has previously been done in

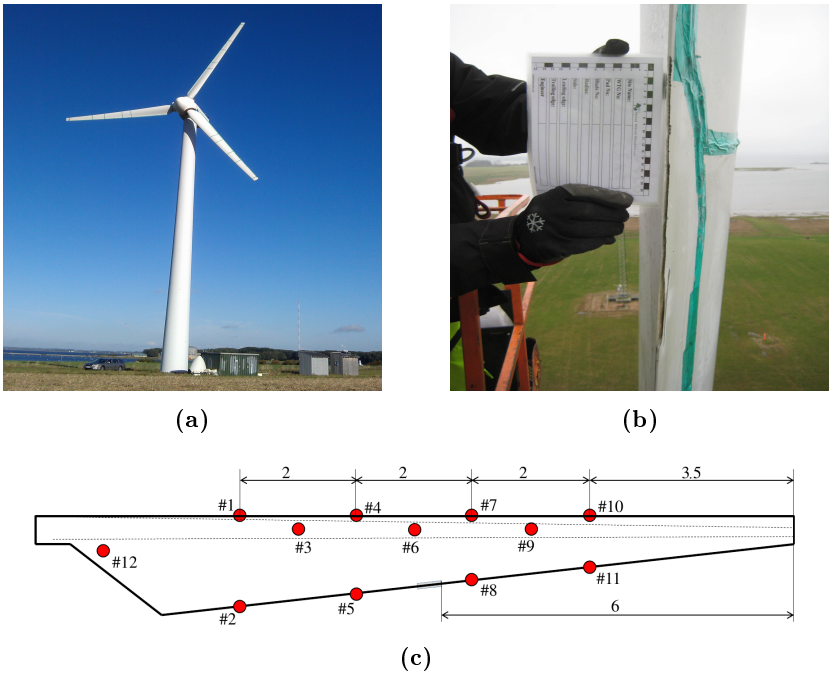

Fig. 4.9: Vestas V27 wind turbine. (a) Overall view. (b) 0.45 m blade edge debonding. (c) Blade sketch with accelerometer (●) and damage (■) positions (all dimensions are in m).

Paper D by Ulriksen et al. (2017), who apply the SDDLV scheme to locate the damage using vibrations induced by the mechanical actuator; with the turbine in idle condition. As can be seen in that study, the debonding can only be located if multiple realizations are gathered in a statistical evaluation to alleviate noise and other variabilities. Now, in the present example, the SEZ scheme is employed to, in a deterministic configuration with just one realization from each of the two structural states, locate the debonding during turbine operation at 32 RPM and without using the actuator.

FE model representation

Following the argumentation in Paper D by Ulriksen et al. (2017), it is sufficient to only model the blade of interest and not the entire turbine. The model is established in the commercial software platform ANSYS® Workbench™ using a formulation with approximately 26,000 first-order shell elements. The model is assigned an orthotropic material model, whose properties, as outlined in Paper D by Ulriksen et al. (2017), are calibrated to the eigenfrequencies and blade-level mode shapes identified in an OMA of the rotor.

Damage localization results

Each measurement sequence consists of 30 s sampling, where the first (approximately) 10 s are turbine operation without any input from the attached actuator. We choose to use these 10 s in the damage localization analysis and, as such, form the experimental feature as $[\tilde{Y}(j\Omega) \;\; Y(j\Omega)]$, where $\Omega \approx 3.35$ rad/s is the frequency at which the rotor operates.

The damage interrogation is conducted by taking each single element as an EZ, which yields the results depicted in Fig. 4.10. As can been seen, the debonding is localized rather clear when inspecting the side of the blade on which the sensors are placed (topmost blade plot in Fig. 4.10). When inspecting the other blade side, some disturbances are, however, present in the vicinity of the actual damage location. These disturbances arise consistently for all

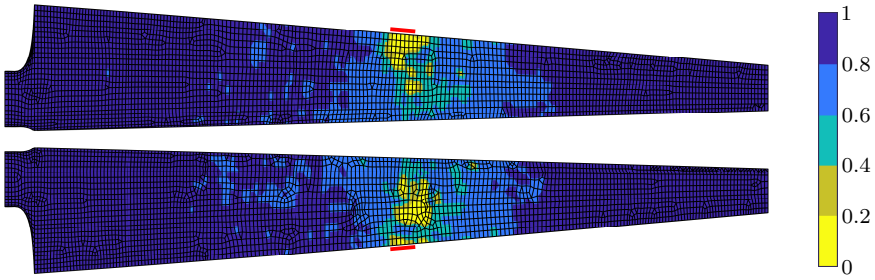

Fig. 4.10: Localization of trailing edge debonding in V27 blade. The colormap is according to $\kappa_l / \max(\kappa)$, and (—) indicates the true debonding location.

combinations of measurement sequences, thus it is contended that they are related to some local errors in the FE model of the blade.

If we compare the results in Fig. 4.10 with those obtained using the SDDLV scheme for the turbine in idle condition, see Paper D by Ulriksen et al. (2017), it is clear that the SEZ scheme provides better results. This despite the fact that the SEZ scheme is implemented for the turbine under operational conditions with 32 RPM. It seems reasonable to assume that the improvement is a direct result of conducting the structural interrogation in a non-parametric mode.

4.7 Concluding remarks

In the present chapter, we have introduced the SEZ scheme, which locates damage from a forward procedure where shifts in measured field quantities are reconstructed by use of subspaces indexed by model-based postulated boundaries. As such, the SEZ scheme, in principle, allows for a user-defined spatial localization resolution while still operating non-parametrically if the input distribution is spatially invariant and the input histories are proportional in the reference and damaged states. If the noted input conditions are not complied with, system identification *must* be used to compute the experimental feature.

In the two first application examples, which are included to demonstrate the basic principles of the SEZ platform and verify its applicability in a non-parametric context, we treat a numerical chain-like system introduced to a non-linearity in the damaged state and a small-scale wind turbine blade treated experimentally with damage emulated by an added "point" mass. In both examples, it is evidenced how the SEZ scheme facilitates unambiguous damage localization, even in the experimental case where an insufficient number of sensors (compared to the theoretical constraint) is available.

In the third application example, the SEZ scheme is used to locate a damage in an operating wind turbine blade. The findings imply that the scheme has merit in real-life applications where the previously established input conditions are, at least to some extent, complied with.

CHAPTER 5

Input control for damage localization

In the present chapter, we introduce the Shaped Damage Locating Input Distribution (SDLID) scheme, which operates unconditionally non-parametric by deploying controllable inputs that are shaped to actively interrogate one structural subdomain at a time for damage. When the subdomain containing damage is rendered dormant, the effect of damage and, as such, its induced shift in steady-state vibration response are canceled. In Section 5.2, the reasoning behind developing the SDLID scheme is given. In Section 5.3, the basic principles of shaping inputs are outlined, and subsequently, in Section 5.4, the theorem constituting the basis of the scheme and how to implement it for damage localization are provided. Following a brief summary of the SDLID scheme in Section 5.5, numerical examples are presented in Section 5.6 to demonstrate the applicability of the scheme. The chapter is completed with some concluding remarks in Section 5.7.

5.1 Dissemination

Parts of this chapter have been published in the following:

- Paper E by Ulriksen et al. (2017a), see Appendix E.
- Paper F by Ulriksen et al. (2017b), see Appendix F.

5.2 Motivation for the SDLID scheme

The SEZ scheme presented in Chapter 4 possesses the feature of being non-parametric if certain input conditions are fulfilled. In such cases, the scheme is implemented in an output-only configuration—requiring more output sensors than DOF on the boundary of the postulated damage—and does not profit further from the fact that certain characteristics of the input are known. The SDLID scheme introduced in this chapter also operates in a forward procedure with postulated damage patterns to circumvent system identification, but unlike the SEZ scheme, the SDLID approach makes active use of the inputs to search for damage. By applying a number of controllable inputs larger than the rank of the postulated damage, the SDLID scheme facilitates non-parametric damage localization using only few output sensors; in fact, one well-placed may

suffice. This low demand on output sensors is an attractive feature, which is conventionally only achieved when using local guided waves-based approaches (Surgeon and Wevers, 1999; Yeum et al., 2014).

Needless to say, the obvious shortcoming of the SDLID scheme is the requirement of deploying multiple controllable inputs. It is noted that for a continuum, the required number of inputs to apply is, in theory, infinite, albeit one expects that some number that is enough to work in a reasonable accurate FE model will suffice. This number can, however, still be large, so, in general, the feasibility of deploying multiple input sources might not seem evident. However, with the latest advances in piezoelectric and electro-mechanical actuators, as utilized in the context of damage localization by, for example, Bernal and Kunwar (2016) and Ulriksen et al. (2017), it should not be substantially more impairing than that of deploying multiple output sensors.

5.3 Basics of input shaping

We return to the LTI system described in time domain by Eq. (2.1) and, under the assumption of zero initial and/or steady-state conditions, in Laplace domain by Eq. (2.5). The fundamental principle of input shaping is to apply a set of controllable inputs, $u(t)$, to a structure and tailor these, preferably by use of a model representation, to induce a certain vibration output response (Singer and Seering, 1988; Murphy and Watanabe, 1992; Singh and Heppler, 1993).

For the purpose of damage localization, the inputs will, as visually exemplified in Fig. 5.1, be shaped such that particular kinematic quantities resulting from these inputs are rendered dormant in a subdomain of the structure in question. It must be noted that as ambient excitation is present in real applications, the shaped inputs need not yield complete suppression in the selected subdomain. Still, in the coming formalization, we assume, for simplicity and without loss of generality, that only the controllable inputs affect the structure.

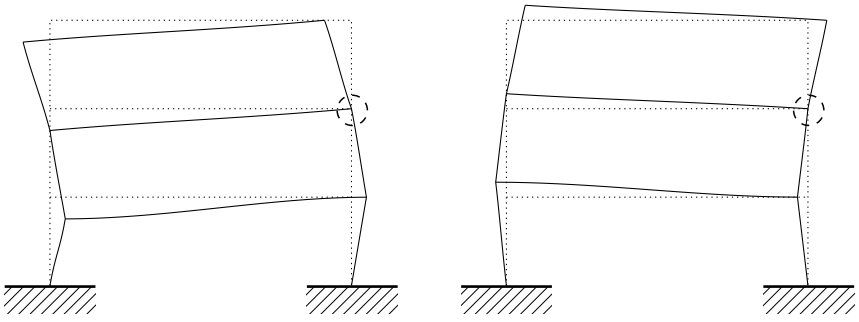

Fig. 5.1: Vibration snapshots at different time instances for frame structure subjected to inputs shaped to suppress translational DOF in the indicated node.

Now, there are numerous ways of shaping inputs to suppress certain vibration quantities; each approach with merits and shortcomings, in terms of computational extent and numerical accuracy, depending on the nature of the input distribution. In Subsections 5.3.1 and 5.3.2, two approaches are outlined. The first one operates in Laplace domain and is, as such, particularly useful when shaping harmonic input sources, while the second one is a time-domain approach in which a deconvolution scheme is employed.

5.3.1 Laplace domain approach

If the structural system adheres to the assumptions made to formulate Eq. (2.5) and p controllable inputs act solely in the DOF indexed by $\mathcal{T}$, then

$$X(s) = G_{\bullet\mathcal{T}}(s)U(s) \tag{5.1}$$

with $G_{\bullet\mathcal{T}}$ being the transfer matrix columns corresponding to the input DOF.

Proposition 5.1. *Let $\Upsilon(s)$ be a subset of DOF or a linear combination hereof obtained from a linear map, $T : X(s) \in \mathbb{C}^n \mapsto \Upsilon(s) \in \mathbb{C}^q$ such $T(X(s)) = \mathscr{L}X(s)$. Then, the p inputs applied to suppress $\Upsilon(s)$ and $\upsilon(t) = \mathcal{L}^{-1}(\Upsilon(s))(t)$ can be extracted from Null$(\mathscr{L}G_{\bullet\mathcal{T}}(s))$, provided that $p > q$.*

Proof. Υ denotes a subset of DOF or a linear combination hereof, thus

$$\Upsilon(s) = \mathscr{L}X(s), \tag{5.2}$$

which, when plugged into Eq. (5.1) and set to zero, yields

$$\Upsilon(s) = \mathscr{L}G_{\bullet\mathcal{T}}(s)U(s) = 0, \tag{5.3}$$

where $\mathscr{L}G_{\bullet\mathcal{T}}(s) \in \mathbb{C}^{q\times p}$. Provided that $p > q$, one obtains Null$(\mathscr{L}G_{\bullet\mathcal{T}}(s)) \in \mathbb{C}^{p\times(p-q)}$ from where relative values of $U(s)$ that, in steady state, yield $\Upsilon \equiv \upsilon \equiv 0$ can be selected. □

Example 5.1. To get an appreciation of the transformation matrix, $\mathscr{L}$, consider the one-dimensional bar element system shown in Fig. 5.2.

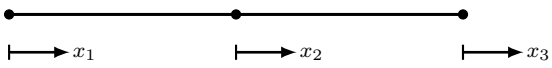

Fig. 5.2: Bar element system with indication of the existing DOF in time domain.

If two inputs are applied (in a spatial context, completely arbitrarily) and shaped to yield $X_1 \equiv x_1 \equiv 0$ in steady state, one finds

$$\Upsilon(s) = \mathscr{L}X(s) = \begin{bmatrix} 1 & 0 & 0 \end{bmatrix} \begin{bmatrix} X_1 \\ X_2 \\ X_3 \end{bmatrix}. \tag{5.4}$$

If, instead, the aim is to suppress the strain across element two, we use the strain-interpolation condition, which is $B = [-1/L \quad 1/L]$ for the one-dimensional bar element of length L. As such,

$$\Upsilon(s) = \begin{bmatrix} 0 & -1 & 1 \end{bmatrix} \begin{bmatrix} X_1 \\ X_2 \\ X_3 \end{bmatrix} \tag{5.5}$$

from where the obvious $\mathscr{L} = [0 \ -1 \ 1]$ is deduced. □

It is gathered from Proposition 5.1 that when $p \geq q + 1$, then any type of characteristic load function can, in theory, be utilized for the p inputs. For harmonic inputs, the desirable steady-state features can be exploited, in the sense that the input amplitudes and phase angles are directly computed as the moduli and arguments of the chosen vector within the span of Null $(\mathscr{L}G_{\bullet\mathcal{T}}(s))$. More generally, however, the outlined approach requires an inverse Laplace transformation along a discretized Bromwich contour. This procedure can, as discussed by Davies and Martin (1979), be both computationally expensive and associated with inaccuracy. Consequently, a time domain approach is presented next that is independent of the nature of the input sources.

5.3.2 Time domain approach

From the discrete state-space formulation provided in Eqs. (2.17a) and (2.17b), one can show that the following input-output relation holds:

$$\begin{pmatrix} y_0 \\ y_1 \\ \vdots \\ y_{N-1} \\ y_N \end{pmatrix} - \begin{bmatrix} C_d \\ C_d A_d \\ \vdots \\ C_d A_d^{N-1} \\ C_d A_d^N \end{bmatrix} z_0 = \begin{bmatrix} Y_0 & 0 & \cdots & 0 \\ Y_1 & Y_0 & \cdots & 0 \\ \vdots & \vdots & \ddots & \vdots \\ Y_{N-1} & Y_{N-2} & \cdots & 0 \\ Y_N & Y_{N-1} & \cdots & Y_0 \end{bmatrix} \begin{pmatrix} u_0 \\ u_1 \\ \vdots \\ u_{N-1} \\ u_N \end{pmatrix} \tag{5.6}$$

or, in analogy to the compact form used by Bernal and Ussia (2015),

$$y_{[0,N]} - Ob_N z_0 = H u_{[0,N]} \tag{5.7}$$

such that

$$u_{[0,N]} = H^\dagger y_{[0,N]} - H^\dagger Ob_N z_0 + \text{Null}\,(H)\,\psi, \tag{5.8}$$

in which $\psi \in \mathbb{R}^{\text{nullity}}$ is an arbitrary vector while Y_j are Markov parameters gathered in the lower triangular Toeplitz matrix H. More specifically, $Y_0 = D_d$ and $\forall j \in [1, N] : Y_j = C_d A_d^{j-1} B_d$.

Let $x_{\mathcal{U}}$ contain the DOF for which a linear combination must be suppressed, then $H_{\mathcal{U}\bullet}$ holds the rows of H associated with these DOF. If $p > q$, $H_{\mathcal{U}\bullet}$ will be wide and, as such, provide an infinite number of solutions to Eq. (5.8). Thus, with one of the p inputs being defined both spatially and temporally, the remaining $p-1$ inputs can be deconvolved to produce the negative response of that obtained by application of the fixed input.

5.4 Locating damage using shaped inputs

Imagine the scenario where a point mass is added to the suppressed DOF in the frame depicted in Fig. 5.1. Obviously, the perturbation, in the form of the added mass, will be inactive, which implies that the steady-state response will be the same in the perturbed state as in the reference one (without the added mass). This simple example captures the principle of using shaped inputs to locate structural damage. The concept is formalized for both mass and stiffness perturbations, viewed upon as damages, in Theorem 5.1.

Theorem 5.1. *$\mathcal{A} = \mathcal{A}_\mathcal{H} \cup \mathcal{A}_\mathcal{D}$ is an LTI system, which is discretized with the DOF indexed by $\mathcal{Q} = \{1, 2, \ldots, n\}$ and described in the reference state by Eq. (2.1) and in the damaged state by Eq. (2.29a) for a mass perturbation and Eq. (2.29b) for a stiffness perturbation. Let $\Delta x(t) = \tilde{x}(t) - x(t)$ be a steady-state displacement shift due to either a mass or stiffness perturbation acting at the DOF indexed by $\mathcal{V} \subset \mathcal{Q}$ and assume the input condition $\tilde{B}_2\tilde{u}(t) = B_2u(t)$. Then, $\Delta x \equiv \Delta\dot{x} \equiv \Delta\ddot{x} \equiv 0$ if $u(t)$ is shaped to yield $\mathscr{L}x_\mathcal{V} \equiv 0$ in the reference state; with $\mathscr{L}$ being the transformation matrix introduced in Proposition 5.1.*

Proof. (1) With damage manifested as a perturbation in the mass, the equilibrium equation describing the damaged steady state, with the same excitation as in the reference state, is given by replacing $\tilde{B}_2\tilde{u}(t)$ with $B_2u(t)$ in Eq. (2.29a). Subtracting Eq. (2.1) from Eq. (2.29a) yields

$$M\Delta\ddot{x}(t) + C\Delta\dot{x}(t) + K\Delta x(t) = \Delta M\ddot{\tilde{x}}(t), \tag{5.9}$$

so with $\ddot{\tilde{x}}_\mathcal{V} \equiv 0$, which must hold if $\Delta x \equiv 0$, one gets $\Delta M\ddot{\tilde{x}} \equiv 0$ and, as such, $\tilde{x} \equiv x$ since $\exists t : u(t) \neq 0$.

(2) For stiffness-related damages, we express the strain energy in the reference steady state as

$$U_\mathcal{A}(t) = \frac{1}{2}\int_\mathcal{A} \epsilon(t)^T E\epsilon(t)\, dV \tag{5.10}$$

and in the damaged steady state—with a stiffness perturbation—as

$$\tilde{U}_\mathcal{A}(t) = \frac{1}{2}\int_{\mathcal{A}_\mathcal{H}} \tilde{\epsilon}(t)^T E\tilde{\epsilon}(t)\, dV + \frac{1}{2}\int_{\mathcal{A}_\mathcal{D}} \tilde{\epsilon}(t)^T \tilde{E}\tilde{\epsilon}(t)\, dV, \tag{5.11}$$

where $\epsilon(t) \in \mathbb{R}^n$ contains the strains and E is the constitutive matrix that maps strains to stresses. In order for the vibration signatures in the two structural states to be identical, one must impose $\tilde{U}_\mathcal{A} \equiv U_\mathcal{A}$ and $\tilde{\epsilon} \equiv \epsilon$, hence

$$\begin{aligned}\int_{\mathcal{A}_\mathcal{H}} \epsilon(t)^T E\epsilon(t)\, dV + \int_{\mathcal{A}_\mathcal{D}} \epsilon(t)^T \tilde{E}\epsilon(t)\, dV = \int_{\mathcal{A}_\mathcal{H}} \epsilon(t)^T E\epsilon(t)\, dV \\ + \int_{\mathcal{A}_\mathcal{D}} \epsilon(t)^T E\epsilon(t)\, dV,\end{aligned} \tag{5.12}$$

which leads to

$$\int_{\mathcal{A}_\mathcal{D}} \epsilon(t)^T \tilde{E}\epsilon(t)\, dV = \int_{\mathcal{A}_\mathcal{D}} \epsilon(t)^T E\epsilon(t)\, dV, \tag{5.13}$$

and since $E \succ 0$, Eq. (5.13) can, for $\tilde{E} \neq E$, only hold if $\epsilon \equiv 0$. We finish the proof by recalling that the strains in a subdomain are a linear transform of the displacements in this subdomain. □

Remark 5.1. *From Eq.* (5.3)*, it is evident that the number of inputs to apply is governed by the rank of the introduced damage, as* $q = rank(\Delta M \vee \Delta K)$ *such* $p > rank(\Delta M \vee \Delta K)$*.*

5.4.1 Damage metric

The procedure for conducting damage localization by use of shaped inputs is to postulate a damage pattern, shape the inputs to suppress this pattern by use of a model representation of the reference state, and then apply these inputs to the damaged structural state and compare the response to a stored signature from the reference state. As such, the lth damage pattern, which is composed of some combination of the DOF indexed by $\mathcal{U}_l$, contains the damage if, under ideal conditions, no shift is present between the steady-state vibration responses from the two structural states.

When ambient excitation is present, $u(t)$ must be shaped such that $v_l(t)$ and, accordingly, $\Upsilon_l(s)$ only contain ambient contributions, that is,

$$\Upsilon_l(s) = W_{\mathcal{U}_l}(s), \tag{5.14}$$

where $W_{\mathcal{U}_l}(s)$ denotes some linear combination of ambient vibrations. Now, it follows from Theorem 5.1 that if $\mathcal{U}_l \supseteq \mathcal{V}$, one gets

$$\tilde{\Upsilon}_l(s) = \tilde{W}_{\mathcal{U}_l}(s), \tag{5.15}$$

while

$$\forall \mathcal{U}_l \not\supseteq \mathcal{V}: \ \tilde{\Upsilon}_l(s) \neq \tilde{W}_{\mathcal{U}_l}(s) \tag{5.16}$$

since $u(t)$ will induce a steady-state response.

Needless to say, one finds $\Delta\Upsilon_l \not\equiv 0$ in practice due to ambient excitation, measurement noise, and so forth. Therefore, some metric must be utilized to quantify the deviation between $\tilde{Y}(s)$ and $Y(s)$, where $Y(s)$ is the Laplace transform of the captured output, $y(t) \in \mathbb{R}^{m_s}$, defined in Eq. (2.10b). This can obviously be done in numerous, more or less sophisticated, ways. Here, we choose the ℓ_2-norm of the residuals, so

$$\mathcal{M}_l = \sqrt{\sum_{i=1}^{N} \left(|\tilde{Y}_l(s_i)| - |Y_l(s_i)| \right)^2} \tag{5.17}$$

because we evaluate at N s-values in m_s output sensor DOF. In practice, one will, of course, choose to evaluate s along $\Im(s)$ to avoid system identification.

A condition for the SDLID scheme to operate as intended is, in general, that the response due to the shaped inputs must be the dominant component in the vibration response. If, however, the inputs are harmonic, this is not a necessary condition since the steady-state harmonics can be extracted using signal filtering techniques. Another aspect worth noting is that the damage localization contrast improves when the response of the damaged area is large for a given suppression pattern not containing the damage.

5.4.2 Resemblance to the (S)DDLV scheme

The SDLID scheme bears resemblance to the (S)DDLV scheme by Bernal (2007, 2010), as both schemes operate on the premise of applying loads that isolate the damage by rendering the damaged subdomain dormant in terms of a particular vibration quantity. The key differences between the two schemes lie in the extraction of the particular load distribution utilized in the localization procedure—using system identification or not—and the implementation of this distribution in a particular localization context. As outlined in Subsection 1.2.1, the (S)DDLV scheme extracts the load distribution from the null space of an experimentally *identified* transfer matrix change (or a surrogate hereof in the stochastic case) and then applies it to a model in the attempt to point directly to the damage; in this way circumventing interrogation with postulated damage patterns.

When it comes to robustness of the two schemes, there is, from a theoretical point of view, no reason to expect any noticeable difference in terms of robustness to model errors. On the other hand, the SDLID scheme stands as more robust to noise since system identification is avoided. Therefore, selecting one of the two schemes to apply boils down to either; using $p > \text{rank}(\Delta M \vee \Delta K)$ controllable input sources and few output sensors (in principle, one may suffice) to increase noise robustness, or avoiding deployment of controllable inputs and, as such, sacrificing some noise robustness while operating with a minimum number of output sensors complying with $m_s > \max\{\text{rank}(\Delta M \vee \Delta K), n_s/2\}$, where n_s is the order of the identified system. In some cases, particularly those involving severe noise contamination and/or poor excitation during the experimental procedure, the SDLID scheme will be preferable.

5.5 Summary of the SDLID scheme

1. Choose the general type of input; of which harmonic and broadband are examples.

2. If harmonic inputs are chosen, select an s-value along $\Im(s)$ (see the notes in Subsection 2.3.2). Otherwise, move on to the next step.

3. Shape the inputs to suppress the lth damage pattern in a model, using either the Laplace domain approach outlined in Subsection 5.3.1 or the

time domain approach outlined in Subsection 5.3.2.

4. Apply the shaped inputs to the actual structure in its healthy state and its damaged state.

5. For non-harmonic inputs, select an s-value along $\Im(s)$ (see the notes in Subsection 2.3.2). For harmonic inputs, move on to the next step.

6. Extract the responses from both states, $Y(s)$ and $\tilde{Y}(s)$.

7. If possible, repeat steps 2 (or 5, depending on the input type) to 6 for other s-values to increase the localization robustness.

8. Calculate the ℓ_2-norm of $\Delta Y(s)$, denoted $\mathcal{M}_l$ in Eq. (5.17).

9. For the same s-value(s), do steps 3, 4, 6, 7, and 8 for each of the remaining damage patterns and declare damage in number k if $\forall l \neq k : \mathcal{M}_k < \mathcal{M}_l$.

5.6 Application examples

Two numerical examples are treated to test the performance of the SDLID method. Each example is cast in a Monte Carlo setting with 100 simulations in both structural states (reference and damaged) for all the selected DOF suppression scenarios. To challenge the robustness of the method, model errors are introduced (in each simulation) to the system matrices of each local element by assigning a random perturbation, which is drawn from a uniform distribution with lower and upper limits of α_L and α_H. Additionally, the output is corrupted with 5 % white Gaussian noise, where the percentage is with regard to the standard deviations of the noise-free output signals.

To provide an insight into the robustness of the SDLID scheme when applied to the two examples, we define a probability of localization (POL) as

$$P_l = \frac{\#\mathcal{B}_l^0}{\#\left\{\mathcal{B}_l^0 \cup \mathcal{B}_l^1\right\}}, \tag{5.18}$$

where

$$\mathcal{B}_l^0 = \left\{\mathcal{M}_l^{(i)} : \mathcal{M}_l^{(i)} = \min\left(\mathcal{M}^{(i)}\right)\right\} \tag{5.19}$$

and

$$\mathcal{B}_l^1 = \left\{\mathcal{M}_l^{(i)} : \mathcal{M}_l^{(i)} \neq \min\left(\mathcal{M}^{(i)}\right)\right\}, \tag{5.20}$$

with $\mathcal{M}^{(i)}$ containing the damage metrics for all postulated patterns in an ith interrogation sequence. In the examples, the results are presented as the POL and the mean, $\bar{\mathcal{M}}_l$, and standard deviation, $S_{\mathcal{M}_l}$, of the discordances for each damage pattern, $\mathcal{M}_l$, as obtained from Eq. (5.17).

5.6.1 Chain-like system

We consider localization of a mass perturbation in the 6-DOF system depicted in Fig. 5.3. The springs and masses in the system are, in any consistent set of units, $k_i \in \{500, 500, 500, 500, 500, 500, 100, 100\}$ and $m_i \in \{1, 2, 3, 1, 3, 1\}$, hereby yielding $\omega_1 = 4.33$ rad/s and $\omega_6 = 35.91$ rad/s, where ω_i is the ith undamped eigenfrequency of the reference structure. Classical damping is assumed such each mode has a damping ratio of $\zeta_i = 5$ %, and the mass perturbation, which is assigned to the third mass in the system, is given by $m_e = 0.2m_3$. To comply with $p \geq \text{rank}\,(\Delta M) + 1$, two inputs are applied, in a spatial context, completely arbitrarily, to masses 2 and 6. The output is taken as noise-corrupted steady-state displacements measured in DOF 2 (that is, only one sensor is employed) with a sampling frequency of 100 Hz.

Shaping the inputs

The input in DOF number 2, denoted $u_1(t)$, is realized from a white Gaussian noise sequence with a frequency range of $0 - 50$ Hz, and then $u_2(t)$ is shaped accordingly by use of the deconvolution technique outlined in Subsec-

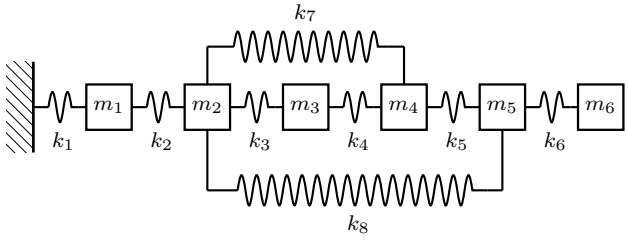

Fig. 5.3: Classically damped 6-DOF chain-like system with inputs applied to masses 2 and 6 and an output sensor at mass 2.

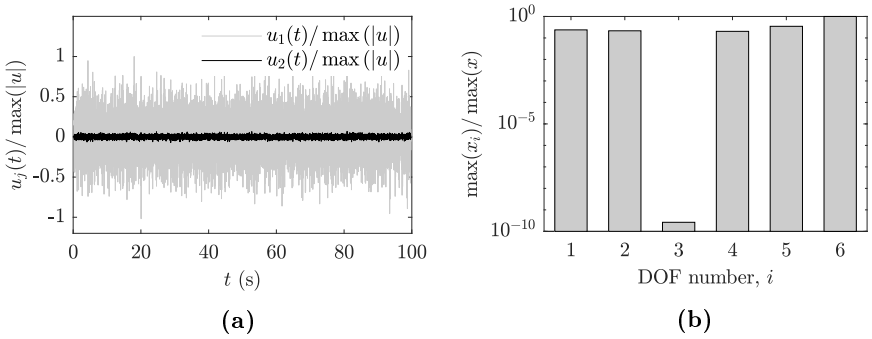

Fig. 5.4: Shaping inputs to suppress DOF 3 in chain-like system (no model errors or noise). (a) Broadband inputs. (b) Steady-state displacement maxima from the excitation in Fig. 5.4a.

tion 5.3.2. The conditions obtained in a single realization for suppressing the displacements in the third DOF by use of broadband excitation are depicted in Figs. 5.4a and 5.4b. As can be deducted, the displacements (and, consequently, the velocities and accelerations) are, for all practical purposes, zero in DOF 3.

Signature discrimination

Theorem 5.1 states that suppression of the steady-state accelerations of mass 3, where the perturbation is located in the damaged state, will yield agreement in the steady-state vibration responses induced solely by the shaped inputs in the two structural states. This is verified in Fig. 5.5, which illustrates the results obtained by interrogating the chain-like system in a noise-free configuration without model errors.

To demonstrate the methodology in a more realistic setup, the previously described Monte Carlo setting is established with 5 % output noise and model errors that are cast from a uniform distribution with lower and upper limits of $\alpha_L = 0.95$ and $\alpha_H = 1.05$. These model errors result in observed maximum eigenfrequency shifts of 2.8 % for modes 1 and 2, 2.9 % for mode 3, 4.1 % for

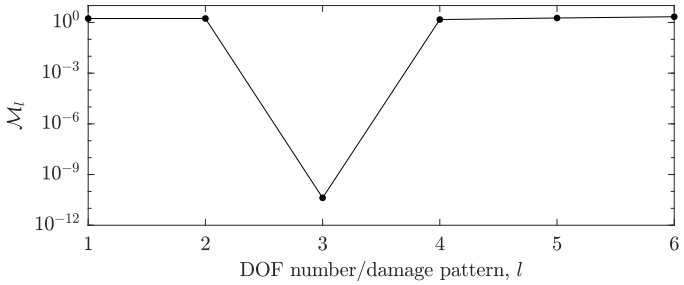

Fig. 5.5: Damage localization in chain-like system (no model errors or noise).

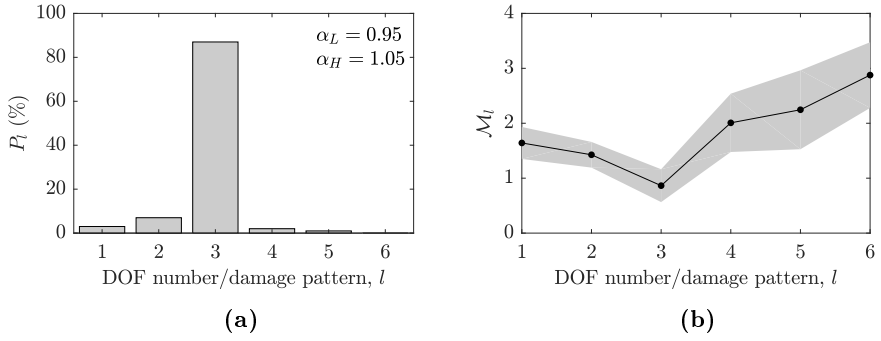

Fig. 5.6: Damage localization in chain-like system with (a) P_l and (b) $\bar{\mathcal{M}}_l$ and $S_{\mathcal{M}_l}$ for the realizations in Fig. 5.6a.

mode 4, 3.2 % for mode 5, and 3.4 % for mode 6. To allow for aggregation of results, which can be used to filter stochastic errors and, thus, improve robustness, the interrogations are conducted for $N = 5$ Fourier realizations of the output, in the range from just below ω_1 to ω_6. The localization results of the Monte Carlo simulation are depicted in Fig. 5.6, where it is evident that the added mass is localized correctly in $P_3 = 87$ % of the interrogations and, as such, incorrectly in 13 %. As will be demonstrated later in this example, these false negatives can be reduced by deploying multiple sensors.

Effect of model errors and single-sensor placement

The results obtained thus far have been for a certain amount of model error and a somewhat arbitrarily chosen output sensor location. Needless to say, there will be some model error extent for which the scheme will no longer work; an extent that will vary from application to application. In the context of this simple chain-like system, we examine the sensitivity to this and the single-sensor placement by implementing Monte Carlo settings with different model error configurations and using a single sensor that is shifted between each DOF. The results are presented in Tb. 5.1, and as it can be seen, the added mass is localized correctly for all single-sensor distributions with model errors up to $\alpha_L = 0.98$ and $\alpha_L = 1.02$ (leading to maximum eigenfrequency shifts of 1.6 %). If $\alpha_L = 0.95$ and $\alpha_L = 1.05$, the observed maximum model error-induced eigenfrequency shift is, as previously noted, 4.1 %, and false localization positives are obtained. These could, of course, be reduced by calibrating the theoretical model with respect to the actual structure, so the most important message is that the method is not hyper-sensitive to model errors.

Effect of deploying multiple sensors

The false localization positives that arise, as seen in Fig. 5.6 and deducted from Tb. 5.1, when operating with a certain extent of model error and a single output sensor can, in general, also be reduced by deploying multiple sensors. This is exemplified from the outset of the configuration providing the results in Fig. 5.6, now extended to the case of an additional output sensor at DOF 5. Fig. 5.7a shows the obtained POL, while Fig. 5.7b depicts $\bar{\mathcal{M}}_l$ and $S_{\mathcal{M}_l}$ to show

Table 5.1: POL for different single-sensor locations and model error configurations, with $\Delta\omega$ being the model error-induced eigenfrequency shifts.

			P_3 (%) with output at DOF;					
α_L	α_H	max($\lvert\Delta\omega\rvert$) (%)	1	2	3	4	5	6
0.98	1.02	1.6	100	100	100	100	100	100
0.95	1.05	4.1	96	94	94	89	90	88
0.90	1.10	8.2	62	57	57	48	48	44

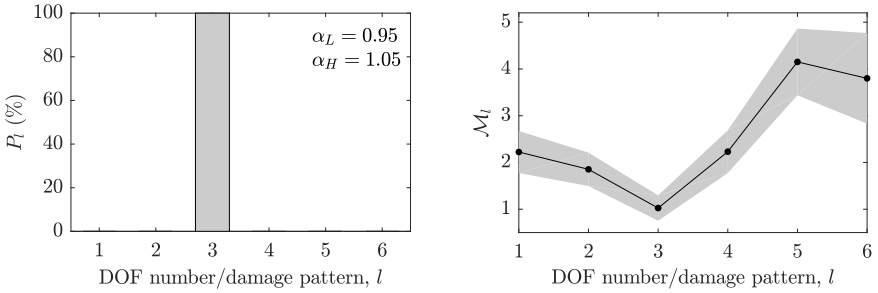

Fig. 5.7: Damage localization in chain-like system with additional output sensor at DOF 5. (a) P_l. (b) $\bar{\mathcal{M}}_l$ and $S_{\mathcal{M}_l}$ for the realizations in Fig. 5.7a.

the localization resolution. As evidenced when comparing these results with those from the similar single-sensor configuration, see Fig. 5.6, the improvement gained by adding an extra sensor is significant.

It is noticed that with the given configuration of model errors, that is, $\alpha_L = 0.95$ and $\alpha_H = 1.05$, only two possible two-sensor combinations—namely, DOF 4 and 6 plus 5 and 6—provide a POL below 100 %. For these particular distributions, we find POL = 96 % when using DOF 4 and 6 and POL = 93 % when using DOF 5 and 6. These reduced POL are due to the fact that almost no damage-induced shift can be observed in the response in DOF 6.

5.6.2 Truss structure

The FE truss model depicted in Fig. 5.8 is examined for damage manifested as a stiffness reduction, smeared across element 9, of magnitude $\chi \in \{40\,\%, 20\,\%\}$. The structure, which is assumed to have a classical damping distribution such each mode has a damping ratio of $\zeta_i = 5$ %, consists of 21 bars that are all assigned a square cross-section and a material model corresponding to typical structural steel. White noise excitation, $r(t)$, with standard deviation $\sigma_r = 1$ kN is applied to node 12 as seen in Fig. 5.8, and two harmonic inputs to be shaped are applied to nodes 8 and 12; with a driving frequency fixed to $\Omega = 0.75\omega_1$, where ω_1 is the fundamental eigenfrequency of the healthy structure. The output is taken as noise-corrupted steady-state vertical accelerations measured in node 5 with a sampling frequency of 1000 Hz.

Structural interrogation

With the introduced stiffness perturbation, Theorem 5.1 states that the two inputs must be shaped such that the steady-state strains are suppressed in one subdomain, that is, one bar element, at a time. For each postulated damage pattern, we extract the moduli and arguments of the two inputs through the

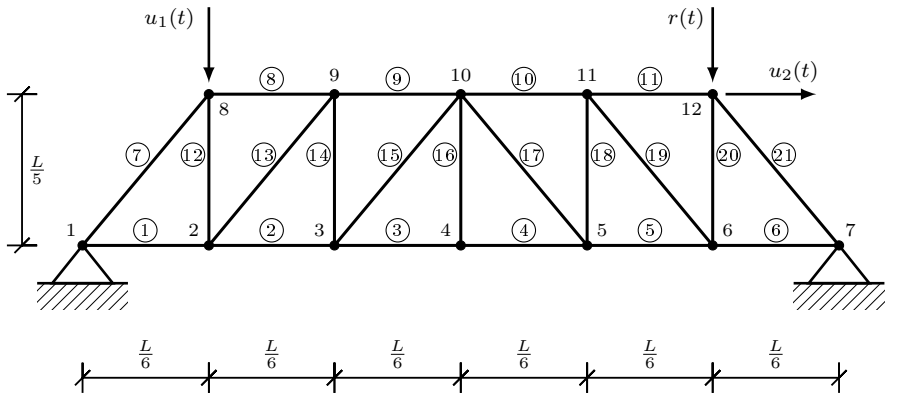

Fig. 5.8: Truss structure subjected to white Gaussian noise excitation, $r(t)$, and two inputs to be shaped, $u(t)$. The output is taken as vertical steady-state accelerations captured in node 5 and corrupted with 5 % white Gaussian noise.

Laplace domain approach described in Subsection 5.3.1 and choose to scale the amplitudes such that $\max(u_1) = 100\sigma_r$, where we recall that σ_r is the standard deviation of r. This scaling is chosen to ensure that the harmonics are not camouflaged by the ambient excitation.

A Monte Carlo simulation is carried out for each of the two damage extents; with 5 % output noise and model errors corresponding to $\alpha_L = 0.98$ and $\alpha_H = 1.02$ (yielding up to 1 % observed shifts in eigenfrequencies). The obtained interrogation results are presented in Fig. 5.9. As evidenced in Figs. 5.9a and 5.9b, the 40 % stiffness reduction in bar element 9 is consistently localized, with a mean discordance value, $\bar{\mathcal{M}}_9$, approximately eight times smaller than the second lowest, which is obtained when interrogating element 8. For the smallest damage, that is, $\chi = 20$ %, interrogation of element 9 yields, as shown in Figs. 5.9c and 5.9d, the lowest discordance in 64 % of the simulations while the remaining 36 % point to element 8.

Aggregation for enhanced robustness

The impaired localization resolution for the 20 % stiffness reduction is governed by the model errors. Therefore, it is contended that this resolution could be improved by taking the discordance between a realization from the damaged state and a statistical baseline model accounting for the variance in the realizations (hence requiring multiple measurements in the undamaged state) and/or by, in some sense, optimizing the spatial distribution of the inputs and output(s).

The previous results are obtained using a single interrogation frequency, $\Omega = 0.75\omega_1$, which has been chosen somewhat arbitrarily. It is recalled that the SDLID scheme operates on the premise of exciting the measurement DOF and the damaged area when this is not intended to be suppressed. This refers to the fact that when all other damage patterns than the correct one are in-

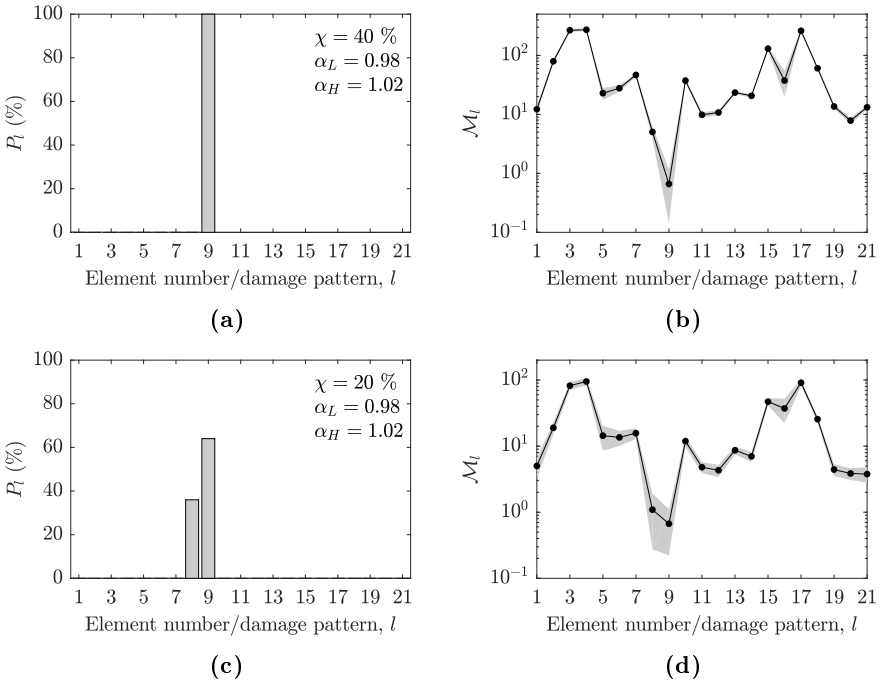

Fig. 5.9: Localization of stiffness reduction in element 9 in the truss with 5 % output noise, $\alpha_L = 0.98$, and $\alpha_H = 1.02$. (a) P_l for $\chi = 40$ %. (b) $\bar{\mathcal{M}}_l$ and $S_{\mathcal{M}_l}$ for the realizations in Fig. 5.9a. (c) P_l for $\chi = 20$ %. (d) $\bar{\mathcal{M}}_l$ and $S_{\mathcal{M}_l}$ for the realizations in Fig. 5.9c.

terrogated, the operating deflection shapes should, ideally, maximize the effect of the damage one seeks for. In the case of stiffness perturbations, this corresponds to maximizing the strain. With this in mind, there most likely exist a set of frequencies that yield worse results than those obtained for $\Omega = 0.75\omega_1$ and a set with which the scheme would perform better. Needless to say, one does not know the correct pattern a priori, so aggregation of multiple excitation setups can be utilized to enhance the localization robustness. In Figs. 5.10a and 5.10b, the results obtained by interrogating with five frequencies, which are evenly spaced between $0.75\omega_1$ and ω_{10}, are shown. Here, the output sensor, damage, noise, and model error conditions are the same as those employed in the analyses providing the results presented in Figs. 5.9c and 5.9d. Thus, it is clearly seen how implementation of multiple interrogation frequencies improve the localization results.

Further aggregation can be implemented by utilizing multiple output sensors, which, as shown for the chain-like system in Subsection 5.6.1, can improve the results. Figs. 5.10c and 5.10d depict the results obtained by adding an output sensor at DOF 21 (capturing the horizontal accelerations in node 11) such $m_s = 2$. Evidently, all clusters of false negatives are removed. Yet, by inspec-

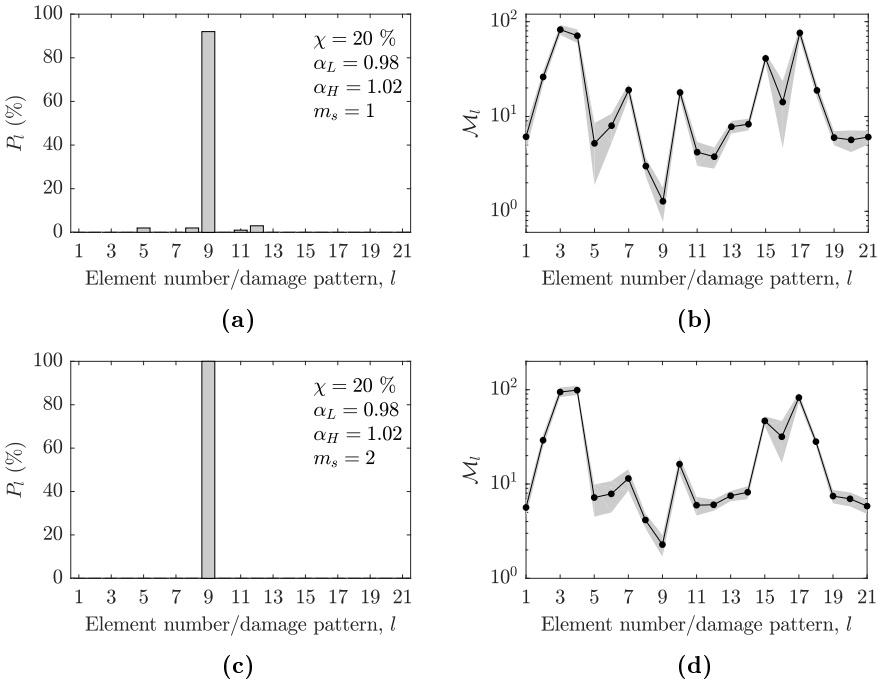

Fig. 5.10: Aggregation of localization results for five driving frequencies (evenly spaced between $0.75\omega_1$ and ω_{10}), $\chi = 20$ %, and different output sensor configurations. (a) $m_s = 1$. (b) $\bar{\mathcal{M}}_l$ and $S_{\mathcal{M}_l}$ for the realizations in Fig. 5.10a. (c) $m_s = 2$. (d) $\bar{\mathcal{M}}_l$ and $S_{\mathcal{M}_l}$ for the realizations in Fig. 5.10c.

tion of the findings plotted in, for example, Figs. 5.10b and 5.10d, we notice that the discordances obtained when interrogating element 8, which is adjacent to the damaged element, are substantially smaller than those obtained when interrogating the remaining undamaged elements. This implies that the input shaping approach also has merit in cases where only spatial locations close to, but not at, the damage are interrogated.

5.7 Concluding remarks

In this chapter, we have introduced the SDLID damage localization scheme, which is based on interrogating structures and structural systems by use of controllable inputs. Despite bearing resemblance to the well-known (S)DDLV platform, the SDLID scheme stands as a conceptual alternative to the traditional vibration-based localization methods, which, typically, operate on the premise of mapping damage-induced vibration signature deviations to the structural domain. Instead, the SDLID scheme localizes damage by deploying multiple inputs that are shaped, using a model representation, to cancel the effect of

the damage.

The applicability of the SDLID scheme has been tested in the context of two numerical examples of engineering interest, namely, a simple chain-like system and a truss structure. The examples demonstrate the major merits of the scheme; including circumvention of system identification, robustness towards noise, and a low demand on output sensors. Regarding the latter, the SDLID method can, in principle, operate with a single output sensor, but as evidenced in the application examples, the localization resolution is improved if multiple output sensors are utilized. Especially in the presence of model errors, which are implemented in the examples to emulate the inevitable discrepancies between a real structure and its model representation, it is suggested to employ multiple output sensors and/or multiple interrogation frequencies to allow for aggregation and, as such, an increased robustness.

CHAPTER 6

Conclusions and future perspectives

This thesis revolves around the topic of vibration-based SHM. More particularly, focus is on damage localization with the aim of exploring new schemes, which, in one way or another, confront the unfavorable ratio between sensitivity to damage and sensitivity to variabilities of the vibration signatures. The exploration has resulted in the development of three new schemes, whose methodological premises have been derived and subsequently tested in the context of examples of engineering interest. This final chapter provides, in Section 6.1, a brief summary of the explored schemes and concludes the observations made in the course of both development and testing of these. Based on this, some suggestions for future work related to the three schemes are outlined in Section 6.2.

6.1 General conclusions

The main conclusions are drawn from those in the preceding chapters and the observations made in the papers that constitute the basis of these chapters; namely, papers A to F as presented in the corresponding appendices.

The CWT-GDTKEO scheme locates damage from identified changes in mode shapes. The location is ascertained from a simple metric comparing processed mode shape signals from the states prior and posterior to damage. The approach can be viewed as offering a small refinement of an existing method, where the robustness to noise has been increased. Application examples illustrate the effectiveness of the refinement, but it is also noticed how the scheme exhibits the difficulties connected with compressing the vibration data into a modal model while preserving sufficient information on the damage. For example, the scheme is applied to locate a damage in a wind turbine blade mounted on a test rig in a laboratory setup. Even under these controlled conditions and with parameter estimation utilizing state-of-art modal analysis techniques, the damage-induced shifts in the modal parameters of the lower modes are camouflaged by the uncertainties associated with the parameter estimation. It thus follows that the CWT-GDTKEO scheme merely applies to cases where the input provides, or can be tailored to provide, excitation of higher modes.

The SEZ scheme locates damage in a forward manner, where shifts in measured vibration quantities are reconstructed by use of stresses acting over

boundaries that are created by the removal of certain portions of the domain. The approach does not directly point to damage, but rather allows one to test whether it is in the interior of any postulated zone. Besides facilitating non-parametric interrogation if the input distribution is spatially invariant and the input histories are proportional in the structural states, an attractive feature of the scheme is that the user can select the zones, more or less, at will. This provides control over the damage localization resolution, which, for example, can be exploited to use large zones to narrow down the set of potentially damaged locations and then, if required, interrogate this set using refined zones. The application examples, particularly the one with a real-life operating wind turbine, suggest that the scheme has merit in those industrial applications where it can work free of system identification and, accordingly, avoid compressing vibration data into a modal model.

The SDLID scheme locates damage using information extracted from the vibration response to inputs, which are shaped to render certain parts of the domain dormant. For mass-related damage, this corresponds to making the steady-state displacements, velocities, and accelerations in the subdomain containing the damage equal to zero, while for stiffness-related damage one suppresses the steady-state strains. As such, the SDLID scheme, like the SEZ platform, operates by interrogating user-selected subdomains for damage instead of pointing directly to it. The applicability of the SDLID scheme has been tested on the basis of numerical examples of engineering interest, and the merits are clearly emphasized; namely, robustness to noise, a low demand on output sensors, and, of course, unconditional circumvention of system identification. Obviously, the scheme has to be tested in the context of experimental campaigns before drawing any final conclusion as to its industrial applicability, but, for now, it stands as a favorable approach to damage localization when deployment of multiple, controllable inputs is feasible.

Generally, the use of any damage localization scheme is governed by the conditions under which it must operate. Since these will vary from one application to the next, one cannot speak of a particular scheme being optimal, or even useful, in all instances. Instead, a method selection must be made for each application, and in this context the SEZ and SDLID schemes exhibit promise for applications where one has control over the excitation imposed on the domain and, in addition, a reasonable accurate model of the structure can be formulated. Needless to say, these two schemes are at a stage of development where further refinements are anticipated before technical maturity is reached.

6.2 Suggestions for future work

Since the scope of this thesis has been to conduct fundamental research on the topic of vibration-based damage localization, there are numerous aspects that

have not been disclosed. Some suggestions for future work related particularly to the three proposed schemes are presented below.

1. The CWT-GDTKEO scheme:
   - The single most important aspect for improvement of the CWT-GDTKEO scheme is to cope with the unfavorable ratio between sensitivity to damage of the mode shapes and sensitivity to noise in the parameter estimation. One approach worth exploring is to extract the uncertainties associated with the mode shape estimates and propagate these throughout the damage localization scheme.
   - Another way of improving the aforementioned ratio could be to develop a procedure for placing the sensors in an optimal sense. Here, balancing the uncertainties associated with the mode shape estimates and the sensitivity to damage must be explored.
2. The SEZ scheme:
   - It is possible to adapt the SEZ scheme to consider entirely arbitrary loading by estimating the experimental feature through system identification. The applicability in this regard should be examined.
   - A crucial step in the scheme is the selection of s-values in the structural interrogation. An interesting and highly relevant research topic could revolve around the development of an automated approach to select these values.
3. The SDLID scheme:
   - At present, the SDLID scheme has only been applied to numerical models, so a natural next step is to implement the scheme in the context of experimental setups.
   - An item of interest is the feasibility of reducing the required amount of controllable inputs. It seems plausible that a least-squares solution, based on fewer inputs than required to provide an exact solution under ideal conditions, may provide useful results.
   - It could also be of interest to examine, more carefully, the influence of the nature and location of the inputs. As the scheme requires the damaged subdomain activated in those instances where it is not to be suppressed, some optimization procedure could, potentially, be implemented in selecting the type and location of the input sources.
   - Just as for the SEZ scheme, an automated approach for selecting the s-value(s) should be established.

Bibliography

Adams, R. D., Cawley, P., Pye, C. J., and Stone, B. J. (1978). "A vibration technique for non-destructively assessing the integrity of structures." *Journal of Mechanical Engineering Science*, 20(2), 93–100.

Allemang, R. J. and Brown, D. L. (1982). "A correlation coefficient for modal vector analysis." *Proceedings of the 1st International Modal Analysis Conference*, Orlando, USA, 110–116.

Antoine, J. P., Murenzi, R., Vandergheynst, P., and Ali, S. T. (2004). *Two-Dimensional Wavelets and their Relatives*. Cambridge University Press.

Balageas, D., Fritzen, C.-P., and Güemes, A. (2006). *Structural Health Monitoring*. ISTE.

Balmès, E., Basseville, M., Mevel, L., Nasser, H., and Zhou, W. (2008). "Statistical model-based damage localization: A combined subspace-based and substructuring approach." *Structural Control and Health Monitoring*, 15(6), 857–875.

Banjevic, D. and Jardine, A. K. S. (2006). "Calculation of reliability function and remaining useful life for a markov failure time process." *IMA Journal of Management Mathematics*, 17(2), 115–130.

Basseville, M., Abdelghani, M., and Benveniste, A. (2000). "Subspace-based fault detection algorithms for vibration monitoring." *Automatica*, 36(1), 101–109.

Basseville, M., Mevel, L., and Goursat, M. (2004). "Statistical model-based damage detection and localization: subspace-based residuals and damage-to-noise sensitivity ratios." *Journal of Sound and Vibration*, 275(3), 769–794.

Bernal, D. (2002). "Load vectors for damage localization." *Journal of Engineering Mechanics*, 128(1), 7–14.

Bernal, D. (2006). "Flexibility-based damage localization from stochastic realization results." *Journal of Engineering Mechanics*, 132(6), 651–658.

Bernal, D. (2007). "Damage localization from the null space of changes in the transfer matrix." *AIAA Journal*, 45(2), 374–381.

Bernal, D. (2010). "Load vectors for damage location in systems identified from operational loads." *Journal of Engineering Mechanics*, 136(1), 31–39.

Bernal, D. (2014). "Damage localization and quantification from the image of changes in flexibility." *Journal of Engineering Mechanics*, 140(2), 279–286.

Bernal, D. and Kunwar, A. (2016). "Steady state shift damage localization." *Meccanica*, 51(11), 2861–2871.

Bernal, D. and Ulriksen, M. D. (2017). "Subspace exclusion zones for damage localization." *Mechanical Systems and Signal Processing*, Under review.

Bernal, D. and Ussia, A. (2015). "Sequential deconvolution input reconstruction." *Mechanical Systems and Signal Processing*, 50-51, 41–55.

Bishof, C. (2006). *Pattern Recognition and Machine Learning*. Springer-Verlag New York.

Bull, T., Markvart, M. K., Sekjær, C., Ulriksen, M. D., Johansen, R. J., Tcherniak, D., and Damkilde, L. (2017). "Statistical discrimination of steady state shift damage localization metrics." *Proceedings of the International Conference on Structural Engineering Dynamics (ICEDyn 2017)*, Ericeira, Portugal.

Burgos, D. A. T., Mujica, L. E., and Rodellar, J. (2015). *Emerging Design Solutions in Structural Health Monitoring Systems*. IGI Global, 1st edition.

Cao, M. and Qiao, P. (2009). "Novel laplacian scheme and multiresolution modal curvatures for structural damage identification." *Mechanical Systems and Signal Processing*, 23(4), 1223–1242.

Cao, M., Xu, W., Ostachowicz, W., and Su, Z. (2014). "Damage identification for beams in noisy conditions based on Teager energy operator-wavelet transform modal curvature." *Journal of Sound and Vibration*, 333(6), 1543–1553.

Caughey, T. K. and O'Kelly, M. E. J. (1965). "Classical normal modes in damped linear dynamic systems." *Journal of Applied Mechanics*, 32(3), 583–588.

Cawley, P. and Adams, R. D. (1979). "The location of defects in structures from measurements of natural frequencies." *The Journal of Strain Analysis for Engineering Design*, 14(2), 49–57.

Cexus, J. C. and Boudraa, A. O. (2007). "Teager-Huang Analysis Applied to Sonar Target Recognition." *International Journal of Electrical, Robotics, Electronics and Communications Engineering*, 1(2), 321–324.

Ciang, C. C., Lee, J.-R., and Bang, H.-J. (2008). "Structural health monitoring for a wind turbine system: a review of damage detection methods." *Measurement Science and Technology*, 19(12), 122001.

Creed, S. G. (1987). "Assessment of large engineering structures using data collected during in-service loading." *Structural Assessment: The Use of Full and Large Scale Testing*, F. K. Garas, J. L. Clarke, and G. S. T. Armer, eds., Butterworth-Heinemann, 55–62.

Davies, B. and Martin, B. (1979). "Numerical inversion of the laplace transform: a survey and comparison of methods." *Journal of Computational Physics*, 33(1), 1–32.

Devriendt, C., Weijtjens, W., El-Kafafy, M., and De Sitter, G. (2014). "Monitoring resonant frequencies and damping values of an offshore wind turbine in parked conditions." *IET Renewable Power Generation*, 8(4), 433–441.

DNV GL (2016). *DNVGL-SE-0439: Certification of condition monitoring*. DNV GL.

Doebling, S. W., Farrar, C. R., and Prime, M. B. (1998). "A Summary Review of Vibration-Based Damage Identification Methods." *Shock Vibration Digest*, 30(2), 91–105.

Döhler, M., Kwan, K., and Bernal, D. (2013). "Optimal sensor placement with a statistical criterion for subspace-based damage detection." *Topics in Dynamics of Civil Structures, Volume 4: Proceedings of the 31st IMAC, A Conference on Structural Dynamics, 2013*, F. N. Catbas, S. Pakzad, V. Racic, A. Pavic, and P. Reynolds, eds., Springer New York, 219–229.

Döhler, M., Mevel, L., and Hille, F. (2014). "Subspace-based damage detection under changes in the ambient excitation statistics." *Mechanical Systems and Signal Processing*, 45(1), 207–224.

Doliński, L. and Krawczuk, M. (2009). "Damage detection in turbine wind blades by vibration based methods." *Journal of Physics: Conference Series*, 181(1), 012086.

Douka, E., Loutridis, S., and Trochidis, A. (2003). "Crack identification in beams using wavelet analysis." *International Journal of Solids and Structures*, 40(13-14), 3557–3569.

Duda, R. O., Hart, P. E., and Stork, D. G. (2001). *Pattern Classification*. John Wiley & Sons, 2nd edition.

Fan, W. and Qiao, P. (2011). "Vibration-based damage identification methods: A review and comparative study." *Structural Health Monitoring*, 10(1), 83–111.

Farrar, C., Doebling, S., Cornwell, P., and Straser, E. (1997). "Variability of modal parameters measured on the Alamosa Canyon Bridge." *Proceedings of the 15th International Modal Analysis Conference*, Orlando, United States, 257–263.

Farrar, C. R., Doebling, S. W., and Nix, D. A. (2001). "Vibration-based structural damage identification." *Philosophical Transactions of the Royal Society A*, 359(1778), 131–149.

Farrar, C. R. and Worden, K. (2013). *Structural Health Monitoring: A Machine Learning Perspective*. John Wiley & Sons, 1st edition.

Friswell, M. I. (2007). "Damage identification using inverse methods." *Philosophical Transactions of the Royal Society A*, 365(1851), 393–410.

Friswell, M. I. and Mottershead, J. E. (1995). *Finite Element Model Updating in Structural Dynamics*. Kluwer Ademic Publishers.

Friswell, M. I. and Penny, J. E. T. (2002). "Crack modeling for structural health monitoring." *Structural Health Monitoring*, 1(2), 139–148.

García, D., Tcherniak, D., and Trendafilova, I. (2015). "Damage assessment for wind turbine blades based on a multivariate statistical approach." *Journal of Physics: Conference Series*, 628(1), 012086.

García, D. and Trendafilova, I. (2014). "A multivariate data analysis approach towards vibration analysis and vibration-based damage assessment: Application for delamination detection in a composite beam." *Journal of Sound and Vibration*, 333(25), 7036–7050.

Gres, S., Ulriksen, M. D., Döhler, M., Johansen, R. J., Andersen, P., Damkilde, L., and Nielsen, S. A. (2017). "Statistical methods for damage detection applied to civil structures." *Procedia Engineering*, 199, 1919–1924.

Guan, R., Lu, Y., Duan, W., and Wang, X. (2017). "Guided waves for damage identification in pipeline structures: A review." *Structural Control and Health Monitoring*, 24(11), 1–17.

Hà, N. V. and Golinval, J.-C. (2010). "Localization and quantification of damage in beam-like structures using sensitivities of principal component analysis results." *Mechanical Systems and Signal Processing*, 24(6), 1831–1843.

Hansen, L. M., Johansen, R. J., Ulriksen, M. D., Tcherniak, D., and Damkilde, L. (2015). "Statistical evaluation of characteristic sddlv-induced stress resultants to discriminate between undamaged and damaged elements." *Journal of Physics: Conference Series*, 628, 012003.

Hellier, C. J. (2001). *Handbook of Nondestructive Evaluation*. McGraw-Hill, 1st edition.

Heylen, W., Lammens, S., and Sas, P. (1998). *Modal Analysis Theory and Testing*. Katholieke Universitet Leuven, 2nd edition.

Iliopoulos, A., Weijtjens, W., Van Hemelrijck, D., and Devriendt, C. (2017). "Fatigue assessment of offshore wind turbines on monopile foundations using multi-band modal expansion." *Wind Energy*, 20(8), 1463–1479.

Janeliukstis, R., Rucevskis, S., Wesolowski, M., and Chate, A. (2017). "Damage identification in beam structure based on thresholded variance of normalized wavelet scalogram." *IOP Conference Series: Materials Science and Engineering*, 251(1), 012089.

Jardine, A. K., Lin, D., and Banjevic, D. (2006). "A review on machinery diagnostics and prognostics implementing condition-based maintenance." *Mechanical Systems and Signal Processing*, 20(7), 1483–1510.

Jiang, L. J., Tang, J. J., and Wang, K. W. (2007). "An optimal sensitivity-enhancing feedback control approach via eigenstructure assignment for structural damage identification." *Journal of Vibration and Acoustics*, 129(6), 771–783.

Johansen, R. J., Hansen, L. M., Ulriksen, M. D., Tcherniak, D., and Damkilde, L. (2015). "Damage localization in a residential-sized wind turbine blade by use of the sddlv method." *Journal of Physics: Conference Series*, 628, 012069.

Ju, F. D. and Mimovich, M. E. (1988). "Experimental diagnosis of fracture damage in structures by the modal frequency method." *Journal of Vibration, Acoustics, Stress, and Reliability in Design*, 110(4), 456–463.

Kaiser, J. F. (1990). "On a simple algorithm to calculate the 'energy' of a signal." *Proceedings of the 1990 International Conference on Acoustics, Speech, and Signal Processing*, Albuquerque, USA, 381–384.

Kopsaftopoulos, F. and Fassois, S. (2010). "Vibration based health monitoring for a lightweight truss structure: Experimental assessment of several statistical time series methods." *Mechanical Systems and Signal Processing*, 24(7), 1977–1997.

Krenk, D. C. and Høgsberg, J. (2013). *Statics and Mechanics of Structures*. Springer, Dordrecht.

Larsen, G. C., Berring, P., Tcherniak, D., Nielsen, P. H., and Branner, K. (2014). "Effect of a damage to modal parameters of a wind turbine blade." *Proceedings of the 7th European Workshop on Structural Health Monitoring*, Bilbao, Spain.

Lieven, N. and Ewins, D. (1988). "Spatial Correlation of Mode Shapes, the Coordinate Modal Assurance Criterion (COMAC)." *Proceedings of the 4th International Modal Analysis Conference*, Kissimmee, USA, 690–695.

Lim, T. W. and Kashangaki, T. A. L. (1994). "Structural damage detection of space truss structures using best achievable eigenvectors." *AIAA Journal*, 32(5), 1049–1057.

Ljung, L. (1987). *System Identification: Theory for the User*. Prentice Hall, 1st edition.

Loutridis, S., Douka, E., Hadjileontiadis, L. J., and Trochidis, A. (2005). "A two-dimensional wavelet transform for detection of cracks in plates." *Engineering Structures*, 27(9), 1327–1338.

Maes, K., Iliopoulos, A., Weijtjens, W., Devriendt, C., and Lombaert, G. (2016). "Dynamic strain estimation for fatigue assessment of an offshore monopile wind turbine using filtering and modal expansion algorithms." *Mechanical Systems and Signal Processing*, 76, 592–611.

Mahalanobis, P. C. (1936). "On the generalised distance in statistics." *The National Institute of Science of India*, 49–55.

Mallat, S. (2009). *A wavelet tour of signal processing*. Academic Press, 3rd edition.

Maragos, P. and Bovik, A. C. (1995). "Image demodulation using multidimensional energy separation." *Journal of the Optical Society of America A*, 12(9), 1867–1876.

Maragos, P., Quatieri, T. F., and Kaiser, J. F. (1991). "Speech nonlinearities, modulations, and energy operators." *Proceedings of the 1991 International Conference on Acoustics, Speech, and Signal Processing*, Toronto, Canada, 421–424.

Marin, L. H. G., Döhler, M., Bernal, D., and Mevel, L. (2015). "Robust statistical damage localization with stochastic load vectors." *Structural Control and Health Monitoring*, 22(3), 557–573.

Markvart, M. K., Bull, T., Sekjær, C., Johansen, R. J., Ulriksen, M. D., Tcherniak, D., and Damkilde, L. (2017). "Steady state shift damage localization in a residential-sized wind turbine blade." *Proceedings of the International Conference on Structural Engineering Dynamics (ICEDyn 2017)*, Ericeira, Portugal.

Messina, A. (2008). "Refinements of damage detection methods based on wavelet analysis of dynamical shapes." *International Journal of Solids and Structures*, 45(14-15), 4068–4097.

Mevel, L., Hermans, L., and Van der Auweraer, H. (1999). "Application of a subspace-based fault detection method to industrial structures." *Mechanical Systems and Signal Processing*, 13(6), 823–838.

Murphy, B. R. and Watanabe, I. (1992). "Digital shaping filters for reducing machine vibration." *IEEE Transactions on Robotics and Automation*, 8(2), 285–289.

Overschee, P. v. and De Moor, B. (1996). *Subspace identification for linear systems: theory - implementation - applications*. Kluwer Academic Publishers, 1st edition.

Pandey, A., Biswas, M., and Samman, M. (1991). "Damage detection from changes in curvature mode shapes." *Journal of Sound and Vibration*, 145(2), 321–332.

Parker, D. L. (2011). "Multi-objective design optimization framework for structural health monitoring." Ph.D. thesis, Mississippi State University, Mississippi, USA.

Peeters, B. and De Roeck, G. (2001). "Stochastic system identification for operational modal analysis: A review." *Journal of Dynamic Systems, Measurement, and Control*, 123(4), 659–667.

Pintelon, R., Guillaume, P., and Schoukens, J. (2007). "Uncertainty calculation in (operational) modal analysis." *Mechanical Systems and Signal Processing*, 21(6), 2359–2373.

Prevosto, M., Olagnon, M., Benveniste, A., Basseville, M., and Vey, G. L. (1991). "State space formulation: A solution to modal parameter estimation." *Journal of Sound and Vibration*, 148(2), 329–342.

Raghavan, A. and Cesnik, C. E. S. (2007). "Review of guided-wave structural health monitoring." *Shock and Vibration Digest*, 39(2), 91–116.

Ratcliffe, C. (1997). "Damage detection using a modified laplacian operator on mode shape data." *Journal of Sound and Vibration*, 204(3), 505–517.

Ray, L. and Tian, L. (1999). "Damage detection in smart structures through sensitivity enhancing feedback control." *Journal of Sound and Vibration*, 227(5), 987–1002.

Ray, L. R., Koh, B.-H., and Tian, L. (2000). "Damage detection and vibration control in smart plates: Towards multifunctional smart structures." *Journal of Intelligent Material Systems and Structures*, 11(9), 725–739.

Rehorn, A. G., Jiang, J., and Orban, P. E. (2005). "State-of-the-art methods and results in tool condition monitoring: a review." *The International Journal of Advanced Manufacturing Technology*, 26(7), 693–710.

Reynders, E., Pintelon, R., and Roeck, G. D. (2008). "Uncertainty bounds on modal parameters obtained from stochastic subspace identification." *Mechanical Systems and Signal Processing*, 22(4), 948–969.

Rucka, M. (2011). "Damage detection in beams using wavelet transform on higher vibration modes." *Journal of Theoretical and Applied Mechanics*, 49(2), 399–417.

Rucka, M. and Wilde, K. (2006). "Application of continuous wavelet transform in vibration based damage detection method for beams and plates." *Journal of Sound and Vibration*, 297(3-5), 536–550.

Rytter, A. (1993). "Vibrational based inspection of civil engineering structures." Ph.D. thesis, Aalborg University, Aalborg, Denmark.

Sakaris, C., Sakellariou, J., and Fassois, S. (2016). "A time series generalized functional model based method for vibration-based damage precise localization in structures consisting of 1d, 2d, and 3d elements." *Mechanical Systems and Signal Processing*, 74, 199–213.

Salawu, O. S. (1997). "Detection of structural damage through changes in frequency: a review." *Engineering Structures*, 19(9), 718–723.

Savage, R. and Hewlett, P. (1978). "A new ndt method for structural integrity assessment." *NDT International*, 11(2), 61–67.

Schroeder, D. (2013). *Repelling inspection.* `https://www.flickr.com/photos/iip-photo-archive/23095738005/` Online; accessed September 3 2017.

Sekjær, C., Bull, T., Markvart, M. K., Johansen, R. J., Ulriksen, M. D., Tcherniak, D., and Damkilde, L. (2017). "Steady state shift damage localization: a super-element approach." *Proceedings of the International Conference on Structural Engineering Dynamics (ICEDyn 2017)*, Ericeira, Portugal.

Shi, Z. Y., Law, S. S., and Zhang, L. M. (2000). "Optimum Sensor Placement for Structural Damage Detection." *Journal of Engineering Mechanics*, 126(11), 1173–1179.

Si, X.-S., Wang, W., Hu, C.-H., and Zhou, D.-H. (2011). "Remaining useful life estimation – a review on the statistical data driven approaches." *European Journal of Operational Research*, 213(1), 1–14.

Simoen, E., De Roeck, G., and Lombaert, G. (2015). "Dealing with uncertainty in model updating for damage assessment: A review." *Mechanical Systems and Signal Processing*, 56-57, 123–149.

Singer, N. C. and Seering, W. P. (1988). "Preshaping command inputs to reduce system vibration." *Journal of Dynamic Systems, Measurement, and Control*, 112(1), 76–82.

Singh, T. and Heppler, G. R. (1993). "Shaped input control of a system with multiple modes." *Journal of Dynamic Systems, Measurement, and Control*, 115(3), 341–347.

Solbeck, J. A. and Ray, L. R. (2005). "Damage identification using sensitivity-enhancing control and identified models." *Journal of Vibration and Acoustics*, 128(2), 210–220.

Straub, D. (2009). "Stochastic modeling of deterioration processes through dynamic bayesian networks." *Journal of Engineering Mechanics*, 135(10), 1089–1099.

Su, Z., Ye, L., and Lu, Y. (2006). "Guided lamb waves for identification of damage in composite structures: A review." *Journal of Sound and Vibration*, 295(3), 753–780.

Surgeon, M. and Wevers, M. (1999). "One sensor linear location of acoustic emission events using plate wave theories." *Materials Science and Engineering: A*, 265(1), 254–261.

Tcherniak, D. and Mølgaard, L. L. (2017). "Active vibration-based structural health monitoring system for wind turbine blade: Demonstration on an operating vestas v27 wind turbine." *Structural Health Monitoring*, 16(5), 536–550.

Teughels, A. and De Roeck, G. (2004). "Structural damage identification of the highway bridge z24 by fe model updating." *Journal of Sound and Vibration*, 278(3), 589–610.

Udwadia, F. E. (1994). "Methodology for optimum sensor locations for parameter identification in dynamic systems." *Journal of Engineering Mechanics*, 120(2), 368–390.

Ulriksen, M. D. and Bernal, D. (2017). "Sensor distributions for structural monitoring: a correlation study." *Proceedings of the International Conference on Structural Engineering Dynamics (ICEDyn 2017)*, Ericeira, Portugal.

Ulriksen, M. D., Bernal, D., and Damkilde, L. (2017a). "Input shaping for steady-state damage localization." *Mechanical Systems and Signal Processing*, Under review.

Ulriksen, M. D., Bernal, D., Nielsen, M. E., and Damkilde, L. (2017b). "Damage localization in offshore structures using shaped inputs." *Procedia Engineering*, 199, 2282–2287.

Ulriksen, M. D. and Damkilde, L. (2016). "Structural damage localization by outlier analysis of signal-processed mode shapes - Analytical and experimental validation." *Mechanical Systems and Signal Processing*, 68-69, 1–14.

Ulriksen, M. D., Skov, J. F., Kirkegaard, P. H., and Damkilde, L. (2014). "Wavelet transformation for damage identification in wind turbine blades." *Structural Health Monitoring, Volume 5*, A. Wicks, ed., Conference Proceedings of the Society for Experimental Mechanics Series, Springer International Publishing, 187–193.

Ulriksen, M. D., Tcherniak, D., and Damkilde, L. (2015). "Damage detection in an operating vestas v27 wind turbine blade by use of outlier analysis." *Proceedings of the 2015 IEEE workshop on environmental, energy and structural monitoring systems (EESMS)*, Trento, Italy, 50–55.

Ulriksen, M. D., Tcherniak, D., Hansen, L. M., Johansen, R. J., Damkilde, L., and Frøyd, L. (2017). "In-situ damage localization for a wind turbine blade through outlier analysis of SDDLV-induced stress resultants." *Structural Health Monitoring*, 16(6), 745–761.

Ulriksen, M. D., Tcherniak, D., Kirkegaard, P. H., and Damkilde, L. (2016). "Operational Modal Analysis and Wavelet Transformation for Damage Identification in Wind Turbine Blades." *Structural Health Monitoring*, 15(4), 381–388.

Wang, Z., Lin, R., and Lim, M. (1997). "Structural damage detection using measured frf data." *Computer Methods in Applied Mechanics and Engineering*, 147(1), 187–197.

Worden, K. and Burrows, A. P. (2001). "Optimal sensor placement for fault detection." *Engineering Structures*, 23(8), 885–901.

Worden, K., Manson, G., and Fieller, N. R. J. (2000). "Damage detection using outlier analysis." *Journal of Sound and Vibration*, 229(3), 647–667.

Xu, W., Cao, M., Ostachowicz, W., Radzieński, M., and Xia, N. (2015). "Two-dimensional curvature mode shape method based on wavelets and Teager energy for damage detection in plates." *Journal of Sound and Vibration*, 347, 266–278.

Yeum, C. M., Sohn, H., Lim, H. J., and Ihn, J. B. (2014). "Reference-free delamination detection using lamb waves." *Structural Control and Health Monitoring*, 21(5), 675–684.

Yuen, M. (1985). "A numerical study of the eigenparameters of a damaged cantilever." *Journal of Sound and Vibration*, 103(3), 301–310.

APPENDIX A

Paper A

Ulriksen, M. D. and Damkilde, L. (2016). "Structural damage localization by outlier analysis of signal-processed mode shapes – Analytical and experimental validation." *Mechanical Systems and Signal Processing*, 68-69, 1-14. https://doi.org/10.1016/j.ymssp.2015.07.021.

APPENDIX B

Paper B

Ulriksen, M. D., Tcherniak, D., Kirkegaard, P. H., and Damkilde, L. (2016). "Operational modal analysis and wavelet transformation for damage identification in wind turbine blades." *Structural Health Monitoring*, 15(4), 381-388. https://doi.org/10.1177/1475921715586623.

APPENDIX C

Paper C

Bernal, D. and Ulriksen, M. D. (2017). "Subspace Exclusion Zones for Damage Localization." *Mechanical Systems and Signal Processing*, Under review.

APPENDIX D

Paper D

Ulriksen, M. D., Tcherniak, D., Hansen, L. M., Johansen, R. J., Frøyd, L., and Damkilde, L. (2017). "In-situ damage localization for a wind turbine blade through outlier analysis of SDDLV-induced stress resultants." *Structural Health Monitoring*, 16(6), 745-761. https://doi.org/10.1177/1475921716681727.

APPENDIX E

Paper E

Ulriksen, M. D., Bernal, D., and Damkilde, L. (2017). "Input shaping for steady-state damage localization." *Mechanical Systems and Signal Processing*, Under review.

APPENDIX F

Paper F

Ulriksen, M. D., Bernal, D., Nielsen, M. E., and Damkilde, L. (2017). "Damage localization in offshore structures using shaped inputs." *Procedia Engineering*, 199, 2282-2287. https://doi.org/10.1016/j.proeng.2017.09.273.

ISSN (online): 2446-1636
ISBN (online): 978-87-7210-122-4

AALBORG UNIVERSITY PRESS